

EVALUATION OF FRONTAL CRASH STIFFNESS MEASURES FROM THE U.S. NEW CAR ASSESSMENT PROGRAM

Christopher Wiacek
Vinay Nagabhushana
Taryn Rockwell
Stephen Summers
Lixin Zhao

National Highway Traffic Safety Administration
USA

Lauren A. Collins
Alpha Technology Associate, Inc.
USA

Paper Number 15-0257

ABSTRACT

Over the years, vehicle manufacturers may have implemented structural changes to light vehicles to comply with upgraded Federal Motor Vehicle Safety Standards (FMVSS) such as advanced air bags (FMVSS No. 208), side impact protection (FMVSS No. 214), and roof crush (FMVSS No. 216), as well as to improve performance in tests conducted by consumer information programs such as NHTSA's New Car Assessment Program (NCAP) and the Insurance Institute for Highway Safety (IIHS). Both programs have undergone changes in recent years. The NCAP was updated in 2010 to include advanced test dummies, new injury criteria, and a side pole test, and the IIHS adopted side impact, small overlap, and roof crush test protocols. Furthermore, as fuel economy requirements become more stringent, vehicle manufacturers may choose to light-weight vehicles and incorporate materials such as advanced high-strength steel and aluminum. This paper will investigate what effect, if any, these changes have had on vehicle crash pulses, as measured under NCAP. Although more stiffness metrics and crash pulse characteristics have been examined, this study mainly updates the analysis from the 2003 ESV paper, *Evaluation of Stiffness Measures from the U.S. NCAP*. [Swanson, 2003]

This paper utilizes data from model year (MY) 2002 to MY 2014 frontal NCAP crash tests to compute vehicle stiffness using four different methods: linear "initial" stiffness, energy equivalent stiffness, dynamic stiffness and static stiffness. The data are averaged and examined historically for three light duty vehicle classes (light duty pickup trucks (PUs), multi-purpose vehicles (MPVs), and passenger cars (PCs)) to provide a fleet perspective on changes to frontal crash characteristics. In addition, various crash pulse characteristics such as duration and peak acceleration are investigated. Collectively, these metrics have been traditionally used to characterize a vehicle's crash behavior and can subsequently influence restraint design.

The Swanson study found that not only were the average stiffnesses of PCs increasing from MY 1982 to 2001, but there was also a large disparity between the average stiffnesses of PCs and those of MPVs and PUs. The current study identified different trends. The average stiffnesses of PCs and MPVs appear to be converging, indicating that these two vehicle classes may have become more structurally homogenous in this respect. This is also evidenced by the changes observed for the crash pulse characteristics. In recent years, the crash pulse durations for both PCs and MPVs have decreased (though MPVs slightly more than PCs) such that the pulse duration is now essentially equal, on average, for both vehicle classes. The average peak accelerations for PCs and MPVs also increased during the years in this study. PU data is presented for completeness, but no extensive conclusions were made on this vehicle class because no statistically significant trends could be identified.

INTRODUCTION

Over the years, new or more stringent Federal Motor Vehicle Safety Standards (FMVSS) such as advanced air bags, side impact protection, and roof crush have been promulgated and implemented for the modern light vehicle fleet. In addition, NHTSA's NCAP consumer information program was updated in 2010 to include advanced test dummies, new injury criteria, and a side pole test, and the IIHS expanded its crash test information program to include not only a 40 percent frontal offset test, but also side impact, small overlap, and roof crush test protocols. As a result, vehicle manufacturers have implemented structural changes throughout their vehicles.

During a crash, the vehicle's front structure manages the crash forces by transferring the crash energy to structural elements throughout the vehicle. Intrusion and forces into the occupant compartment must be limited so that the restraints can manage the energy transferred to the occupant(s). Side impact and roof crush tests have driven vehicle manufacturers

to make additional improvements to the occupant compartment structure in an attempt to limit door and roof intrusion, respectively.

Concurrently, as fuel economy requirements became more stringent, vehicle manufacturers may have chosen to lightweight vehicles by incorporating materials such as advanced high-strength steel and aluminum while continuing to comply with FMVSS requirements and perform well in consumer information programs. Being successful in such an approach most likely requires optimization of the vehicle structure while giving consideration to the special material properties for these higher strength and lightweighted materials. This paper will explore what impact these additional tests and regulations may have had on vehicle front stiffness as measured in MY 2002 to MY 2014 frontal NCAP tests.

Stiffness is one factor studied to understand how vehicles interact with their collision partners in the real world. Stiffness, as well as other factors such as mass and geometry, provides insight into how energy is managed in crashes. It is also an important factor in understanding the energy that the frontal restraint systems will have to manage in crashes in order to protect the occupants.

Swanson examined three methods of evaluating vehicle front-end stiffness using passenger car data from NCAP tests conducted between MY 1982 and MY 2001. The methods included: initial stiffness, static stiffness, and dynamic stiffness. Two of these methods, initial stiffness and dynamic stiffness, showed a steady increase for PCs over the model years analyzed (21 percent and 34 percent, respectively). The static stiffness method predicted much greater increases (61 percent) in stiffness due to its reliance on static crush data that does not account for the elasticity in front-end structures like dynamic stiffness does.

Average force-deflection plots generated in the Swanson paper for the various PC classes (compact, midsize, full-size) confirmed the increasing stiffness trends predicted by the initial stiffness and dynamic stiffness methods. Similar plots were generated for three other vehicle classes, light trucks, vans, and sport utility vehicles (SUVs), known collectively as LTVs. While stiffness values for the LTV classes tended to be much higher than those for the PC classes, their stiffness characteristics had not changed as much over the same time period.

A recent study using full-frontal rigid-barrier tests data from the NHTSA and Transport Canada crash test databases was conducted to analyze the vehicle crash pulse. [Caitlin, 2012] The paper grouped the data by vehicle type (PC, PU, minivan, and SUV) and size (small, midsize, and large) using the Highway Loss Data Institute classification based upon size and weight. The authors examined crash pulse characteristics, such as peak acceleration and crash pulse duration, for tested MY 2000–2010 vehicles. The paper showed an overall increasing trend in peak acceleration and a decrease in pulse duration, by year, for most vehicle classes. The authors concluded that the shorter, more severe pulse is consistent with stiffening vehicle structure for the current vehicles within the fleet. However, they also found that for later model year vehicles, the crash pulse characteristics were becoming more homogeneous for different vehicle classes.

As with Swanson, this paper will investigate initial stiffness (now termed linear “initial” stiffness), and static and dynamic stiffness. In addition, energy-equivalent stiffness will be calculated using the Kw400 methodology. [Patel, 2007] To expand upon the findings of Caitlin, this paper will also investigate various crash pulse characteristics for severity and duration as measured by time-to-zero velocity and peak acceleration, and will study the characteristics of force-deflection profiles seen in the modern fleet. Though the earlier papers divided their data based on vehicle type and size, since there is not a standard definition for vehicle size classification, this paper will utilize only vehicle type (as identified on the FMVSS certification label) in an effort to gain a fleet perspective on changes to frontal crash characteristics.

METHODOLOGY

Since 1979, NHTSA has been providing consumers with comparative frontal crashworthiness information on new passenger vehicles through NCAP. In the frontal NCAP test, vehicles are evaluated based on the crash protection they provide in a 56 km/h full-frontal rigid barrier crash. This is determined from injury readings recorded by Hybrid III test dummies positioned in the driver and right front passenger seats. Frontal NCAP test data can also be used to characterize a vehicle’s crash behavior.

In this study, available frontal NCAP data collected for MY 2002-2014 test vehicles was used to compute vehicle stiffness using four different methodologies – linear “initial” stiffness, energy-equivalent stiffness, dynamic stiffness, and static stiffness – each of which will be detailed in the next section.

For the first two of these methodologies, linear “initial” stiffness and energy-equivalent stiffness, stiffness is derived using data from (1) accelerometers that are mounted onto the vehicle structure near the driver or front passenger’s seating location, and (2) load cells that have been added to the rigid barrier face to measure the total force the vehicle exerts on the barrier. The data from the vehicle accelerometer is double-integrated to obtain the vehicle’s dynamic displacement, or crush, and the outputs from all of the individual load cells on a barrier are summed to obtain the total barrier force. (All accelerometer and load cell data were filtered according to the Society of Automotive Engineers Recommended Practice J211/1 rev. Mar 95, “Instrumentation for Impact Test – Part 1 – Electronic Instrumentation.”) Although the sizes and numbers of load cells varied among NCAP testing laboratories over the years under study, this should have negligible effect on the total force exerted on a barrier; therefore, it is appropriate to use data from the various arrays for this study.

To compute dynamic stiffness and static stiffness, a vehicle’s mass and velocity are used in combination with dynamic displacement data (again, derived from the vehicle accelerometers in the occupant compartments) and post-test vehicle crush measurements, respectively. For this study, crush measurements were calculated to be the difference between pre- and post-test measurements of the vehicle length, as recorded in the NCAP final test reports. It should also be noted that test weight, not curb weight, was used for these calculations since test weight includes the weight of the two Hybrid III test dummies and the vehicle-rated cargo weight, and best reflects the weight of the vehicle at impact and the resulting forces on the load cells on the barrier.

Although the original data set was comprised of 611 passenger vehicles, the data set for a given metric has been reduced because either the required data was lost, or because the available data was deemed invalid. The final data sets for each of the four stiffness metrics were divided into three vehicle class categories – PCs, MPVs (comprised of SUVs and vans), and light PUs. SUVs and vans were combined into one class, MPVs, because only a small number of vans were tested by NCAP over the years studied. The class category for a given vehicle was dictated by the classification noted on the vehicle’s certification label – PC, MPV, or truck (PU).

Additionally, vehicle crash pulse data such as peak acceleration and time to zero velocity were grouped by vehicle class to observe any changes during the model years considered.

The trends in vehicle dynamic and static stiffness from MY 1982-2014 were examined. In doing so, the MY 2002-2014 data is added to that from Swanson. For the trend analysis spanning from MY 1982-2014, the data was subdivided into model year clusters, with each cluster spanning two model years, and the computed stiffness values for each cluster were then averaged. Three-year intervals were used to present force-deflection profiles for each vehicle class.

As this study is limited to only those vehicles selected for NCAP testing during the given model years, and data was not weighted based on vehicle sales or registration volumes, findings are not necessarily representative of the vehicle fleet as a whole. Trends observed can only be inferred for those vehicles tested by NCAP for the model years under study. Further, no effort was made to relate occupant injury values collected in these tests to the stiffness metrics explored.

RESULTS AND DISCUSSION

For each of the stiffness metrics and the vehicle parameter analysis, the data was primarily analyzed by grouping the first four MY of the study (2002-2005) and the last four MY of the study (2011-2014) and comparing the averages found for each interval. For ease of discussion, these intervals will be referred to as the “first four years” and the “last four years.”

Linear “Initial” Stiffness

For this first method, vehicle stiffness was defined to be the slope of a linear regression line fit to the early portion of a vehicle’s force-deflection profile. A force-deflection profile reflects the total force exerted on the load cell barrier versus the dynamic deformation, or crush, that a vehicle experiences during the duration of a crash test. As mentioned above, this crush is calculated by double-integrating the acceleration recorded by vehicle accelerometers in the occupant compartments.

Force-deflection profiles were generated for the 611 passenger vehicles subjected to frontal NCAP testing spanning model years 2002 through 2014; however, 89 tests were ultimately eliminated because of errors in accelerometer or load cell data collection or because a linear fit of the data could not be achieved. This resulted in a final data set of 522 vehicles for this metric. In the absence of a standard technique, the authors developed a method for resolving differences in the data collected by load cell barriers and vehicle accelerometers. The data collected from the load cell wall and vehicle accelerometers were verified for accuracy by analyzing the momentum balance. Data was considered acceptable if the vehicle velocity (calculated by integrating the vehicle accelerometer data): (1) shared a similar slope to the momentum curve (determined by the force measured at the load cell wall) for the first 400 mm of crush, which was generally 30 ms or less into the crash event, and (2) reflected the actual delta-V. The data was visually inspected to ensure the force on the load cell wall (i.e., momentum curve) led the velocity response and did not diverge from the velocity response prior to the first 400 mm of crush.

For the 522 qualifying tests, linear “initial” stiffness was determined by applying the following criteria: (1) good correlation of linear fit (R^2 value greater than 0.95), (2) correlation begins within the first 200 millimeters of deflection to emphasize what is considered the “initial” deformation of the vehicle, (3) correlation is maintained for a minimum distance of 150 millimeters in order to reflect the overall slope, and (4) linear fit is not constrained to zero force at zero deflection to compensate for small variations in time zero data collection. For a given vehicle, the longest linear correlation that met all four criteria was estimated to be indicative of the vehicle’s linear stiffness. [Summers, 2002], [Swanson, 2003] If a linear fit meeting the preceding criteria could not be achieved for a particular force-deflection profile, linear “initial” stiffness was not quantified for the corresponding vehicle. Figure 1 depicts the results for the three vehicle classes studied. The associated data is provided in the Appendix.

The average linear “initial” stiffness was 1,678 N/mm for all vehicles tested since MY 2002. By class, the average was 2,448 N/mm for PUs, 1,895 N/mm for MPVs, and 1,336 N/mm for PCs during this time period. As shown in Figure 1, average linear “initial” stiffness decreased for MPVs and slightly increased for PCs over the years studied. The average linear “initial” stiffness for the first four years was 1,292 N/mm for PCs, whereas for the last four years, the average was 1,431 N/mm. This was an increase of 10.7 percent, which was found to be significant at the 95% confidence level. MPVs, however, have shown a clear decrease in linear “initial” stiffness since MY 2002. For the first four years, MPVs had an average linear “initial” stiffness of 2,054 N/mm, while for the last four years, this average dropped 14.4 percent to 1,759 N/mm. This result was also significant at the 95% confidence level. It appears that linear “initial” stiffness values for MPVs and PCs are converging. The difference in the average linear “initial” stiffness for the first four years between MPVs and PCs was 45.5 percent. This difference has dropped to 20.6 percent for the last four years. This is consistent with the trend to construct MPVs on more car-like, unibody platforms instead of truck-based, body-on-frame construction. There are more unibody-based MPV offerings than there were during the time period studied in Swanson. Figure 1 shows that average linear “initial” stiffness values for PUs remained higher than those for PCs and MPVs. No statistically significant trend in linear “initial” stiffness could be identified for PUs.

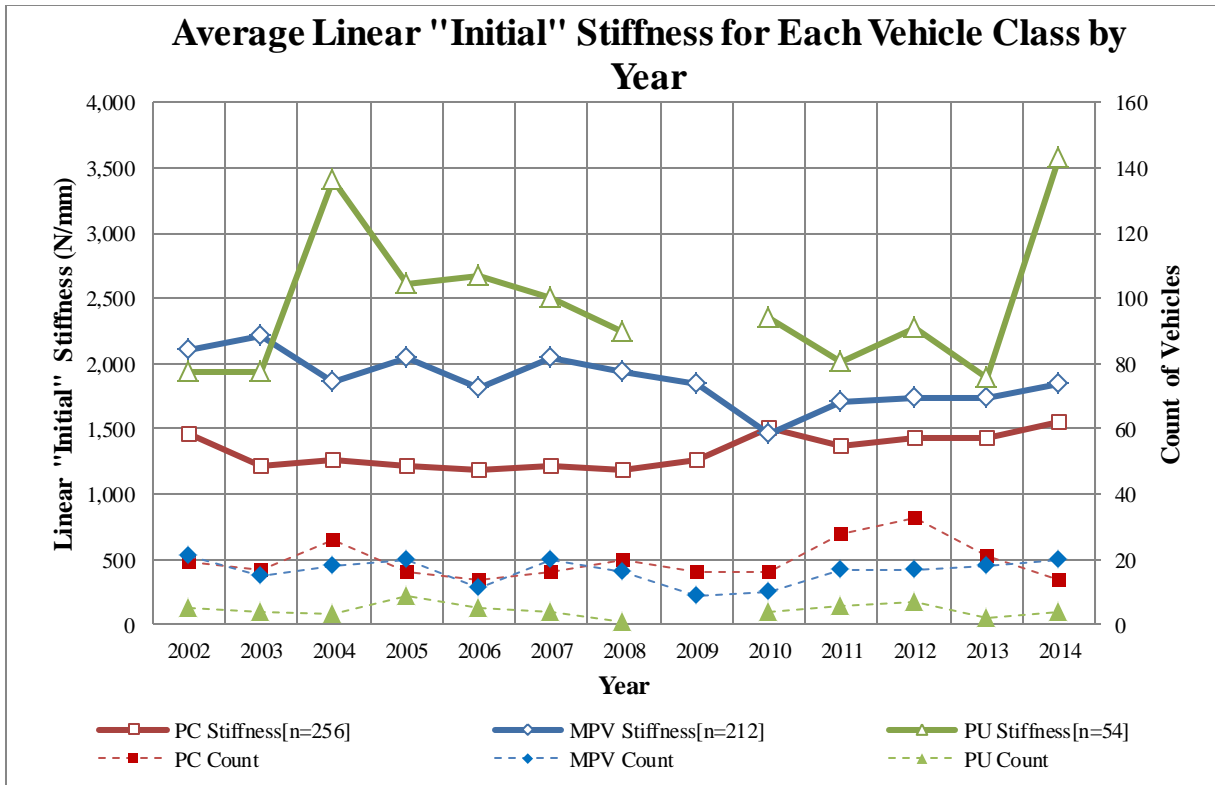


Figure 1: Average linear "initial" stiffness values computed for MY 2002-2014 NCAP test vehicles.

Energy-Equivalent Stiffness: Kw400

Like the linear "initial" stiffness method, this second method, energy-equivalent stiffness, is also designed to characterize a vehicle's stiffness based on its force-deflection profile. However, where the linear stiffness method approximates initial stiffness based on the slope of a line fit to the force-deflection curve over a given displacement range, this second method is based on the crash energy (or area under the force-deflection curve) over a given range.

One metric that can be used to approximate energy-equivalent stiffness is Kw400. Kw400 is derived from equating the energy stored in an ideal spring ($\frac{1}{2} Kx^2$) to the work of crushing the front end of a vehicle ($\int Fdx$). Contrary to the linear "initial" stiffness method, in which the displacement range is variable, the displacement range for the energy-equivalent stiffness method, as defined by Kw400, is fixed. To calculate energy-equivalent stiffness, the integral of the area under the force-deflection curve is evaluated between 25 and 400 mm of vehicle frontal crush. The equation for Kw400 is shown below. [Patel, 2007]

$$Kw400 = \frac{2 \int_{25mm}^{400mm} Fdx}{(400^2 - 25^2)}$$

This equation was used to calculate energy-equivalent stiffness for the same 522 qualifying tests discussed in the linear "initial" stiffness section.

The average energy-equivalent stiffness was 1,362 N/mm for all vehicles tested from MY 2002 to MY 2014. By class, the average energy-equivalent stiffness was 1,720 N/mm for PUs, 1,502 N/mm for MPVs and 1,171 N/mm for PCs during this time period. More specifically, Figure 2 shows that PCs had an average energy-equivalent stiffness

of 1,106 N/mm during the first four years, and 1,245 N/mm for the last four years – a 12.6 percent increase that was statistically significant at the 95% confidence level. Conversely, the average energy-equivalent stiffness for MPVs was 1,561 N/mm for the first four years, and decreased 7.8 percent to 1,439 N/mm for the last four years. Again, this difference was found to be statistically significant at the 95% confident level. The difference in energy-equivalent stiffness between MPVs and PCs was 34.2 percent for the first four years of the data set. This difference dropped to 14.5 percent for during the last four years. Directionally, the results are consistent with those found for linear “initial” stiffness; however, the energy-equivalent stiffness metric identified a smaller difference in stiffness between PCs and MPVs than the linear “initial” stiffness metric. No statistically significant changes were identified for the PU fleet. Similar to that mentioned for linear “initial” stiffness, the average energy-equivalent stiffness for PUs is higher than that for PCs and MPVs as shown in Figure 2.

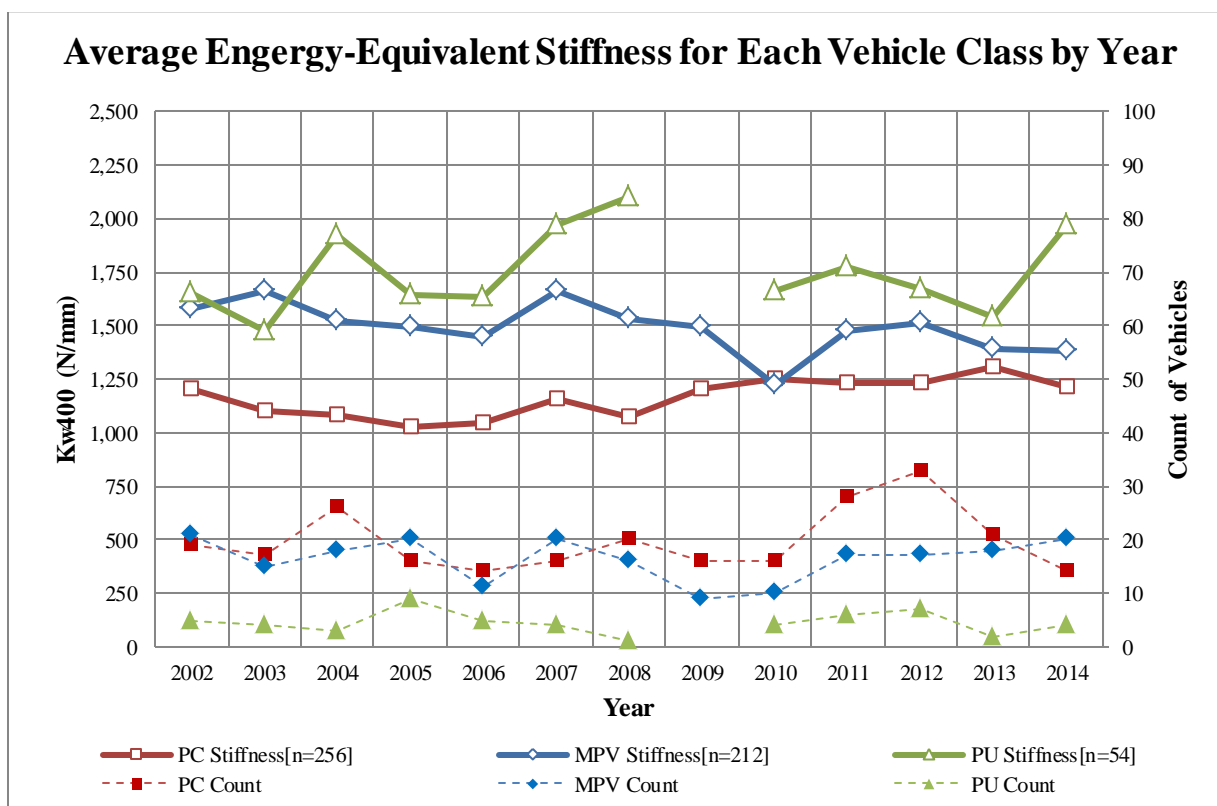


Figure 2: Average energy-equivalent stiffness values computed for MY 2002-2014 NCAP test vehicles.

Dynamic Stiffness

For the third method, dynamic stiffness, a vehicle’s stiffness, K , is computed using the equation $K = mv^2/x^2$, where m is the test weight of the vehicle, v is the closing speed of the vehicle, and x is the maximum dynamic displacement. This equation was derived using the approximation of the conservation of total energy, $E = \frac{1}{2} mv^2 = \frac{1}{2} Kx^2$. As mentioned previously, the maximum dynamic displacement (or crush) for a vehicle is found by taking the maximum of the double integral of the vehicle acceleration in the front occupant compartment. Dynamic displacement accounts for the elastic behavior often found in the vehicle front-end structure. [Swanson, 2003]

There were 611 passenger vehicles subjected to frontal NCAP testing from MY 2002 through MY 2014; however, 10 of the tests were ultimately eliminated because of errors in accelerometer data, resulting in a final data set of 601 for dynamic stiffness, static stiffness and vehicle acceleration data. The average dynamic stiffness from MY 2002 to MY 2014 for all vehicles was 1,101 N/mm. By class, the average dynamic stiffness for the model years studied was 1,409 N/mm for PUs, 1,191 N/mm for MPVs, and 959 N/mm for PCs. During the first four years, the average dynamic stiffness for PCs was 916 N/mm. For the last four years, the average dynamic stiffness for PCs was 980 N/mm – an increase of 7.0 percent over the earlier interval. This increase was statistically significant at the 95% confidence interval. When examining the same intervals, dynamic stiffness values decreased for MPVs. In the first

four years, the average dynamic stiffness for MPVs was 1,221 N/mm. This value decreased 6.7 percent to an average of 1,138 N/mm for the last four years. These results were also found to be statistically significant at the same level of confidence. The dynamic stiffness decrease for MPVs, again, likely corresponds to the trend of constructing MPVs on more car-like, unibody structures and not on pickup truck-based, body-on-frame structures. The difference in average dynamic stiffness between MPVs and PCs was 28.5 percent during the first four years. This difference dropped to 15.0 percent in the last four years. This converging trend is directionally consistent with the other stiffness metrics already discussed and very similar to the 14.5 percent difference found when using the Kw400 (energy-equivalent) approach. Again, although no significant differences could be identified for the PU data set, dynamic stiffness is higher, on average, for PUs than for PCs and MPVs.

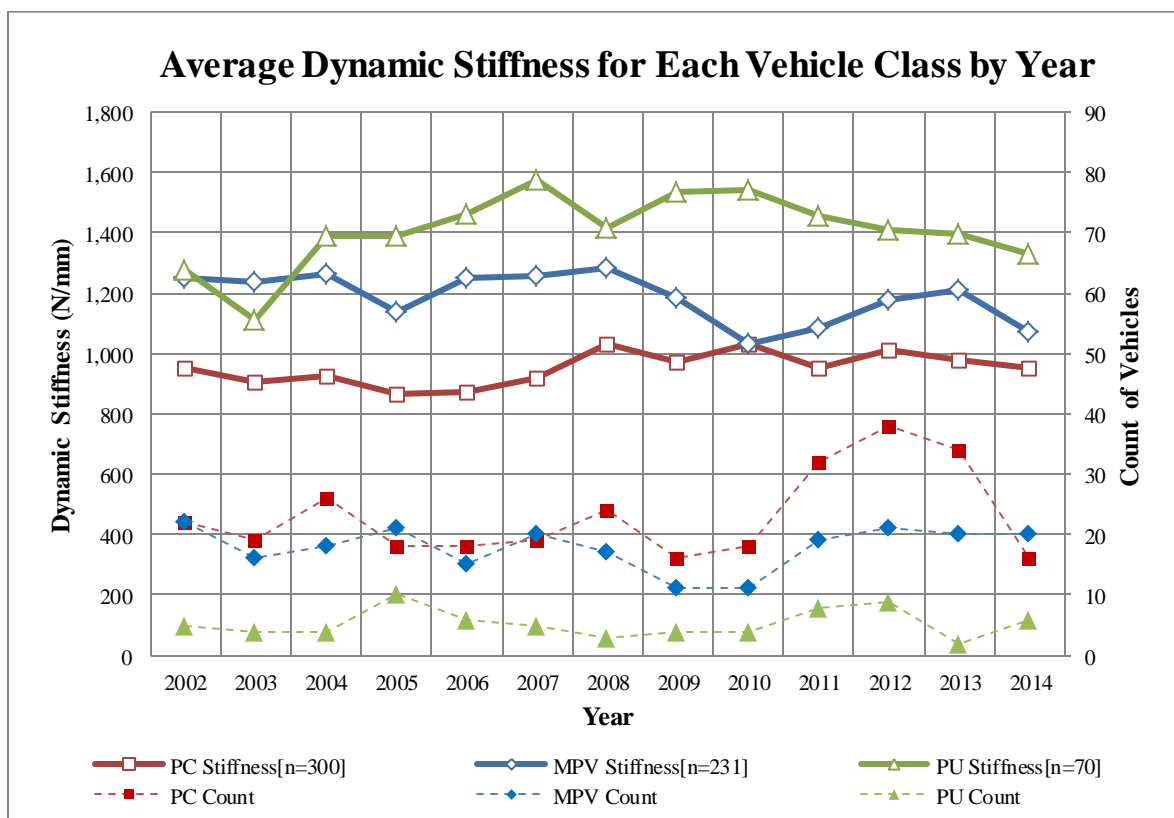


Figure 3: Average dynamic stiffness values computed for MY 2002-2014 NCAP test vehicles.

Static Stiffness

The fourth stiffness calculation method, static stiffness, is similar to dynamic stiffness in that it uses the same equation derived from the conservation of energy ($K = mv^2/x^2$); however, x instead reflects the maximum static crush measured for the vehicle post-test. Unlike dynamic stiffness, static stiffness does not account for the elastic deformation of the vehicle front-end. [Swanson, 2003]

Static stiffness was computed for the same 601-vehicle data set used to calculate dynamic stiffness. The average static stiffness for all vehicles from MY 2002 to MY 2014 was 2,035 N/mm. By class, the average stiffness was 2,149 N/mm for PUs, 2,160 N/mm for MPVs, and 1,913 N/mm for PCs over this time period. As shown in Figure 4, the static stiffness for PCs has generally been increasing since MY 2002. In the first four years, the average static stiffness for PCs was 1,691 N/mm, which increased 24.0 percent to 2,097 N/mm in the last four years. This was a statistically significant increase at the 95% confidence level. Conversely, in the first four years, the average static stiffness for MPVs was 2,183 N/mm, which decreased 3.6 percent in the last four years to 2,104 N/mm. This difference was not found to have statistical significance at the 95% confidence interval. The difference in static stiffness between MPVs and PCs was 25.4 percent during the first four years; this difference dropped to 0.3 percent in the last four model years. In general, it also yielded the highest average values among the methods. As with the

other stiffness metrics discussed, there currently appears to be more homogeneity in stiffness between PCs and MPVs compared to earlier model years. As with the other stiffness metrics, no statistically significant changes could be identified for PUs. However, it should be noted that the magnitude of static stiffness values for PUs appears to be more comparable to those for MPVs and PCs when compared to results seen for the other three stiffness metrics.

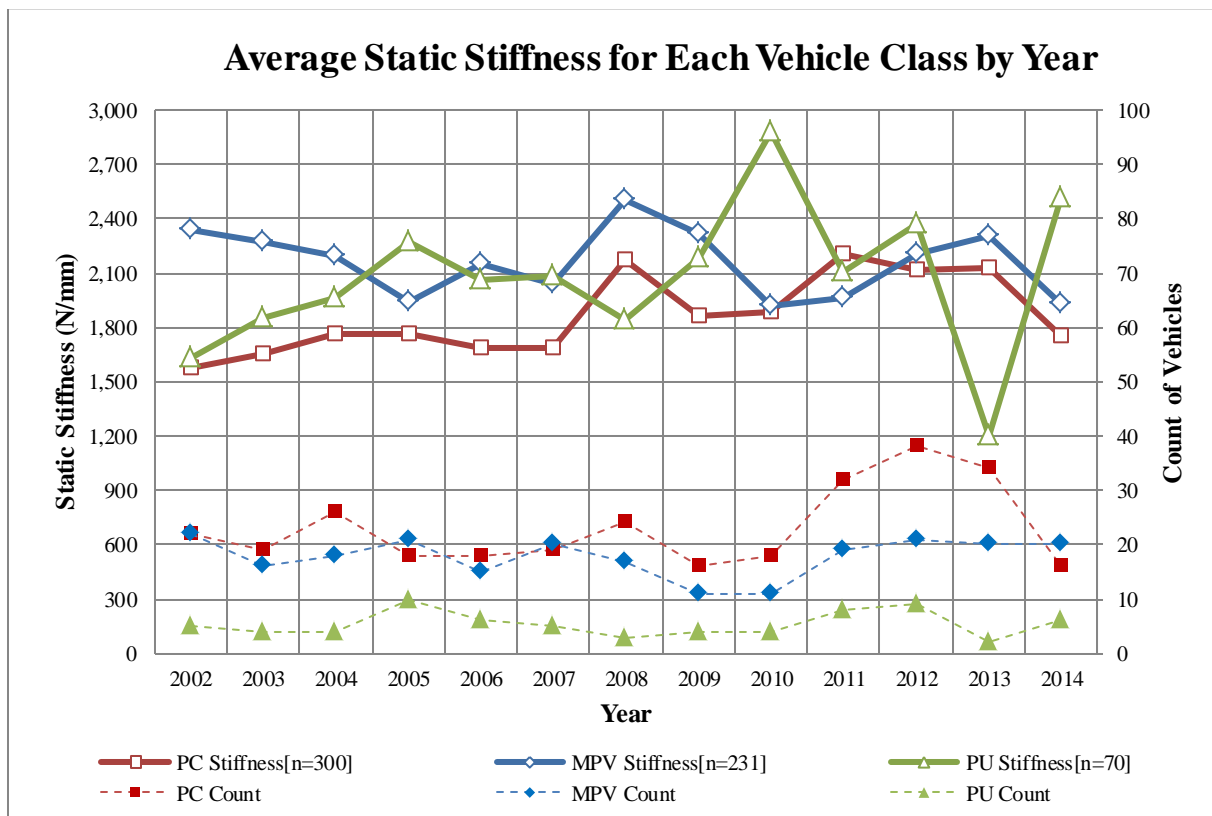


Figure 4: Average static stiffness values computed for MY 2002-2014 NCAP test vehicles.

Overall, the four methods of computing vehicle stiffness showed similar trends. They each showed a slight increasing trend in average stiffness for PCs, and a concurrent responding decreasing trend in average stiffness for MPVs, with both classes becoming more homogenous with respect to their front-end stiffnesses. When comparing the first four years to the last four, average percent increases in stiffnesses for PCs when compared to average percent decreases in stiffnesses for MPVs varied depending on the metric used. This is illustrated in Table 1. Table 2 shows, by stiffness metric, the percent difference between the average stiffnesses of PCs and MPVs when comparing the first four years to the last four. All of the metrics showed a decrease in the difference between PC average stiffnesses and MPV average stiffnesses, again supporting the notion that the two are converging. The metric that showed the least difference when comparing MPVs versus PCs for the first four years with the last four was static stiffness.

Table 1. Differences in average stiffnesses for PCs and MPVs between the first and last four years.

	PCs	MPVs
Linear “Initial” Stiffness	10.7%	-14.4%
Energy-Equivalent Stiffness	12.6%	-7.8%
Dynamic Stiffness	7.0%	-6.7%
Static Stiffness	24.0%	-3.6%

Table 2.
Differences in average stiffnesses, MPVs versus PCs, for the first and last four years.

	MY 2002-2005	MY 2011-2014
Linear “Initial” Stiffness	45.5%	20.6%
Energy-Equivalent Stiffness	34.2%	14.5%
Dynamic Stiffness	28.5%	15.0%
Static Stiffness	25.4%	0.3%

Differences between static stiffness trends and the other three stiffness metrics may largely be due to the fact that the static stiffness metric relies upon post-test vehicle crush measurements for displacement rather than dynamic (accelerometer-based) measurements, which are used for the other three metrics. Unlike dynamic deformation, static post-test crush measurements cannot account for the elastic deformation that occurred during the crash. Instead, static measurements represent only the inelastic residual crush. As such, static crush measurements are inherently smaller than calculated values for dynamic displacement, and this translates into higher stiffness values for static stiffness compared to the other three metrics evaluated.

To better understand the role elastic vehicle components play in stiffness results for the metrics studied, it was of interest to compare static and dynamic stiffness results directly since the same equation is used to calculate both; the only difference between the two calculations is the source of displacement - either post-test vehicle measurements (for static stiffness) or vehicle accelerometer readings (for dynamic stiffness).

Figure 5 depicts the average calculated static stiffness and dynamic stiffness for PCs tested by NCAP since MY 1982. For this comparison, data from Swanson (MY 1982-2001) was added to that used for the current study (MY 2002-2014). The static and dynamic stiffness data was subdivided into two-year intervals and then averaged for each interval. This figure shows that there was a gradual upward trend in static and dynamic stiffness from MY 1982 to MY 2014. It is also of interest that the values for both seemed to stabilize just prior to the last four years in this study. It can also be seen that the difference between average dynamic and static stiffness values has grown larger over the years. This indicates an increase in elasticity of the front-end vehicle structure. Therefore, results using linear “initial” stiffness, energy-equivalent stiffness, and dynamic stiffness – the three methods that use dynamic displacement in their calculations – may more realistically approximate the stiffness of the current fleet, since dynamic deformation accounts for the elastic and energy-absorbing front-end components.

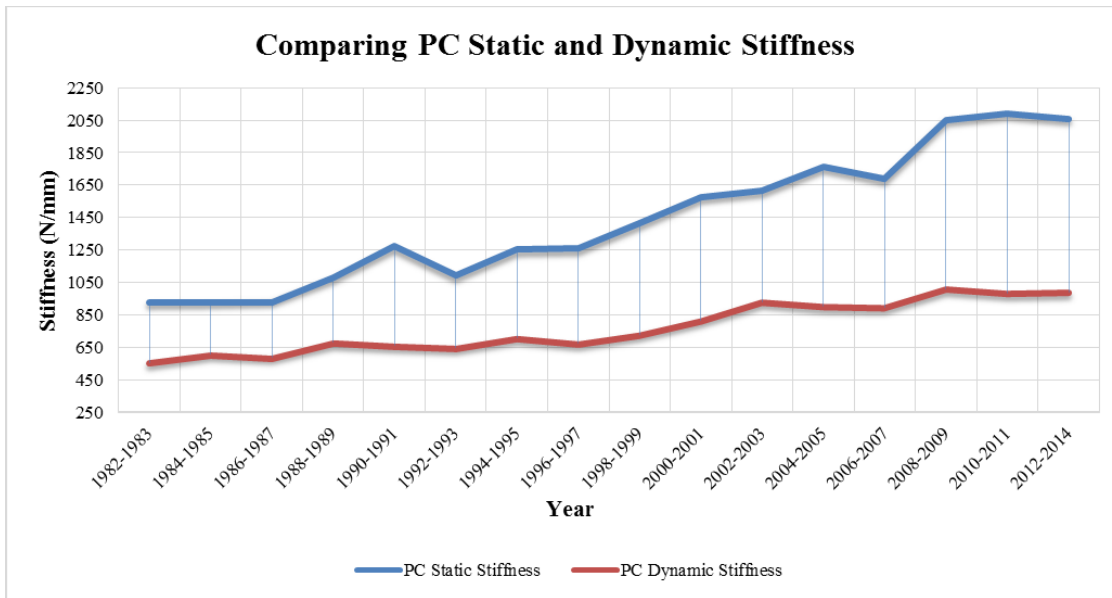


Figure 5. Comparing static and dynamic stiffnesses for NCAP-tested vehicles.

Considering the previous discussion, it is not surprising that a correlation was found between energy-equivalent and dynamic stiffness, which is shown in Figure 6. This is also demonstrated by a similar percent decrease in stiffness observed using the energy-equivalent and dynamic stiffness metrics. These metrics showed stiffness decreases of 14.5 percent and 15.0 percent, respectively, for the last four model year interval when compared to the first four model year interval. As both metrics rely on test instrumentation, and in particular, vehicle acceleration data, to calculate stiffness, both metrics may be more reliable than methods that do not take these into account. Although linear “initial” stiffness also relies on vehicle acceleration data to compute stiffness, a similar correlation to energy-equivalent stiffness and/or dynamic stiffness was not observed for this metric. This may be because of the potential error introduced by fitting a straight line to the force-deflection curve. Fitting a line slightly earlier or later in time along the curve, or over a longer stretch of time, could significantly influence the slope of the line, and therefore, the approximated stiffness.

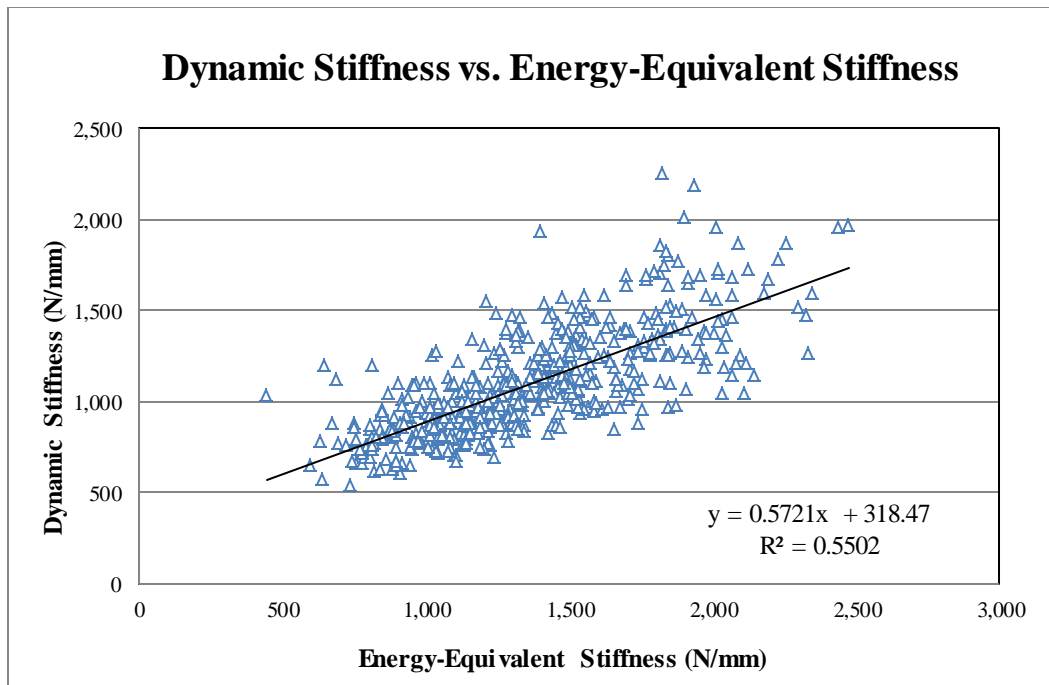


Figure 6. Comparing energy-equivalent stiffness and dynamic stiffness for NCAP-tested vehicles.

As an additional check, the force-deflection profiles used for the linear “initial” stiffness and energy-equivalent stiffness metrics were studied. Similar to that done for the comparison of static and dynamic stiffness, the force-deflection data was subdivided into three-year intervals and then averaged for each interval. The slope of each of the averaged force-deflection profiles was then examined for the first ~200 mm of deflection as an indicator of vehicle stiffness (i.e., the sharper the rise of the curve, the stiffer the vehicle front-end). Figure 7 illustrates the concept previously discussed, that the linear stiffnesses of PCs and MPVs are converging. This is shown by the similar amount of force required to crush each of these vehicle types 200 mm in the later model years. Furthermore, the stiffness of PUs, on average, is higher than that of both PCs and MPVs.

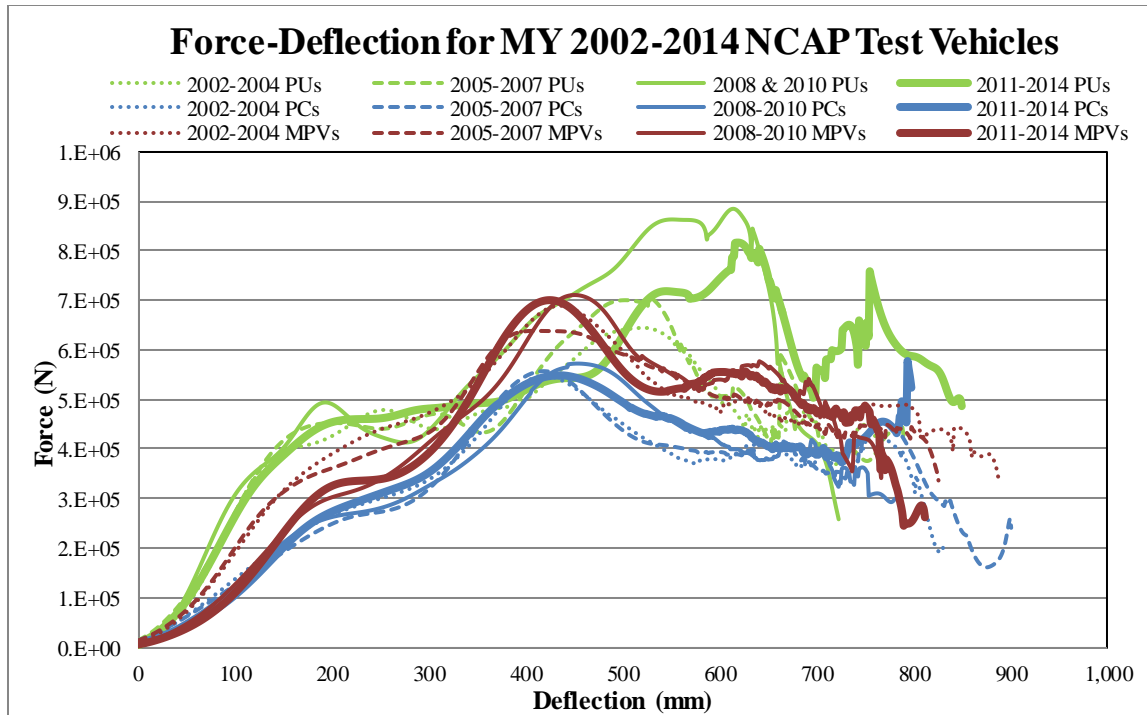


Figure 7. Force-Deflection Plot for MY2002-2014 NCAP Test Vehicles.

Changes to the fleet in response to things such as new regulatory requirements, revisions to consumer information programs, and shifting consumer preferences do not occur all at once and are generally phased in over time. This is evidenced by the steady increase in offerings of unibody-based MPVs compared to the prior (Swanson) study. However, the analysis of vehicle stiffness appears to support the notion that just prior to the last four years of this data set, a change affecting the front-end design of PCs and MPVs may have occurred in the fleet. To expand upon this finding, and build upon the Caitlin study, an additional analysis that focused on crash pulse characteristics was conducted. Specifically, peak acceleration and crash pulse duration for the vehicles tested during the model years under study were examined. With this analysis, there was a desire to see how vehicles designed to the latest regulatory and consumer information programs are managing crash forces. It was of particular interest to note any change in the amount of force translated to the occupant compartment over the years studied. It was also hoped that the trends observed for the stiffness metrics would correspond, in time, to any observations made for the crash pulse characteristics. To be consistent with the stiffness analysis, the same model year intervals were used for this analysis.

Peak Acceleration

The first crash pulse characteristic reviewed was the peak x-axis acceleration, measured in G's. Once again, this measurement is recorded by accelerometers that are mounted onto the vehicle structure near the driver or front passenger's seating location. Peak acceleration is typically indicative of the crash severity and correlates, in combination with the occupant's mass, to the amount of force the restraint system would need to manage during the crash. Effectively, this metric reflects how much of the crash forces are translated to the occupant compartment during the crash.

The average peak acceleration for all vehicles tested during the model years under study was 43G. By vehicle class, the average peak acceleration was 41G for PUs, 44G for MPVs, and 43G for PCs over this same time period. Averages for each model year by vehicle type are shown in Figure 8. Of interest is the relatively narrow range of average peak acceleration values calculated for the model years under study. The peak acceleration range for PUs was 36G to 49G; for MPVs, the range was 39G to 51G, and for PCs, the range was 39G to 48G. For the first four years, the average peak acceleration for PCs was 41G, and for the last four years, it increased 10.0 percent to 45G. This was a statistically significant increase at the 95% confidence interval. The average peak acceleration for MPVs from these same intervals increased 16.3 percent from 40 G to 47 G. This was also a significant finding at the 95% confidence level. Furthermore, for both PCs and MPVs, average peak accelerations have increased in the most recent

years, even though, when comparing the first four years to the last four years, the average stiffnesses of PCs were increasing while the average stiffnesses of MPVs were decreasing. A statistically significant trend was not identified for PUs.

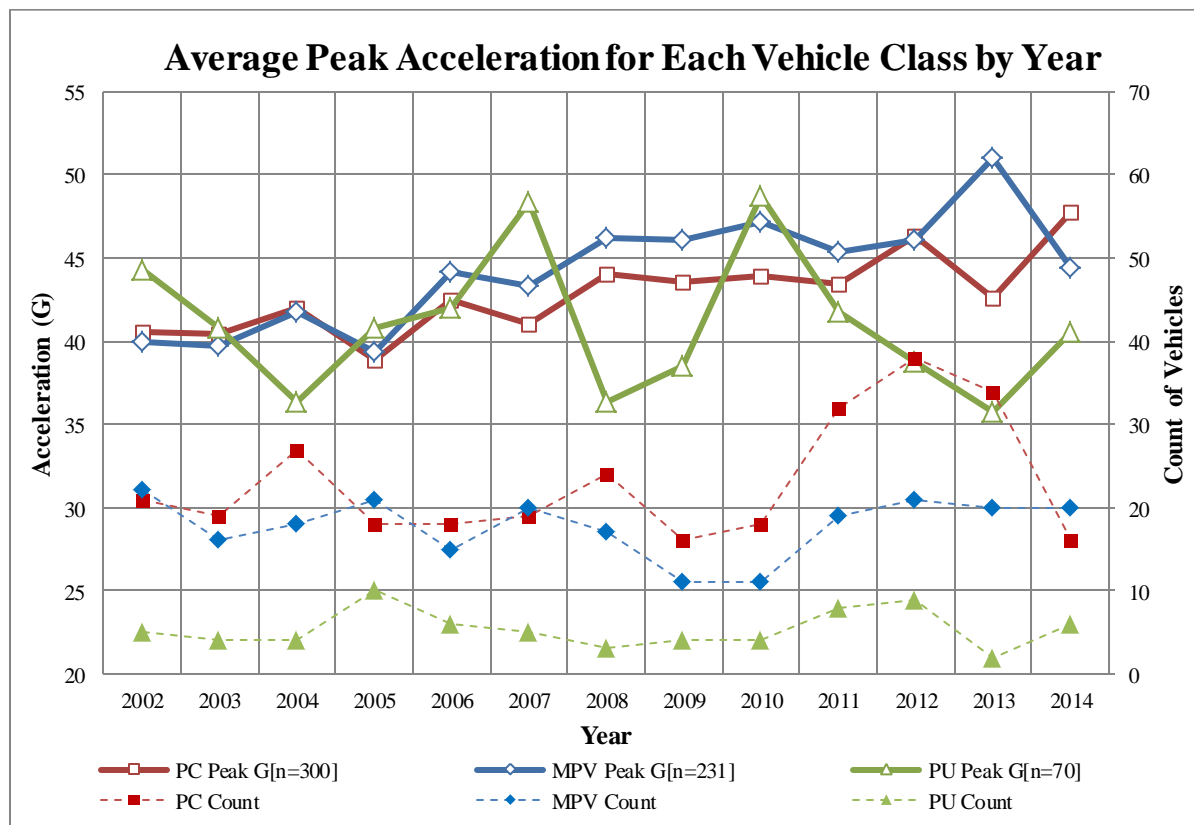


Figure 8. Average peak acceleration.

Time-to-Zero Velocity

The second pulse characteristic analyzed was the crash pulse duration, which is measured in milliseconds. This measurement is determined from single integration of the vehicle's x-axis acceleration and spans from the point of impact (t=0) until barrier separation, or when the vehicle velocity is equal to zero. Like peak acceleration, the crash pulse duration is also indicative of crash severity. If the duration of the crash event is shorter, the occupant and the restraint system may have to absorb the crash energy over a shorter period of time, which could make the event more severe.

For all MY 2002-2014 vehicles tested, the average time-to-zero velocity was 72 ms. By vehicle class, the time-to-zero velocity was 74 ms for PUs, 73 ms for MPVs, and 71 ms for PCs over this same time period. Figure 9 shows that there do not appear to be any significant trends overall; however, the results for PCs for the first four years show an average crash duration of 72 ms, which decreased by 3.8 percent to 70ms for the last four years. For MPVs, the average pulse duration for the first four years was 75 ms, and this decreased 5.7 percent to 71 ms during the last four years. For all practical purposes, on average the crash duration for both PCs and MPVs is now nearly the same.

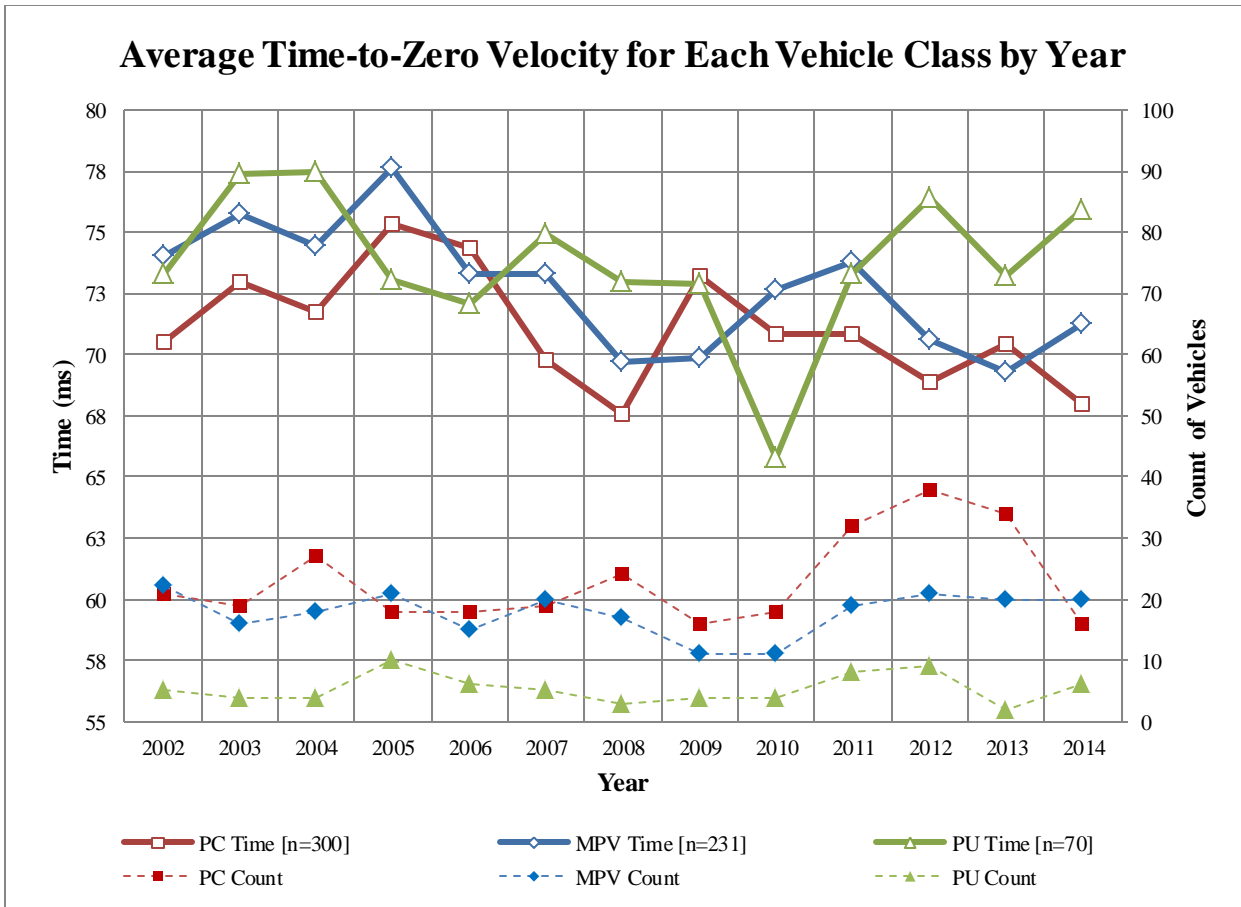


Figure 9. Average time-to-zero velocity.

The results for the pulse characteristics suggest that an increase in pulse severity (i.e., an increase in peak acceleration and/or a decrease in duration) does not necessarily equate to an increase in vehicle stiffness. This is evident from the stiffness trends previously discussed for MPVs during recent model years. Although average peak accelerations increased when comparing the last four years to the first four years, average MPV stiffness was shown to have decreased. The same phenomenon exists when looking at pulse durations: average MPV pulse durations decreased during the same time period in which a decrease in stiffness was observed. In sum, average traditional vehicle pulse characteristics may be in contrast to these front-end stiffness findings. This finding is also supported by Figure 10, which compares peak acceleration values to stiffness values computed using the energy-equivalent stiffness method. As shown, there is no correlation between peak acceleration and energy-equivalent stiffness. Comparisons of linear “initial,” dynamic, and static stiffness to peak acceleration showed similar results..

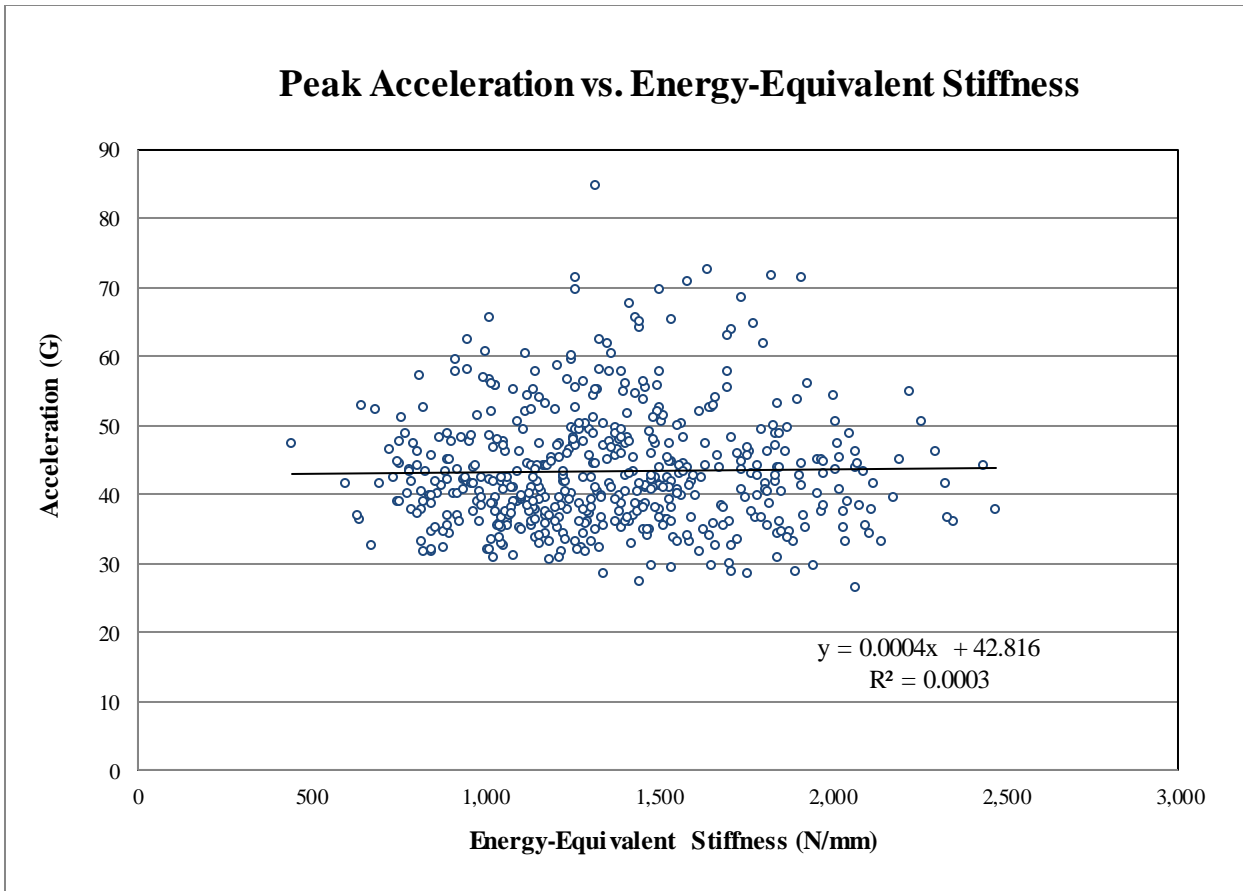


Figure 10. Comparing peak acceleration and energy-equivalent stiffness for NCAP-tested vehicles.

CONCLUSIONS

This study examined four methods of calculating front-end stiffness using vehicle crash data collected from NCAP tests conducted from MY 2002 through 2014. These methods included linear “initial” stiffness, energy-equivalent stiffness, dynamic stiffness, and static stiffness. This approach was similar to a study conducted by Swanson et al. that examined the MY 1982-2001 fleet. The Swanson study, which also used frontal NCAP data, found that not only were the average stiffnesses of PCs increasing over time, but there was also a large disparity between the average stiffnesses of PCs and that of MPVs and PUs. The results presented herein identified different trends. Generally, PCs continued to increase in average stiffness until stabilizing just prior to the last four years of this study, while MPVs decreased in average stiffness when considering the same time period. The average stiffnesses for PCs and MPVs appear to be converging, indicating that the fleet has become more homogenous with respect to these two vehicle classes. This is supported by the increase in MPV offerings utilizing unibody construction rather than traditional body-on-frame techniques. This study also examined the changes in crash pulse characteristics. While average peak accelerations generally increased for MPVs and PCs and pulse duration slightly decreased when comparing the first four years to the last four years of data, these findings do not appear to correlate to any of the stiffness metrics discussed. This analysis also further confirms the findings in Caitlin, which identified a slightly more severe, but homogeneous, crash pulse in the fleet.

REFERENCES

- [1] Swanson, J., Rockwell, T., Beuse, N., Summers, L., Summers, S., Park, B., "Evaluation of Stiffness Measures from the U.S. New Car Assessment Program", Enhanced Safety of Vehicles Conference, Paper Number 527, 2003
- [2] Caitlin M. Locey, BS, J. Felipe Garcia-Espana, PhD, Akira Toh, MS, Aditya Belwadi, PhD, Kristy B. Arbogast, PhD, and Matthew R. Maltese, PhD, Homogenization of Vehicle Fleet Frontal Crash Pulses from 2000–2010, Annals of Advances in Automotive Medicine/Annual Scientific Conference, 2012
- [3] O'Reilly, Peter, "Status Report of IHRA Compatibility and Frontal Impact Working Group," Enhanced Safety of Vehicles Conference, Paper Number 402, 2003
- [3] Summers, Stephen and Prasad, Alok, "NHTSA's Recent Compatibility Test Program," Enhanced Safety of Vehicles Conference, Paper Number 05-027, 2005
- [4] Summers, Stephen, Hollowell, W.T., and Prasad, A., "Design Considerations for a Compatibility Test Procedure," Society of Automotive Engineers Paper No. 02B-169, 2002
- [5] Patel, S., Smith, D., Prasad, A., and Mohan, P., "NHTSA's Recent Vehicle Crash Test Program on Compatibility in Front-to-Front Impacts," Enhanced Safety of Vehicles Conference, Paper Number 07-0231, 2007

Appendix

Linear "Initial" Stiffness (N/mm)														
Year	MPV				PC				PU				Avg of 3 Classes	Total Count
	Stiffness	Min	Max	Count	Stiffness	Min	Max	Count	Stiffness	Min	Max	Count		
2002	2,111	1,053	3,375	21	1,468	985	2,848	19	1,936	1,473	2,732	5	1,820	45
2003	2,207	894	3,578	15	1,221	769	1,702	17	1,929	1,613	2,505	4	1,711	36
2004	1,866	962	3,601	18	1,261	803	1,761	26	3,402	2,828	4,456	3	1,630	47
2005	2,049	1,045	4,289	20	1,210	759	1,700	16	2,613	1,929	3,809	9	1,863	45
2006	1,806	952	4,276	11	1,189	723	1,608	14	2,673	1,921	3,444	5	1,663	30
2007	2,050	819	3,951	20	1,208	440	1,667	16	2,504	2,374	2,811	4	1,759	40
2008	1,939	857	3,041	16	1,188	577	2,439	20	2,240	2,240	2,240	1	1,541	37
2009	1,843	1,258	2,857	9	1,261	655	1,955	16	-	-	-	-	1,471	25
2010	1,457	838	2,683	10	1,506	599	2,308	16	2,344	916	3,039	4	1,602	30
2011	1,713	866	3,387	17	1,366	489	2,059	28	2,016	1,684	2,486	6	1,558	51
2012	1,741	942	3,373	17	1,426	761	2,631	33	2,277	1,041	3,206	7	1,624	57
2013	1,733	731	3,044	18	1,437	723	2,286	21	1,892	1,572	2,212	2	1,589	41
2014	1,836	816	2,745	20	1,560	943	2,774	14	3,570	1,520	5,381	4	1,917	38
Avg/Total	1,895	731	4,289	212	1,336	440	2,848	256	2,448	916	5,381	54	1,678	522

Energy-Equivalent Stiffness (Kw400) (N/mm)														
Year	MPV				PC				PU				Avg of 3 Classes	Total Count
	Stiffness	Min	Max	Count	Stiffness	Min	Max	Count	Stiffness	Min	Max	Count		
2002	1,582	1,044	2,257	21	1,203	805	1,870	19	1,650	1,408	2,022	5	1,429	45
2003	1,667	752	2,441	15	1,104	639	1,635	17	1,474	1,395	1,619	4	1,380	36
2004	1,527	644	2,472	18	1,085	754	1,787	26	1,928	1,769	2,038	3	1,308	47
2005	1,491	1,008	2,181	20	1,024	747	1,376	16	1,645	1,336	1,913	9	1,356	45
2006	1,447	882	2,334	11	1,047	736	1,295	14	1,633	1,430	1,961	5	1,291	30
2007	1,660	859	2,331	20	1,158	756	1,566	16	1,973	1,901	2,051	4	1,490	40
2008	1,533	688	2,302	16	1,072	444	1,816	20	2,098	2,098	2,098	1	1,299	37
2009	1,492	1,101	1,851	9	1,204	597	1,909	16	0	0	0	0	1,307	25
2010	1,221	848	1,640	10	1,250	698	1,766	16	1,666	1,027	2,228	4	1,296	30
2011	1,478	760	2,084	17	1,231	727	2,072	28	1,771	1,413	1,917	6	1,377	51
2012	1,513	1,139	2,067	17	1,233	674	1,825	33	1,676	1,020	1,969	7	1,371	57
2013	1,396	917	1,712	18	1,305	895	1,753	21	1,542	1,539	1,544	2	1,356	41
2014	1,382	969	1,853	20	1,214	805	1,588	14	1,974	1,590	2,143	4	1,382	38
Avg/Total	1,502	644	2,472	212	1,171	444	2,072	256	1,720	1,020	2,228	54	1,362	522

Static Stiffness (N/mm)														
Year	MPV				PC				PU				Avg of 3 Classes	Total Count
	Stiffness	Min	Max	Count	Stiffness	Min	Max	Count	Stiffness	Min	Max	Count		
2002	2,341	1,104	7,762	22	1,578	1,051	2,758	22	1,635	1,312	2,065	5	1,926	49
2003	2,267	1,585	4,927	16	1,657	1,035	4,230	19	1,850	1,359	2,615	4	1,927	39
2004	2,194	1,477	3,602	18	1,762	926	3,597	26	1,967	1,827	2,111	4	1,941	48
2005	1,944	1,156	3,041	21	1,762	979	4,113	18	2,271	1,330	3,474	10	1,944	49
2006	2,152	1,226	3,910	15	1,688	899	2,746	18	2,060	1,721	2,306	6	1,924	39
2007	2,045	1,294	3,252	20	1,687	1,024	2,477	19	2,081	1,439	3,143	5	1,895	44
2008	2,509	1,511	5,434	17	2,178	1,093	5,883	24	1,844	1,507	2,035	3	2,283	44
2009	2,312	1,259	5,689	11	1,864	1,108	3,613	16	2,189	1,693	3,144	4	2,065	31
2010	1,923	1,224	3,977	11	1,887	1,258	3,039	18	2,881	1,224	4,638	4	2,020	33
2011	1,960	1,304	2,941	19	2,203	912	9,679	32	2,103	1,588	3,039	8	2,111	59
2012	2,209	1,244	3,797	21	2,120	1,015	4,612	38	2,373	1,180	4,692	9	2,181	68
2013	2,305	1,392	4,567	20	2,133	1,027	4,617	34	1,199	562	1,835	2	2,161	56
2014	1,931	1,015	4,765	20	1,754	1,257	2,620	16	2,515	1,506	4,453	6	1,947	42
Avg/Total	2,160	1,015	7,762	231	1,913	899	9,679	300	2,149	562	4,692	70	2,035	601

Dynamic Stiffness (N/mm)														
Year	MPV				PC				PU				Avg of 3 Classes	Total Count
	Stiffness	Min	Max	Count	Stiffness	Min	Max	Count	Stiffness	Min	Max	Count		
2002	1,253	798	1,867	22	953	731	1,407	22	1,277	1,027	1,704	5	1,121	49
2003	1,238	840	1,949	16	905	565	1,358	19	1,112	954	1,193	4	1,063	39
2004	1,263	799	1,965	18	926	624	1,380	26	1,391	1,224	1,672	4	1,091	48
2005	1,138	743	1,827	21	868	616	1,289	18	1,389	1,035	1,795	10	1,090	49
2006	1,250	755	1,746	15	871	537	1,304	18	1,460	1,016	1,715	6	1,107	39
2007	1,260	868	1,668	20	922	748	1,295	19	1,577	1,109	2,009	5	1,150	44
2008	1,282	832	1,851	17	1,033	672	1,706	24	1,418	1,250	1,568	3	1,156	44
2009	1,186	881	1,563	11	975	648	1,342	16	1,539	1,463	1,581	4	1,123	31
2010	1,031	812	1,576	11	1,034	732	1,479	18	1,541	889	1,933	4	1,094	33
2011	1,085	727	1,680	19	954	662	1,681	32	1,457	1,240	1,745	8	1,064	59
2012	1,180	870	1,638	21	1,012	605	2,250	38	1,409	915	2,184	9	1,117	68
2013	1,209	871	1,566	20	982	668	1,481	34	1,397	1,339	1,454	2	1,078	56
2014	1,075	858	1,397	20	951	650	1,219	16	1,333	939	1,771	6	1,065	42
Avg/Total	1,191	727	1,965	231	959	537	2,250	300	1,409	889	2,184	70	1,101	601

Peak Acceleration (G's)														
Year	MPV				PC				PU				Avg of 3 Classes	Total Count
	Accl.	Min	Max	Count	Accel.	Min	Max	Count	Accel.	Min	Max	Count		
2002	40	58	30	22	41	55	29	21	44	54	40	5	41	48
2003	40	49	29	16	40	60	30	19	41	55	32	4	40	39
2004	42	55	28	18	42	62	32	27	36	43	32	4	41	49
2005	39	54	29	21	39	55	31	18	41	50	27	10	39	49
2006	44	65	32	15	42	70	32	18	42	49	35	6	43	39
2007	43	58	32	20	41	61	32	19	48	54	35	5	43	44
2008	46	58	33	17	44	71	32	24	36	38	36	3	44	44
2009	46	61	36	11	44	62	34	16	39	45	34	4	44	31
2010	47	56	34	11	44	68	29	18	49	58	39	4	46	33
2011	45	71	33	19	43	66	31	32	42	52	33	8	44	59
2012	46	60	26	21	46	72	32	38	39	56	27	9	45	68
2013	51	85	30	20	43	67	30	34	36	38	34	2	45	56
2014	44	63	35	20	48	71	33	16	41	51	33	6	45	42
Avg/Total	44	85	26	231	43	72	29	300	41	58	27	70	43	601

Time to Zero Velocity (ms)														
Year	MPV				PC				PU				Avg of 3 Classes	Total Count
	Time	Min	Max	Count	Time	Min	Max	Count	Time	Min	Max	Count		
2002	74	63	98	22	70	58	84	21	73	69	79	5	72	48
2003	76	61	96	16	73	61	91	19	77	70	91	4	75	39
2004	74	62	91	18	72	61	91	27	78	70	85	4	73	49
2005	78	60	95	21	75	61	93	18	73	63	87	10	76	49
2006	73	64	97	15	74	60	93	18	72	62	82	6	74	39
2007	73	63	98	20	70	62	78	19	75	57	106	5	72	44
2008	70	59	80	17	68	46	84	24	73	68	78	3	69	44
2009	70	58	76	11	73	64	89	16	73	69	77	4	72	31
2010	73	60	84	11	71	60	82	18	66	56	79	4	71	33
2011	74	64	85	19	71	57	86	32	73	62	81	8	72	59
2012	71	61	96	21	69	42	85	38	76	57	98	9	70	68
2013	69	55	79	20	70	47	87	34	73	69	78	2	70	56
2014	71	60	79	20	68	61	78	16	76	62	92	6	71	42
Avg/Total	73	55	98	231	71	42	93	300	74	56	106	70	72	601

Preliminary Study of the Responses of Hybrid III 5th female, 50th male, Q6 and Hybrid III 5th pregnant female dummy seated in the 2nd row seats of passenger vehicles in sled tests

SIWOO KIM, JAEWAN LEE, JONGSOO KIM, GYUHYUN KIM
Korea Automobile Testing & Research Institute

KOREA

MYUNGWON SUH

School of mechanical Engineering, Sungkyunkwan Univ.,
KOREA

Paper Number 15-0282

ABSTRACT

The objective of this study was a preliminary study of the responses of dummies seated in the 2nd row seat of passenger vehicles in frontal crashes using a sled system. Q6, Hybrid III 5th female, Hybrid III 5th pregnant female, and Hybrid III 50th male ATD were used in the tests. 8-tests were carried out according to a draft protocol for the 2nd row seat evaluation program. The vehicle type was a sedan and SUV's. The cut-body or jig was used to simulate the ATD in the 2nd row seat/belts of a passenger vehicle. The frontal crash pulse in sled tests was an average acceleration of about 30 vehicle acceleration pulses tested according the KNCAP FFRB test. ATD seating positions were set using the H-point machine. Injury criteria were considered among the HIC₁₅, upper neck tension force, chest deflection. The HIC₁₅ ranged from 350 to 800 for both a Hybrid III 5th female and a pregnant female. The upper neck tension forces of a 5th female dummy and a 5th pregnant female dummy were also higher than that in FMVSS 208. The kinematics was influenced by the seat and seatbelt characteristics. The sled test results were compared with those of the same vehicle KNCAP FFRB test results. The possibility of fatal injury of Hybrid III 5th female and 50th male ATD in the rear seat could have much higher than in the front seat, especially case of the chest deflection. In addition, the further consideration should be given regarding Y- axis in the regulation at the seat belt anchorage point.

INTRODUCTION

The motor vehicle safety standard refers to a fundamental regulation that should be complied by all vehicles. It should be enacted to prevent traffic accidents and to reduce injuries among vehicle occupants and/or pedestrians at a traffic accident. The Korean government established the "Korea motor vehicle safety standard" in September 1987 under an ordinance of the Ministry of Transportation. For the safety standard regarding the occupant safety of a vehicle at a crash, parts of FMVSS 208 - Occupant Crash Protection, a U.S. motor vehicle safety standard, were introduced in 1993, and the safety standard for occupant safety was established for the FFRB (Full-width Frontal Rigid Barrier) test. Article 102 of the "Korea motor vehicle safety standard" specifies the standard for occupant safety in a head-on collision. The FFRB test is designed the injury criteria of a dummy, by using a Hybrid III 50th male ATD in the driver's seat and the front passenger seat of a vehicle during the impact speed at 48.3km/h.

Therefore, the KMOVSS (Korea Motor Vehicle Safety Standard) to protect a vehicle occupant at the FFRB test is applied to the driver's seat and front passenger seat only. The KMOVSS includes a standard for seat strength and seat belt anchorage strength for the protection of occupants seated on the second or other rows also. In other words, this can be interpreted in such a way that seats after the 2nd row does not have to meet the safety requirement during the FFRB test. We can see that the safety of the driver's seat and front passenger seat has been dramatically improved over the last ten years, largely as a result of the motor vehicle safety standard and the new car assessment system. KNCAP (Korea New Car Assessment System) introduced the FFRB test in 1999 and has used it ever since. The trend of a star rating shows that only three vehicles (18.8%) out of nineteen tested between 1999 and 2001 received

a five-star rating, whereas thirty-seven (97.4%) out of thirty-eight vehicles tested between 2011 and October 2014 received a five-star rating. As shown in Figure 1, a comparison of the 3-year-average AIS (Abbreviated Injury Scale) 4+ injury risk probability for head and chest injuries measured in a 56km/h FFRB test by the KNCAP. It shows that the probability of sustaining a AIS4+ injury risk probability of head injury was reduced from 12.2% to 4.7%, whereas the probability of a joint injury was reduced from 21.6% to 15.1%. This result shows that the probability of a joint injury has been reduced by 70%, compared with the initial stages.

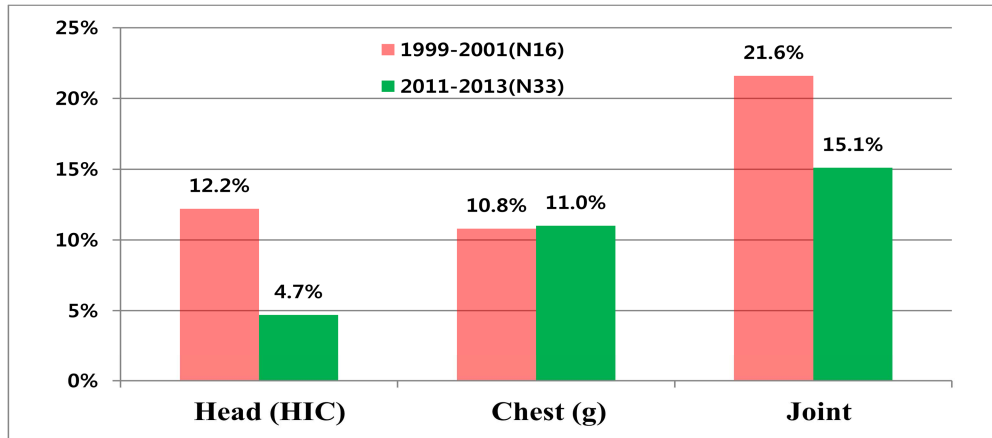


Figure 1. Average Injury risk possibility (AIS 4+) of ATD in KNCAP FFRB test

When we compared the effects of introducing the FFRB test in KNCAP, based on real accident analysis in Korea, vehicles with a higher star rating were found to be safer. Thus, the MAIS3+ (Maximum Abbreviated Injury Scale) occurrence rate of vehicles with a 4-star rating was found to be 34.2% lower than that of vehicles with from 1 to 3 stars in a frontal crash accident. As described above, the safety of the driver's seat and front passenger seat has been significantly improved owing to the considerable efforts made by car manufacturers, the government, and research institutes. Also, the rate of injury is now quite low. However, little attention has been paid to rear seats, because we can see that a motor vehicle safety standard for the rear seat passengers based on an FFRB test, offset test has not yet been established.

Evans (1987) analyzed that the rear seat lap belt reduces the likelihood of by 18±9 percent, whereas the 3-point seat belt has a 41±4 percent effect for the front passenger seat. Morgan (1999) found that the level of safety increased by 25%, compared with two-point seat belt, as the regulation for the rear seat had changed from the two-point seat belt to the three-point seat belt. Paranteau and Viano (2003) found that torso injuries generally occur due to the seat belt, according to data about frontal crash accidents suggesting that rear seat passengers wear the 3-point seat belt. They also found that abdominal injuries among rear seat occupants caused by the type 1 seat belt also occur when the type 2 seat belt is worn. Suzanne et al (2012) evaluated Hybrid III 5th female ATD and Hybrid III 10 years old on the rear seat. Even when the dummy wore a 3-point seat belt, the dummy in the rear seat was subjected to a more forward movement, compared with the occupant of the front seat. As movements become frequent, the measurement value has an important effect on the head, neck, chest, and lower spine. Sometimes, the head and neck injury value was likely to exceed the reference value. Chest displacement occurs more frequently when the seatbelt is well maintained from the center of the shoulder to the center of the torso.

When we reviewed the results of past studies, analysis was performed on the excellence of the 3-point safety belt, the abdominal injury when the 3-point safety belt is used, and the injury of the 5th female ATD. However, the possibility of injury did not much analyzed by comparing the front and rear seat occupant. The occupation rate of the rear seat in Korea is 21.1%, which is somewhat smaller than the front passenger seat (39.6%). However, we

cannot disregard the vehicle safety of the rear seat due to a low rear seat occupation rate, in order to reduce traffic casualties. Therefore, this study ran a frontal sled test by using a Hybrid III 50th male ATD, Hybrid III 5th female ATD, Hybrid III 5th pregnant female ATD, and a child Q6 on the rear seat, in order to stimulate greater interest in the safety of the rear seat occupant, which generally attracts little attention, and to compare the possibility of injury with the occupant of the front seat, which will require further studies.

TEST METHOD

DUMMY

The sled comparison test was performed by using a Hybrid III 50th male ATD, Hybrid III 5th female ATD, Hybrid III 5th female ATD pregnant, and child Q6 in the booster seat on the rear seat of a sedan and SUV type vehicles. The Hybrid III 5th female ATD and Q6 were seated in the rear seat for the test, while the Hybrid III 5th female ATD pregnant and Hybrid III 50th male ATD were seated in the same vehicle rear seat for another test (See Figure 2).



Figure 2. Test set up of Hybrid III 5th & Q6, MAMA & Hybrid III 50th male ATD

The new rear seat and safety belt were installed with each test. The rear seat cushion, seat backs, and safety belt D-ring points were set on the design point. The dummy was seated by checking the H-point machine. In particular, the seating reference point of the Hybrid III 5th female ATD was different from the H-point machine. Hybrid III 5th female ATD was lowered by 6mm below the H-point machine, and the H-point was reset by reducing the seat length rate by the same degree as the forward direction of the car. The Hybrid III 5th pregnant female ATD was seated in the same way as the Hybrid III 5th female ATD. The Hybrid III 50th male ATD was seated with the same seating method as the dummy used for the FFRB test in the motor vehicle safety standard. As there was no steering handle, the upper arm was placed on the seat back and the ring finger was placed on the outer thigh and seat cushion. The Q6 was seated in the booster seat, according to the child safety test method that is being prepared by KNCAP. The frontal sled test speed was 56km/h, and the average acceleration speed pulse was used, regarding the upper and lower limit of the KNCAP FFRB test acceleration speed conducted in 2013 (See Figure 3).

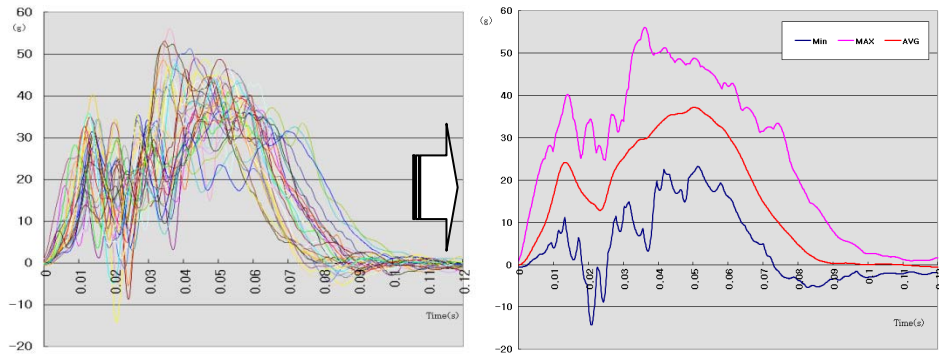


Figure 3. FFRB test acceleration and mean acceleration

TEST EQUIPMENT

The test data was recorded in 10 kHz and filtered according to SAE J211. The scene was recorded from the left and right sides and the upper front, using a 1,000 frame high-speed digital camera. The parts needed for the rear seat test was cut from the actual car (sedan) and made in a jig form. For the SUV car, the second row seat and safety belt part were made in a jig form for the test. The baseline ATD instrumentation included a tri-axial accelerometer at the head CG; a 6-axis load cell at the upper and lower neck; tri-axial accelerometers at the chest and chest potentiometer at chest the Hybrid III 50th male, Hybrid III 5th female, and Hybrid III 5th pregnant female ATD. The same equipment was installed on the Q6 dummy, except that the IR-TRACCs were installed on the lower and upper sternum.

TEST RESULTS

Total 4 vehicles were conducted using the sled system in KATRI (Korea Automobile Testing & Research Institute). The responses of the Hybrid III 50th male, Hybrid III 5th female, and Hybrid III 5th pregnant female ATD seated on the rear seat were compared. The HIC₁₅ of the Hybrid III 50th male ATD were 333, 356, 446 and 498. The HIC₁₅ of the Hybrid III 5th female ATD were 354, 705, 723 and 745. The HIC₁₅ of the Hybrid III 5th female pregnant ATD were 580, 698, 787 and 794. The HIC₁₅ of female ATD had higher than the male ATD, and either came close to or exceeded HIC₁₅ 700, which is the injury reference value in FFRB test in the regulation.

The upper neck tension force of the Hybrid III 5th pregnant female ATD were 2.42kN, 2.79 kN, 2.19kN and 1.93kN which is similar to the Hybrid III 5th female ATD (2.62kN, 2.12kN, 2.14kN, 1.52kN). The value for the Hybrid III 50th male ATD were 2.76kN, 2.31kN, 2.27kN and 1.75kN.

The chest displacement of the Hybrid III 5th female ATD were 42.76mm, 42.14mm, 40.3mm and 40.6mm respectively, while those of Hybrid III 50th male ATD were 43.76mm, 49.52mm, 44.8mm and 40.9mm. The chest acceleration 3msec clips of the Hybrid III 5th female ATD were 44.92g, 63g, 63.67g and 52.82g. The chest acceleration 3msec clips of the Hybrid III 5th pregnant female ATD were 41.1g, 51.14g, 58.5g and 61.5g. The female ATD chest acceleration 3msec clip of two vehicles was found to exceed the limits referenced in compliance. The chest acceleration 3msec clip observed for the Hybrid III 50th male ATD were 54.28g, 52.11g, 54.3g and 43.4g. The chest displacement of the Hybrid III 5th female ATD were 47.26mm, 42.14mm, 40.3mm and 40.6mm. The chest displacement of the Hybrid III 50th male ATD were 43.76mm, 49.52mm, 44.8mm and 40.9mm. When comparing the injury criteria between male and female ATD, the male ATD showed a higher value, with the exception of the HIC₁₅. The HIC₁₅ of the child Q5 seated on the booster seat were 502 and 491, and those for upper neck tension force were 2.23kN and 2.17kN, which exceeded the AIS3+20% reference value suggested by the EEVC.

COMPARISON WITH THE RESPONSES OBTAINED FOR THE FRONT SWAR OF SAME VEHICLE FFRB TEST

The results of the FFRB test conducted by the KNCAP were compared with the ATD responses seated on the rear seat, by positioning a Hybrid III 50th male ATD on the driver's seat and a Hybrid III 5th female ATD on the front passenger seat. Figure 4 (left) compares the HIC₁₅ and upper neck tension force, which were both found to be lower than the ATD responses recorded for the rear seat, due to the influence of the load limiter in the airbag and the seat belt. Figure 4 (right) shows the comparison between the head acceleration 3m sec clip and the upper neck tension force. Head acceleration is similar to the front seat, but the upper neck tension force in the rear seat is higher than the front seat.

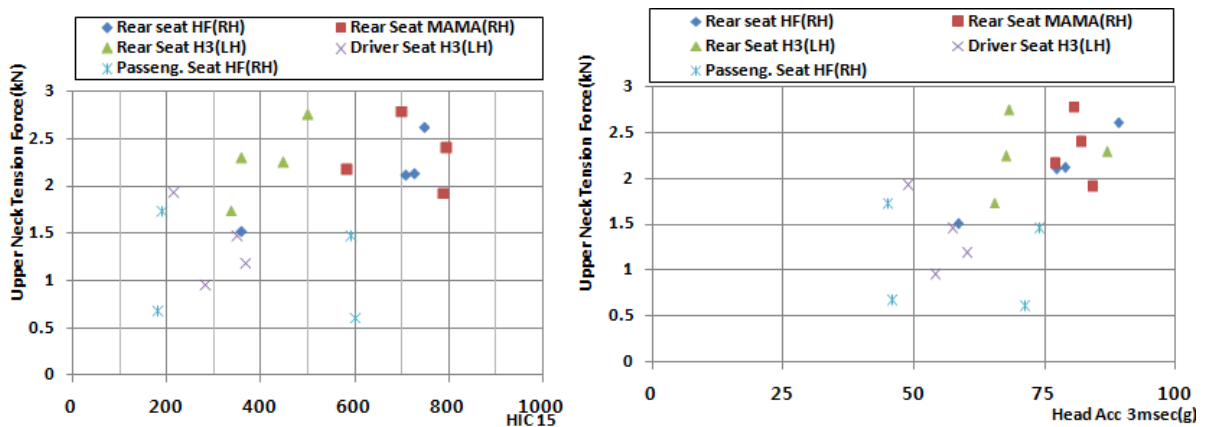


Figure 4. Peak upper neck tension force and HIC₁₅ (left) / Peak upper neck tension force and peak resultant head acceleration of 3msec(right)

Figure 5 shows the chest deflection of the comparison between shoulder belt load and lap belt load, respectively. The shoulder belt load of the front seat was under 4kN, whereas the lap belt load was distributed between 4.99kN and 11.25kN. The Hybrid III 50th male ATD has a greater lap belt load than the Hybrid III 5th female ATD on the front seat, because the former weighs more. However, the shoulder belt load was similar. It was found that the Hybrid III 50th male ATD received a greater lap belt load and shoulder belt load in the rear seat. When compared with the front seat, the shoulder belt load was applied to the torso more than three times in the rear seat, and chest deflection compared with the front seat was increased.

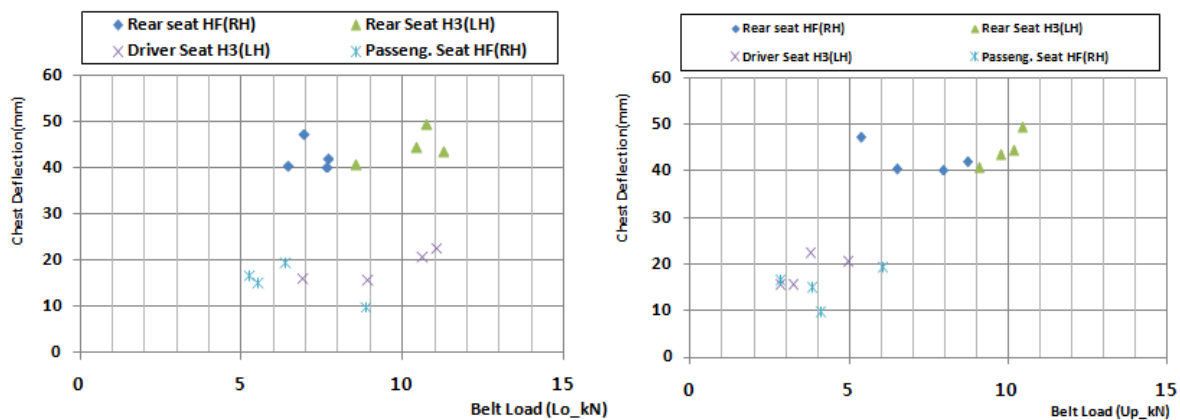


Figure 5. Peak chest deflection and peak lap belt load (left) / Peak chest deflection and peak shoulder belt load (right)

COMPARISON WITH THE FFRB TEST IN KNCAP

To compare our results with those of the KNCAP, 52 FFRB test results were reviewed among the test results of KNCAP from 2011 to 2014. The Hybrid III 50th male ATD was seated in the driver's seat and the front passenger seat in 2011 and 2012. The Hybrid III 50th male ATD was seated in the driver's seat but the Hybrid III 5th female ATD was seated in the front passenger seat for the evaluations conducted in 2013 and 2014. As a result, the rear seat and front passenger seat were compared for the Hybrid III 5th female ATD, and the test results of the driver's seat, front passenger seat, and rear seat were compared for the Hybrid III 50th male ATD.

The average HIC₁₅ of the Hybrid III 5th female ATD response of the front passenger seat was 452.72, while the average upper neck tension force was 0.911kN. On the other hand, the average of HIC₁₅ and upper neck tension force responses recorded for the rear seat were 631.75 and 2.1kN, respectively. The HIC₁₅ of the Hybrid III 5th female ATD in the rear seat was about 140% greater than that of the front seat, whereas the upper neck tension force was about 230% greater. On the contrary, the average HIC₁₅ among driver, front passenger and rear seat occupant did not show a big difference (i.e. driver's seat: 353.29; front passenger seat: 409.65; rear seat: 427). The average upper neck tension force of ATDs for the driver's seat, front passenger seat and rear seat was 1.42kN, 1.3kN, and 2.27kN, respectively. These results indicate that the female ATD in the rear seat could have sustained more injuries than the male ATD in the front and rear seats (See Figures 6).

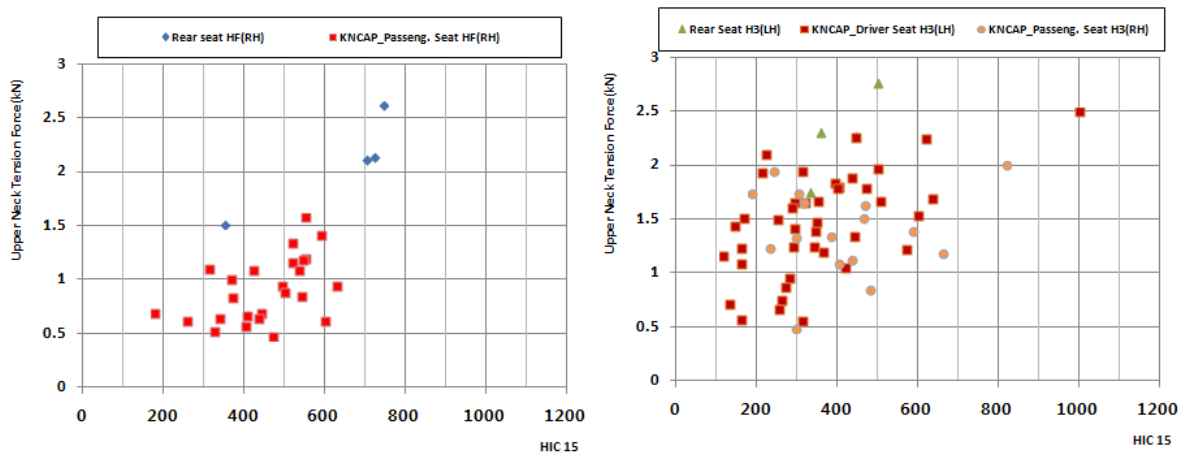


Figure 6. Peak upper neck tension force and HIC₁₅ of 5th female ATD(left) / Peak upper neck tension force and HIC₁₅ of 50th male ATD(right)

The chest deflection of both the driver's seat and the front passenger seat was under 30mm in the Hybrid III 50th male ATD and the Hybrid III 5th female ATD. However, that of the rear seat was 40 - 49mm. The chest deflection of the Hybrid III 5th female ATD was about 270% more compressed than the front seat average (See Figures 7). Furthermore, it was found that chest deflection in the driver's seat and front passenger seat is not as great as in the rear seat, even though the lap belt load and shoulder belt load increase, regardless of the type of ATD. Figure 8 (right) shows the comparison between shoulder belt load and chest deflection in KNCAP and rear seat frontal sled test. The ATDs of FFRB test in KNCAP is controlled by chest deflection of about 30mm and a shoulder belt load of about 7kN.

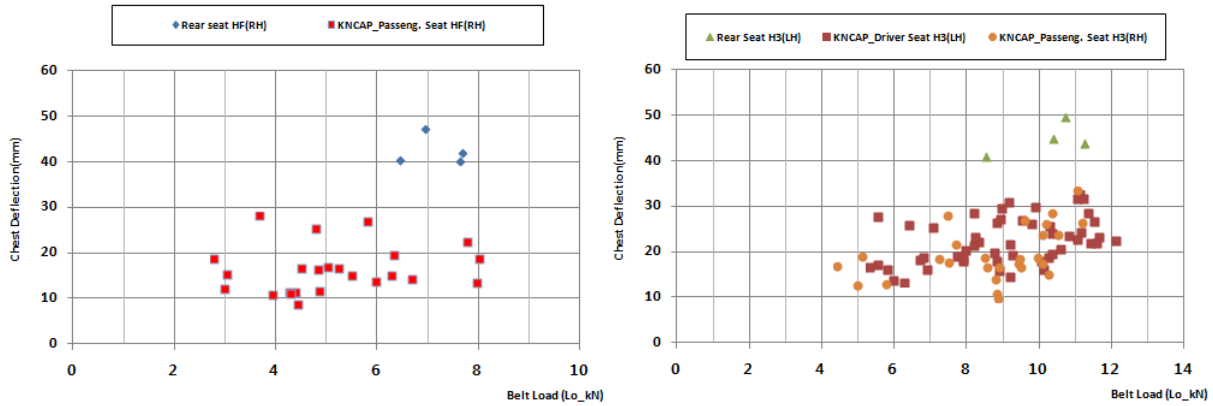


Figure 7. Peak chest deflection and lap belt load of 5th female ATD(left) / Peak chest deflection and lap belt load of 50th male ATD(right)

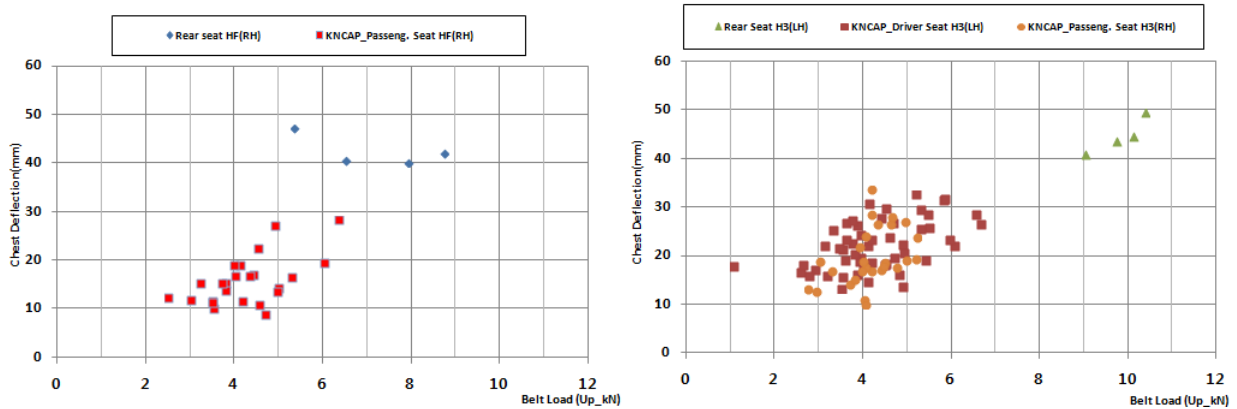


Figure 8. Peak chest deflection and shoulder belt load of 5th female ATD(left) / Peak chest deflection and shoulder belt load of 50th male ATD(right)

KINEMATICS ANALYSIS

Figure 9 shows photos of the ATD prior to the frontal sled test. As the torso position of the seat belt for the Hybrid III 50th male ATD in the rear seat is correct, the seat belt is fastened from the center of the shoulder to the center of the chest. However, the seat belt did not protect the torso of the Hybrid III 5th pregnant female ATD properly in the test, because its sitting height is short and the shoulder belt leans toward the neck due to the presence of the fetus in the abdomen.



Figure 9. 5th female pregnant ATD(left) and 50th male ATD(right) set up in the rear seats

The ATD loaded onto the rear seat moves forward more strongly than that in the front seat. In particular, the test was performed without the front seat. Therefore, restriction of the ATD movement by the front seat could not be tested. It was also found that the seat belt could not control chest displacement at a proper position, due to the presence of the fetus in the lower abdomen of the Hybrid III 5th pregnant female ATD (See Figure 10). The frontal movement displacement of the Hybrid III 50th male ATD was the greatest followed by the 5th female ATD, pregnant female ATD and Q6.

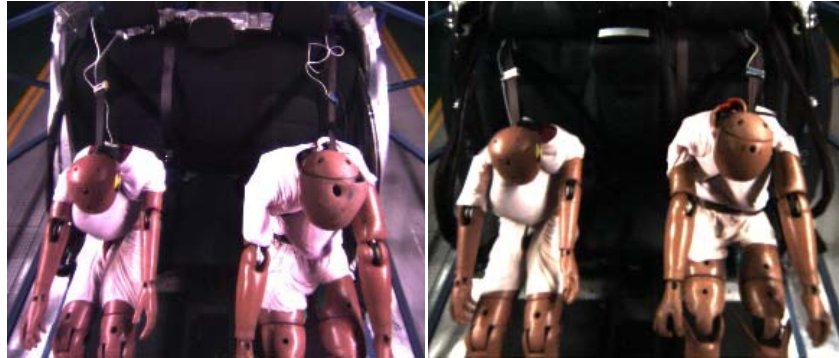


Figure 9. Examples of kinematic responses observed 5th female pregnant ATD and 50th male ATD in the rear seat

DISCUSSION

This study presents the same conclusion as the data of Paranteau and Viano (2003) regarding frontal crash accidents in which rear seat passengers put on the 3-point seat belt, confirming that a torso injury generally occurs due to the safety seatbelt, and that abdominal injuries of the rear seat occupants caused by the 3-point seat belt also occur when the type-3 seat belt is worn. Even though the abdominal load on the dummy was not checked due to the lack of measurement system, the chest deflection of the female ATD in the rear seat was observed to increase by 270% greater than the front seat. Also, the shoulder belt load of the front passenger seat is 5.13kN, whereas rear seat was about 7kN, indicating that the possibility of abdominal injury increases. The test results suggest that we need to devise a method of reducing injuries in actual accidents, by taking into account the fact that the lap belt load on the abdominal area is high.

The percentage of injury risk possibility was analyzed according to the average values of injury criteria of the same vehicle FFRB test conducted by the KNCAP, and the results of the rear seat frontal sled test. For the Hybrid III 50th male ATD on the driver's seat, the injury risk possibility (AIS3+) of HIC₁₅ in the FFRB test was found to be 0.9%; that of chest deflection, 1.1%; and that of upper neck tension force, 0.05%. The joint possibility of an injury being caused by all three factors was 2.04%. Meanwhile, for the Hybrid III 50th male ATD, the injury risk possibility (AIS3+) of HIC₁₅ in the rear seat frontal sled test was 2.6%; that of chest deflection, 18.3%; and that of upper neck tension force, 0.4%. The joint possibility of an injury being caused by all three items was 20.74%. These results indicate that the joint possibility of an injury in a rear seat is greater than in the case of the driver's seat.

For the front passenger seat of the Hybrid III 5th female ATD, the injury risk possibility (AIS3+) of HIC₁₅ in the FFRB test conducted by the KNCAP was found to be 3.5%; that of chest deflection, 1.3%; and that of upper neck tension force, 0.1%. The joint possibility of an injury being caused by all three factors was 4.85%. However, for the Hybrid III 5th female ATD, the injury risk possibility (AIS3+) of HIC₁₅ in the rear seat frontal sled test was 8.7%; that of chest deflection, 30.2%; and that of upper neck tension force, 4.6%. The joint possibility of an injury being caused by all three factors was 39.2%. These results indicate that the joint possibility of injury is also greater than in the case of the front passenger seat. The Hybrid III 5th pregnant female ATD, the injury risk possibility (AIS3+) of

HIC15 in the rear seat frontal sled test was 11.7%, and that of upper neck tension force, 0.4%. As a result, the rear seat is concluded to be less safe than the front seat in the case of both the male and female ATDs.

The shoulder belt part was found to be inappropriate for each dummy, as it was pushed into the lower neck during the test, making it impossible for the chest to absorb the energy properly. As such, it seems that more regulation should be proposed regarding the adjustable Y-axis for short adults, besides the regulation on the X-axis and Z-axis, when defining the shoulder belt of the rear seat belt in the motor vehicle safety standard. It seems that the motor vehicle safety standard and NCAP for rear seat safety and new car safety assessment should be implemented immediately, as the possibility of a head, neck, or chest injury is higher in the rear seat than in the front seat.

SUMMARY AND FUTURE WORKS

It was observed that the performance of safety for the rear seats and restraints was different compared with the front seat in a same vehicle. The possibility of fatal injury of Hybrid III 5th female and 50th male ATD in the rear seat could have greater than in the front seat, especially case of the chest deflection. For the Hybrid III 50th male ATD on the driver's seat in FFRB test, the joint possibility of an injury risk (AIS3+) was 2.04%. But for the 50th male ATD on rear seat, the joint possibility of an injury risk (AIS3+) was 20.74%.

For the Hybrid III 5th female ATD on the front passenger seat in FFRB test, the joint possibility of an injury risk (AIS3+) was 4.85%. However, for the 5th female ATD on rear seat, the joint possibility of an injury risk (AIS3+) was 39.2%. In case of the injury risk possibility (AIS3+) of chest deflection of passenger seat in the FFRB test was 1.3%, but rear seat frontal sled test was 30.2%. As a result, it was found that the rear seat was to be less safe than the front seat in the case of both the male and female ATDs. Also it was found that the possibility of injury risk for the female ATD on rear seat in frontal crash was greater than male ATD. In addition, the further consideration should be given regarding Y- axis in the regulation at the seat belt anchorage point.

Acknowledgements

This research was supported by the Korea Ministry of Land, Transport and Maritime Affairs. It was also supported by the Korea Institute of Construction and Transportation Evaluation and Planning (Project No.: 12PTSI-C054118-04).

REFERENCES

- [1] Evans, L., 1987. "Rear Compared to Front Seat Restraint System Effectiveness in Preventing Fatalities," Society of Automotive Engineers, Warrendale, PA, SAE Paper No. 870485.
- [2] Korea motor vehicle safety standard, 2014, <http://www.law.go.kr/>
- [3] Korea Auto-vehicle Safety Association, 2014, "A study on the introducing benefit and analysis of vehicle crash test protocols in KNCAP", Report.
- [4] Morgan, C., 1999. "Effectiveness of Lap/Shoulder Belts in the Back Outboard Seating Positions," NHTSA Report No. DOT HS 808 945.
- [5] Paranteau, C., Viano, D., 2003. "Field Data Analysis of Rear Occupant Injuries Part 1: Adults and Teenagers," SAE World Congress, Society of Automotive Engineers, Warrendale, PA, SAE Paper No. 2003-01-0153.
- [6] Richard Kent¹, Jason Forman¹, Daniel P. Parent¹, Shashi Kuppaa², 2007, "Rear seat occupant protection in frontal crashes and its feasibility", 20th ESV conference, pp 07-0386
- [7] Smith, K., Cummings, P., 2004. "Passenger Seating Position and the Risk of Passenger death or Injury in Traffic Crashes," Accident Analysis and Prevention, Vol. 36, pp. 257-260.

- [8] Shashi Kuppala¹, James Saunders¹, Osvaldo Fessahaie², 2005, "Rear seat occupant protection in frontal crashes", 19th ESV conference, pp 05-0212
- [9] Suzanne Tylko¹, Alain Bussièrès², 2012, "Responses of the Hybrid III 5th Female and 10-year-old ATD", IRCOBI conference 2012, pp IRC-12-65
- [10] YW Kim, 2013, "Korea NCAP status and future plan", Seminar of Safest vehicle of year

CONSIDERATION OF REPRESENTATIVENESS OF REAL-WORLD ACCIDENTS AND REPEATABILITY OF NEW NHTSA OBLIQUE OFFSET FRONTAL IMPACT TEST

Ryuuji Ootani
Taisuke Watanabe
Tomosaburo Okabe
Nissan Motor Co., Ltd.
Japan

Dix Jeff
Lam Joyce
Nissan Technical Center North America
USA

Muthanandam Muthukumar
Renault Nissan Technology and Business Center in India
India

Paper Number 15-0261

ABSTRACT

The National Highway Traffic Safety Administration has been considering introducing an oblique frontal offset impact test (oblique test) as a new crash test procedure. By means of accident data analysis, it was examined whether this oblique test can represent real-world accidents. Tests were also conducted using two identical vehicles to examine the repeatability of the oblique test. Representativeness of real-world accidents was examined by using the National Automotive Sampling System Crash Worthiness Data System (NASS-CDS) to investigate frontal impact accidents from 2004 to 2008. Repeatability of the oblique test was investigated by conducting the same crash test twice using a midsize sedan. In terms of percentage of the total number of real-world accidents, the most frequent accident modes observed were Full-engagement and Offset frontal impacts, accounting for about 30%. Accidents similar to the oblique test accounted for about 10%. In terms of representativeness of severe injuries, the percentage of brain rotational injuries and lower extremity injuries differed from real-world accident statistics. Brain rotational injuries were considerably different from real-world accidents. With regard to repeatability, vehicle deceleration (G) was almost the same. However, the degree of cabin deformation differed because of a difference in the buckling mode of the front longitudinal member. Another notable point in the oblique test is that, as the test vehicle weight increases, the Delta-V decreases. However, this tendency is not observed in real-world accidents. To ensure the validity and significance of introducing this test procedure, more test data are required along with continued evaluation and analysis of occupant protection performance based on actual test results.

INTRODUCTION

Occupant protection performance in frontal impacts is currently assessed in tests conducted under the New Car Assessment Program (NCAP) and by the Insurance Institute for Highway Safety (IIHS). The National Highway Traffic Safety Administration (NHTSA) has proposed introducing a frontal oblique offset impact test, which is different from the traditional test method. The NHTSA has been publishing results obtained from oblique tests and accident analysis. In 2011, Rudd et al. [1] conducted an analysis of small overlap and oblique accidents and also reported the factors causing injuries. In 2012, Saunders et al. [2] reported a small overlap and oblique test method and the results obtained for vehicle G and deformation. In 2013, Saunders and Parent [3] reported the results of additional oblique tests. Regarding the repeatability of the oblique test, the same authors [4] also published the results of a three-vehicle comparison using the same vehicle. For the THOR dummy, which is to be used in the oblique test, introduction of the Brain Injury Criteria (BrIC) is being considered. Saunders and Parent [5] discussed BrIC, and Dokko and Hasegawa [6] reported an evaluation of thoracic injuries using a human finite element model. Recent publications indicate that the studies related to the oblique test method and new THOR dummy have been increasing. In this study, attention was focused on analyzing the representativeness of real-world accidents and the repeatability of the oblique test.

REPRESENTATIVENESS OF REAL-WORLD ACCIDENTS

Method of accident analysis

The National Automotive Sampling System Crash Worthiness Data System (NASS-CDS) was used in this study to analyze injured occupants. Table 1 summarizes the extraction conditions of the accident analysis. The total number of MAIS3+ injured occupants was 3,214. The injured occupants were classified in nine types of crash configurations shown in Figure 1. In making this classification, “Small overlap” was classified based on the method proposed by the Medical College of Wisconsin [7]. “Offset”, “Full-Engagement”, “Narrow”, “DYZ-NoRail”, “Oblique”, and “High/Low Vertical” were classified according to the taxonomy proposed by Sullivan et al. [8]. “Front-other” and “Side-other” were classified as other accident types.

Table 1.
Summary of NASS-CDS data extraction conditions

Data years	2004-2008
Vehicle model years	1959-2009
Deformation location	Front, Left & Right
PDOF (Principal Direction of Force) [degrees]	Left & Right: 0-40, 320-360
Rollover collisions	Not involved
MAIS	3+ injuries

Results of Accident Analysis

Figure 1 shows a breakdown of the accidents by crash configuration. The most frequent accident types are the Full-Engagement and Offset frontal impact, each of them accounts for 27% of the total. The second most frequent accident type is the Small overlap impact, which accounts for 13%. The next frequent accident types are the Narrow, DYZ-NoRail, Oblique, and High/Low Vertical in decreasing order. Other accidents (Front-other and Side-other) are 15%.

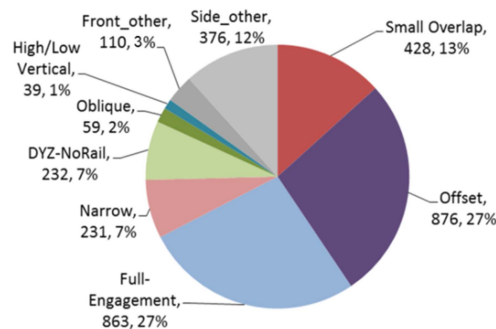


Figure 1. Accident breakdown by crash configuration

Among the results in Figure 1, Offset and Small overlap accidents were segmentalized in two directions: “Offset-Oblique” and “Offset-Colinear”, “Small Overlap-Oblique” and “Small Overlap-Colinear”. The results are shown in Figure 2. As a result of the segmentalization, the second most frequent accident type is “Offset-Oblique”, which accounts for 15%. The next most frequent accident type is “Offset-Colinear”, which accounts for 13%.

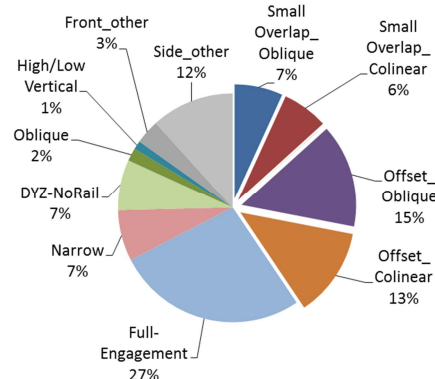


Figure 2. Accident breakdown by crash configuration segmentalized by direction

Among the results in Figure 2, Offset and Small overlap accidents were further segmentalized in terms of three types of collision partners: vehicle, pole and other object. The results are shown in Figure 3. As a result of the resegmentalization it is seen that the most frequent accident type is Full-Engagement, and the second most frequent type is “Offset-Oblique-Vehicle”, which accounts for 12%. This “Offset-Oblique-Vehicle” is considered to be a crash configuration similar to the offset oblique impact test.

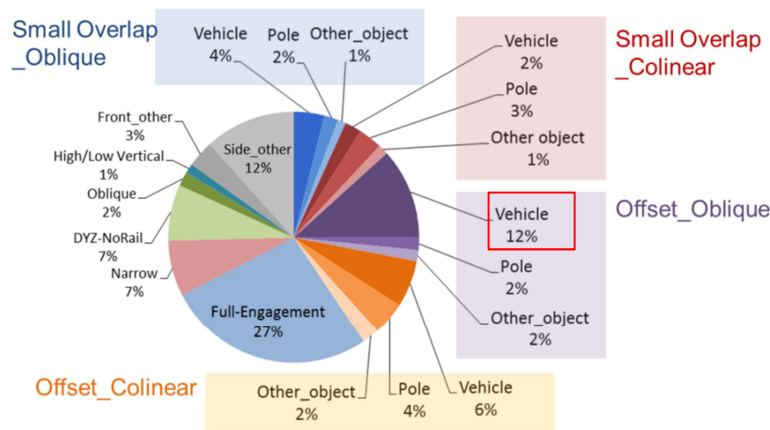


Figure 3. Accident breakdown by crash configuration segmentalized by direction and collision partner

Figure 4 shows the cumulative distribution of Delta-V of the “Offset-Oblique-Vehicle” type, and Figure 5 shows the frequency distribution. These data exclude unknown Delta-Vs. The number of seriously injured occupants (MAIS3+) was 256. The results indicate that Delta-V of 56 km/h covers 90% of the cases and the cumulative percentage of Delta-V less than 45 km/h was 75%.

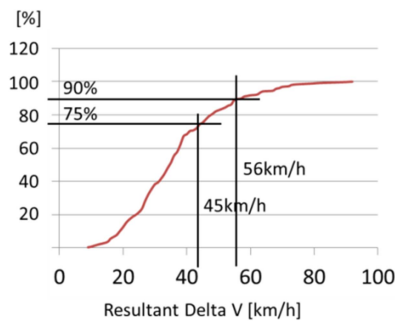


Figure 4. Cumulative distribution of Delta-V

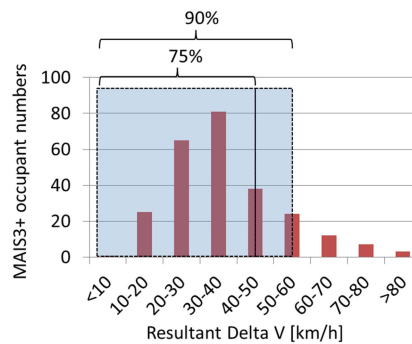


Figure 5. Frequency distribution of Delta-V

Method of Detailed Accident Analysis

A more detailed accident analysis was then conducted using NASS-CDS data. The data sets were the same as those used in [1]. Table 2 shows the extraction conditions of this accident analysis. These conditions were applicable to 19 out of 117 number of total occupants used in [1]. The accidents involving these 19 occupants were analyzed.

Table 2.
Summary of NASS-CDS data extraction conditions for detailed analysis

Data years	1998-2009
Vehicle model years	1998-2005
Deformation location	Left offset only
PDOF (Principal Direction of Force) [degrees]	320-350
Collision partner	Vehicle only
Rollover collisions and multiple crashes	Not involved
Occupants	Driver only
	Belted
	Not ejected
AIS	3+ injuries

Comparison between NHTSA test results and detailed accident analysis results

The results of the accident analysis were compared with the results obtained for 16 vehicles in oblique frontal impact tests (Table 3) in a study conducted by NHTSA. Figure 6 shows the configuration of the oblique frontal impact test, and Table 3 is the list of vehicles used. In this oblique frontal impact test, the dolly with barrier impacts the target vehicle at 56mph (90 km/h) and the angle of the stationary vehicle is 15 degrees and the overlap is 35 percent on the driver side of the vehicle. In this paper, an oblique offset impact in real-world accidents is referred to as an Accident Oblique Offset Impact (AOOI) and an oblique offset impact in the NHTSA research test is referred to as an Oblique Offset Impact (OOI).

Table 3.
List of vehicles used in oblique frontal impact test conducted by NHTSA

Report No.	Name	Model Year	Test vehicle weight [kg]
7458	Smart For two	2011	1034
7441	Toyota Yaris	2011	1331
8086	Nissan Versa R	2013	1438
8084	Nissan Versa	2013	1451
8089	Hyundai Elantra	2013	1590
7431	Chevrolet Cruze	2011	1662
7428	Ford Fiesta	2011	1671
8085	Toyota Camry R	2012	1752
8096	Honda CRV	2012	1757
8088	Toyota Camry	2012	1759
7467	Buick Lacrosse	2011	1944
8087	Ford Taurus	2013	2123
8097	Honda Odyssey	2012	2210
7476	Ford Explorer	2011	2363
7457	Dodge Ram 1500	2011	2611
8099	Chevrolet Silverado	2012	2624

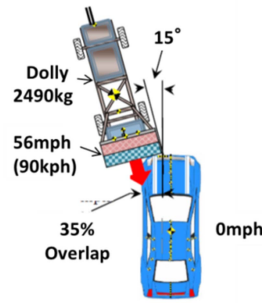


Figure 6. NHTSA offset oblique impact test

Delta-V Direction Figure 7 compares the results for the Delta-V direction, which is calculated with Eq. (I). Most of the Delta V-direction is within 10-20 degrees, and the average Delta-V direction of AOOI and OOI is almost the same.

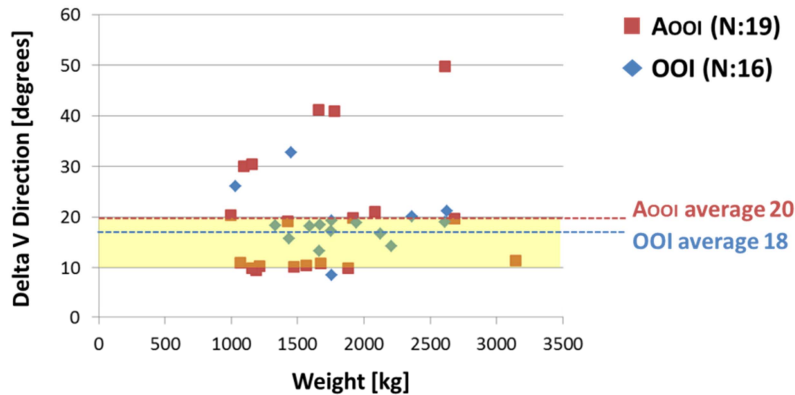


Figure 7. Relationship between Delta-V direction and vehicle weight

$$\Delta V \text{ Direction} = \text{Tangent} (\text{longitudinal } \Delta V / \text{Lateral } \Delta V) \quad (I)$$

Relationship between Delta-V and Vehicle Weight Figure 8 shows the relationship between the resultant Delta-V (longitudinal and lateral) and vehicle weight. In OOI, a strong correlation exists between the two. Delta-V of 41 km/h for the heaviest vehicle is the minimum velocity of all the Delta-V values; Delta-V of 67 km/h for the lightest vehicle is the maximum velocity and is approximately 1.6 times higher than that of the heaviest vehicle. On the other hand, weak correlation is observed between Delta-V and vehicle weight in AOOI. Delta-V in OOI is almost at the upper limit of Delta-V in AOOI.

Figure 9 shows the relationship between the resultant Delta-V and vehicle weight ratio. The vehicle weight ratio used in this study is explained here. The vehicle weight ratio in AOOI is found by dividing the weight of the impacted vehicle by the weight of the collision partner because the crash configuration is a car-to-car collision. In contrast, OOI is a research moving deformable barrier (RMDB)-into-stationary vehicle impact test. For this reason, the vehicle weight ratio cannot be calculated in the same way. For a better comparison between AOOI and OOI, as shown in Figure 10, the OOI test condition was translated into a car-to-car test at an initial velocity of 64 km/h and a vehicle weight of 1750 kg. The initial velocity and vehicle weight were derived using the law of conservation of momentum. The initial velocity was the same as in the offset deformable barrier (ODB) impact test conducted by IIHS and EuroNCAP, and the vehicle weight was calculated with Eq. (II). For reference, the resultant Delta-V of the Toyota Camry R (1752 kg) and the Honda CRV (1757 kg), both of which weigh close to 1750 kg, was 52 km/h and 54 km/h, respectively. These values are similar to Delta-V of 56 km/h, having a cumulative composition ratio of

90% in Figure 4. The weight of the collision partner was 1750 kg, and the vehicle weight ratio was calculated by dividing the impacted vehicle weight by 1750 kg.

The results plotted in Figure 9 are almost the same as those in Figure 8. It is seen that the resultant Delta-V and vehicle weight ratio have a strong correlation in OOI but little correlation in AOOI.

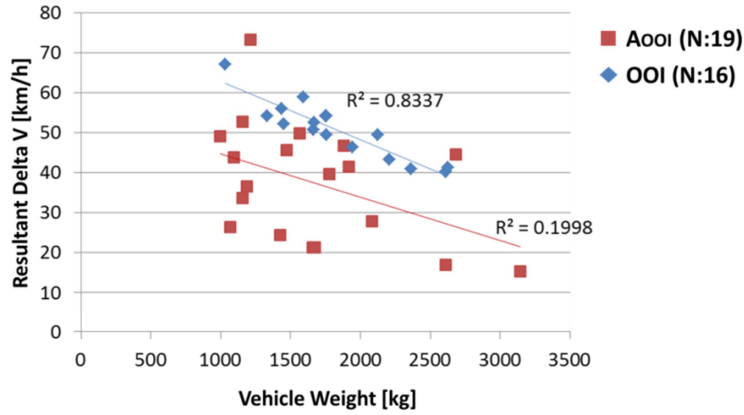


Figure 8. Relationship between resultant Delta-V and vehicle weight

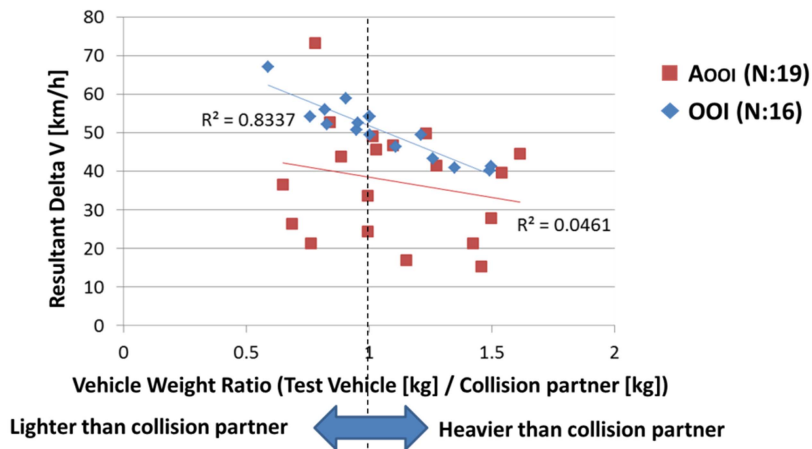


Figure 9. Relationship between resultant Delta-V and vehicle weight ratio

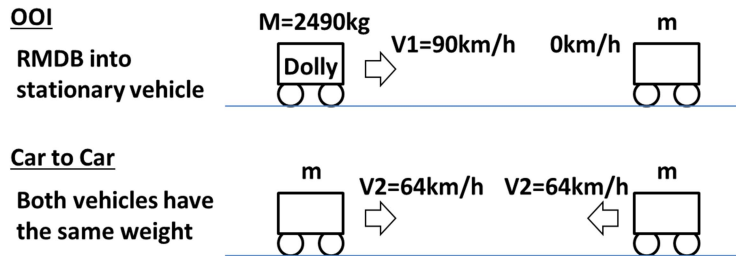


Figure 10. Translation method to equivalent car-to-car impact

$$2*m*V2 = M *V1 \quad m=1750 \text{ kg} \quad (II)$$

Injuries in AOOI Figure 11 shows the percentages of AIS3+ injuries by body region in AOOI. The most frequent type is knee, thigh, and hip (KTH) & lower leg (40%) injuries, followed by upper extremity (28%) and thorax (20%) injuries. Small percentages of injuries are seen for head (8%) and abdomen (2%).

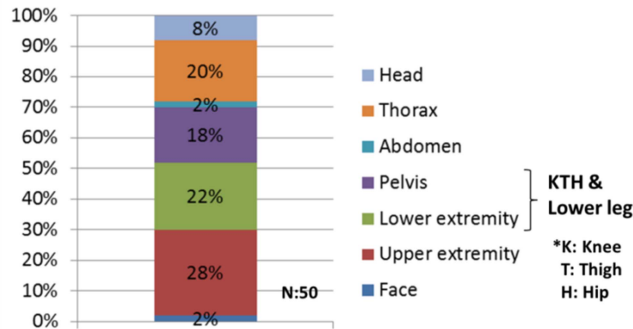


Figure 11. AIS3+ injury percentages by body region

Figures 12 and 13 show the details of AIS3+ head injuries and injury sources in AOOI. Number of injuries N:4 in Figure 12 is small and all of them involve brain damage. Injury sources are safety belt and left B-pillar.

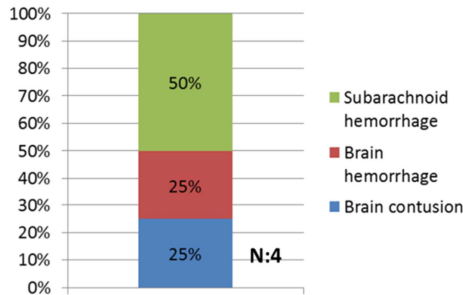


Figure 12. Details of AIS3+ head injuries

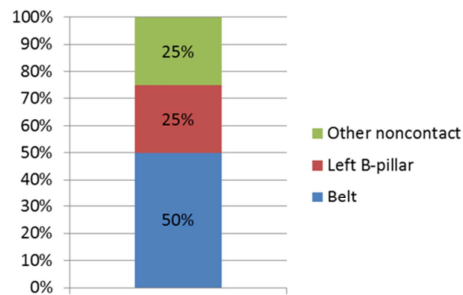


Figure 13. Sources of head injuries

Figures 14 and 15 show the details of AIS3+ thorax injuries and injury sources in AOOI. Thorax injuries comprise rib fracture, lung contusion, and thorax cavity damage. The main injury sources are left-side object and steering wheel.

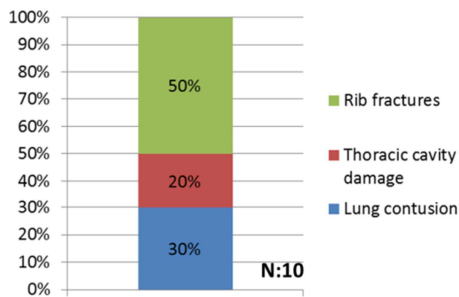


Figure 14. Details of AIS3+ thorax injuries

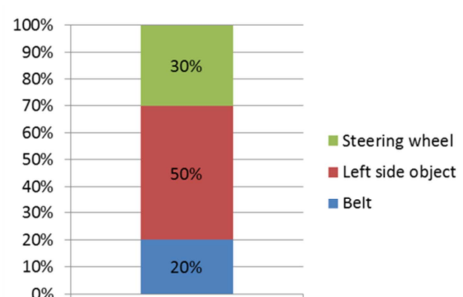


Figure 15. Sources of thorax injuries

Figures 16 and 17 show the details of AIS3+ KTH & lower leg injuries and injury sources in AOOI. All injuries are fractures, the most frequent of which are femur fractures, followed by acetabulum and tibia fractures. The main injury sources are the knee bolster, the left-side object and the floor panel.

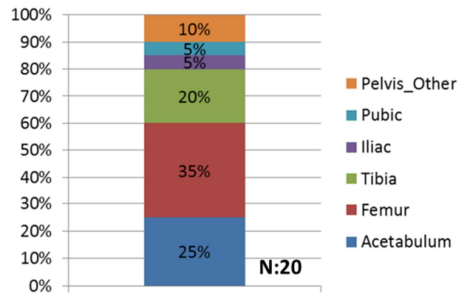


Figure 16. Details of AIS3+ KTH & lower leg injuries

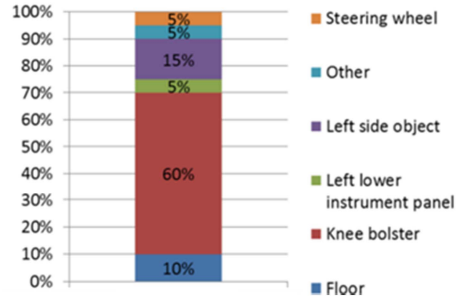


Figure 17. Sources of KTH & lower leg injuries

Figures 18 and 19 show the fracture points of AIS3+ KTH & lower leg injuries and injury sources for the femur, acetabulum and tibia in AOOI. Fracture occurs equally in both the right and left legs. Pelvis and upper leg fractures in particular occur frequently. Tibia fracture occurs in only the right leg. The injury sources for the acetabulum are the knee bolster, left lower instrument panel, and the steering wheel. The injury sources for the femur are the knee bolster and the left-side object, and for the tibia the knee bolster and the floor panel.

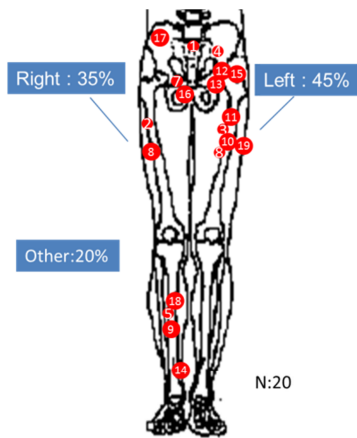


Figure 18. Fracture points of KTH & lower leg

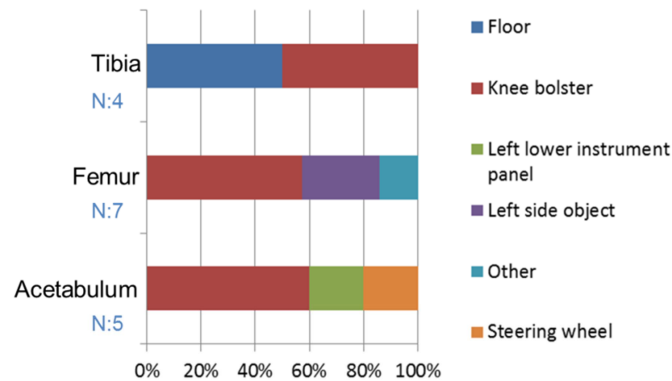


Figure 19. Sources of acetabulum, femur, and tibia injuries

Comparison of injuries between AOOI and OOI Figure 20 compares the percentages of serious injuries occurring in AOOI and OOI. In AOOI, AIS3+ injuries were treated as serious injuries, and the percentage of serious injuries was calculated in the following way: (a) at first, AIS3+ injury numbers of the driverside occupant were counted and (b) then it is divided by the total number of injuries of the body region. For example, regarding the percentage of head serious injury, the percentage of serious injuries is 16% (3/19), where 3 was AIS 3+ and total numbers of injuries was 19. In OOI, the percentage of serious injuries was calculated in the following way: (a) at first, the injury numbers of the driverside dummy which exceeded the reference Injury Assessment Reference Value (IARV) were counted and (b) then it is divided by the total number of injuries of the body region. For example, regarding the percentage of head serious injury, the percentage of serious injuries is 25% (4/16), where 4 exceeded IARV and total numbers of injuries was 16. It will be noted that the IARV of thorax injuries was not determined, so the upper deflection (53 mm) and lower deflection (46 mm) [2] were used as provisional values. The Brain Rotational Injury Criterion (BRIC) was also used as head injury value. As a result, the percentage of BRIC head injuries in OOI differed greatly from the percentage of AIS3+ head injuries in AOOI. As for KTH & lower leg injuries, the percentage of acetabulum and femur serious injuries differed between AOOI and OOI.

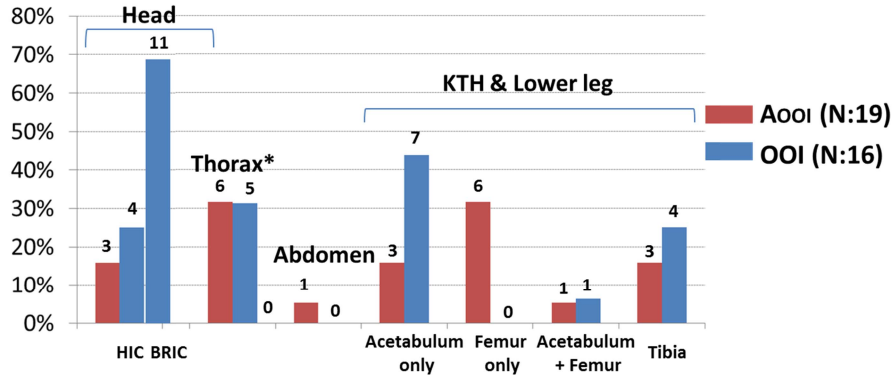


Figure 20. Comparison of serious injury percentages between AOOI and OOI

REPEATABILITY OF OBLIQUE TEST

Test Conditions

To examine the repeatability of the oblique offset impact test (OOI), a comparison was made for the vehicle deformation and G level in two tests conducted with the same vehicle. Table 4 shows the test conditions and vehicle specification for OOI. The vehicle used was a midsize sedan. The initial velocity and the test vehicle weight were almost the same in OOI#1 and OOI#2 tests. A 50th percentile male THOR-NT frontal impact test dummy was seated in the driver's seat. A Hybrid-III dummy was seated in the front passenger's seat. The THOR-NT dummy was a tentative version manufactured by GESAC and was different from the THOR dummies used in NHTSA's OOI research tests.

Table 4.
Test conditions and vehicle specification of OOI test

No.	Vehicle	Weight [kg]	Velocity [km/h]
OOI #1	V6 3.5L 2WD	1868	90.1
OOI #2		1870	90.4

Dummy	
Driver (Left)	THOR-NT (GESAC)
Passenger (Right)	Hybrid-III

Comparison results

Summary Figure 21 shows photographs of the post-test vehicles and barriers. The comparison did not show any significant difference for the vehicle and the barrier deformations between OOI#1 and OOI#2.



Figure 21. Photographs of the post-test vehicles and barriers

Difference in Vehicle Deformation Figures 22 and 23 compare the cabin deformation and floor deformation of the post-test vehicles, respectively. The cabin deformation around the front door opening was almost the same in OOI#1 and OOI#2; the maximum deformation point was the part of the door front near the lower A-Pillar, and the amount of deformation was 44 mm. On the other hand, floor deformation differed in the longitudinal and vertical directions. In the longitudinal direction, C2 and D2 showed large differences, with the maximum difference being 36 mm. In the vertical direction, B2, C2 and D2 showed large differences, with the maximum difference being 58 mm. Generally the vehicle deformation is greater in OOI#2 than in OOI#1.

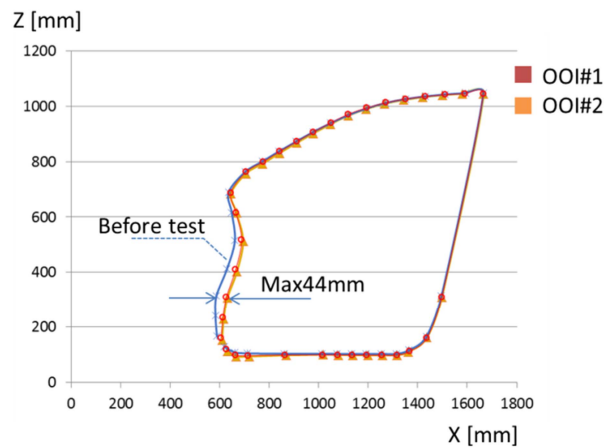


Figure 22. Comparison of cabin deformation

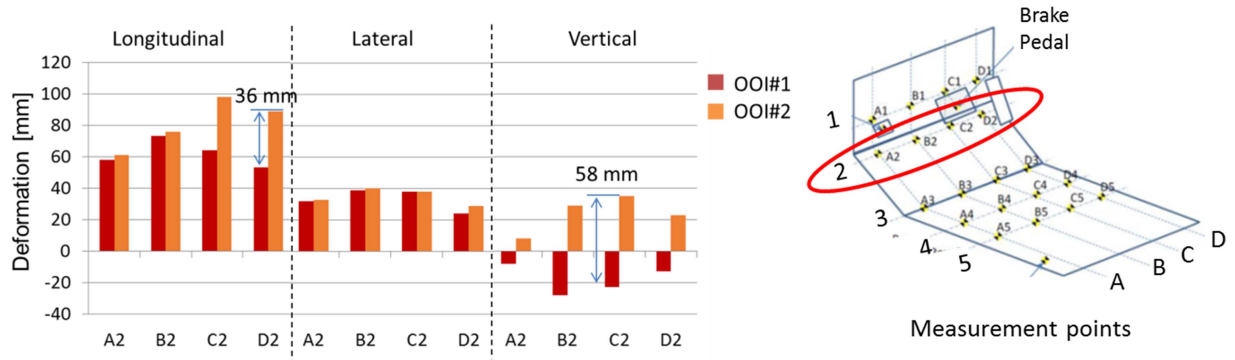


Figure 23. Comparison of floor deformation

The factors causing the difference in the floor deformation seen in Figure 23 were then examined. Figure 24 shows the deformation of Row 1 on the dash panel and measurement points 6, 7, 8 on the dash lower cross member. Figure 25 presents photographs of the post-test dash panels. The difference (52 mm) in the deformation at location 8 was especially large. In addition, as seen in Figure 25, the deformation mode of the dash panel near the dash lower cross member differed. In order to investigate the reason of these differences, the deformation of the front longitudinal member which is connected to the dash lower cross member in the engine compartment was then examined.

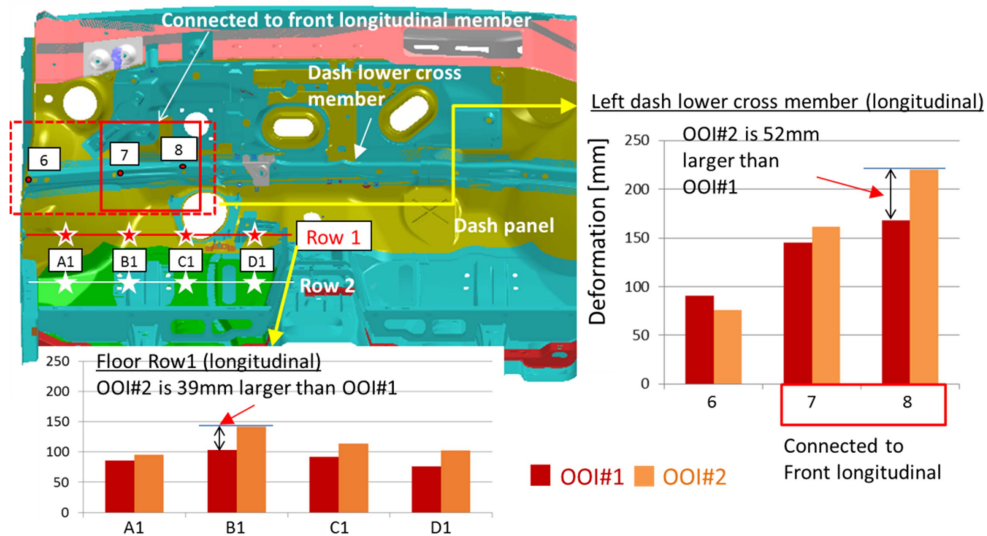


Figure 24. Comparison of dash panel and dash lower cross member deformation

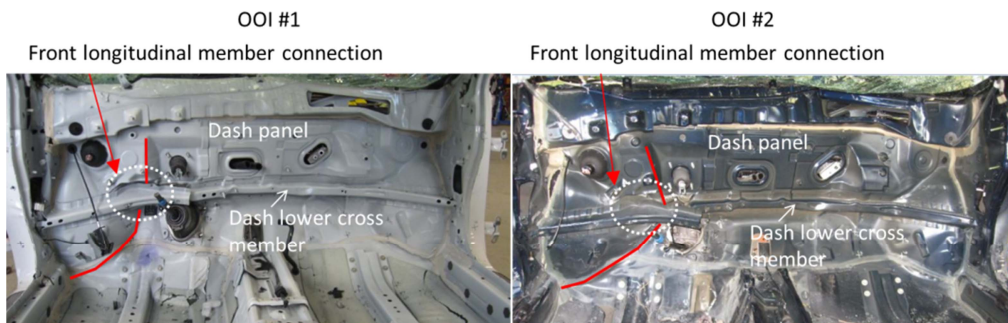


Figure 25. Photographs of dash panel deformation

Figures 26 and 27 show the measured deformation modes of the front longitudinal member. These results indicate that the deformation mode in OOI#1 differed from that in OOI#2 and that rearward displacement in OOI#2 was

larger than that in OOI#1. Two bending points occurred in the front longitudinal member and bumper reinforcement beam in OOI#1 and OOI#2, but the bending locations were different. The bending points in OOI#1 occurred only in the front longitudinal member, whereas in OOI#2, there were one bending point each on the front longitudinal member and the bumper reinforcement beam. Figures 28 and 29 show photographs of the post-test front longitudinal member and bumper reinforcement beam, respectively. It is seen in these photographs that the deformation mode and bending locations of the front longitudinal member and bumper reinforcement beam differed between the two tests.

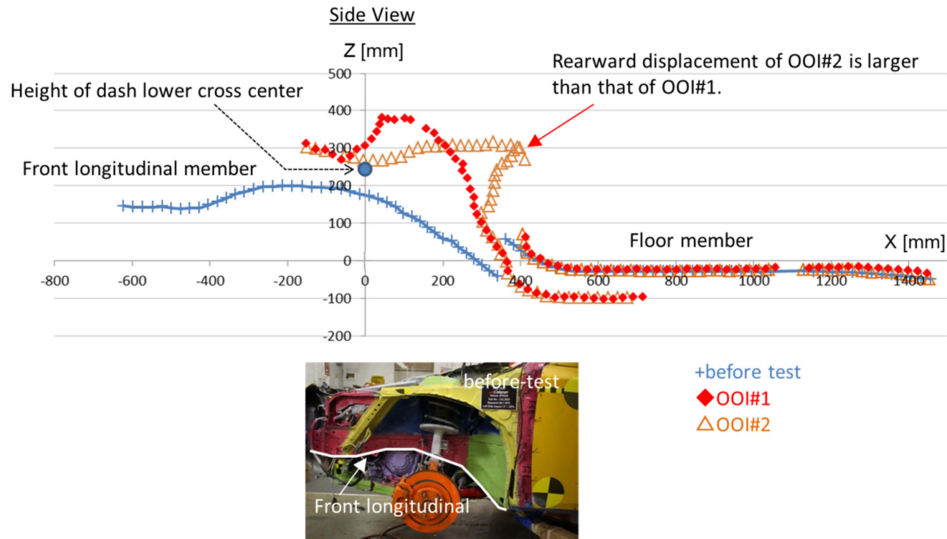


Figure 26. Comparison of front longitudinal member deformation (side view)

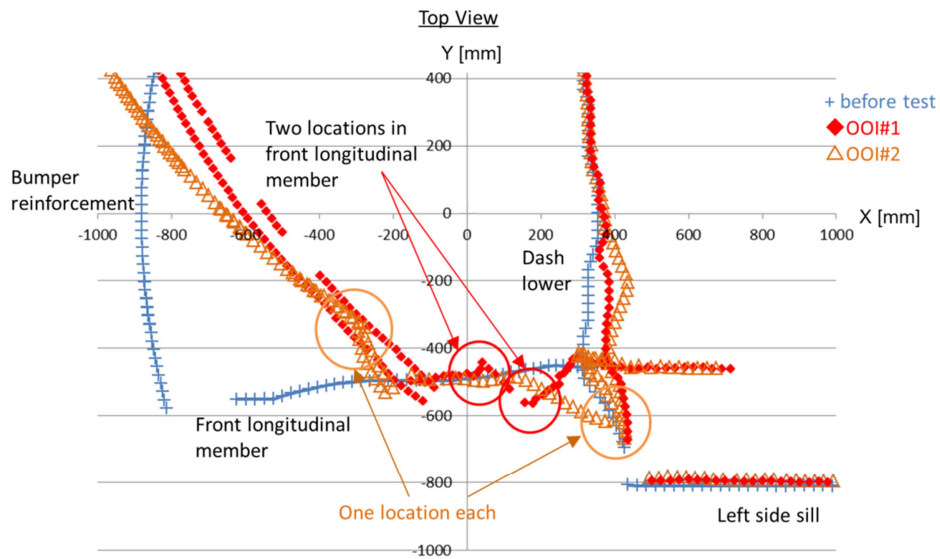


Figure 27. Comparison of front longitudinal member deformation (top view)

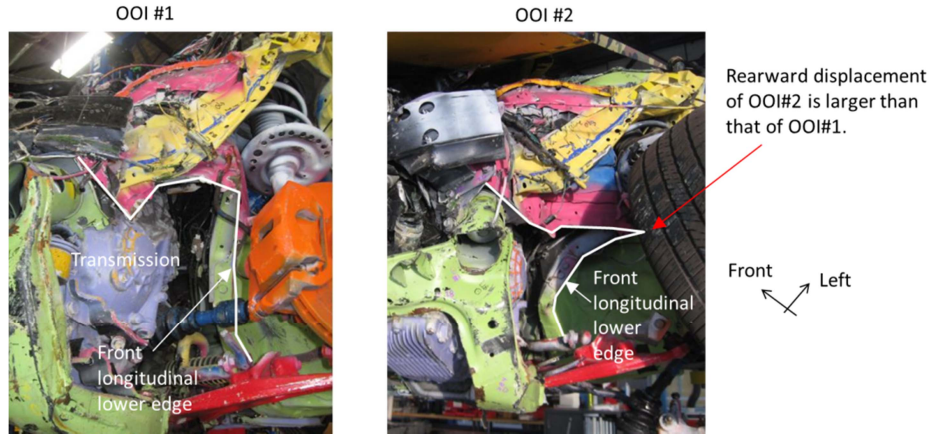


Figure 28. Photographs of front longitudinal member deformation

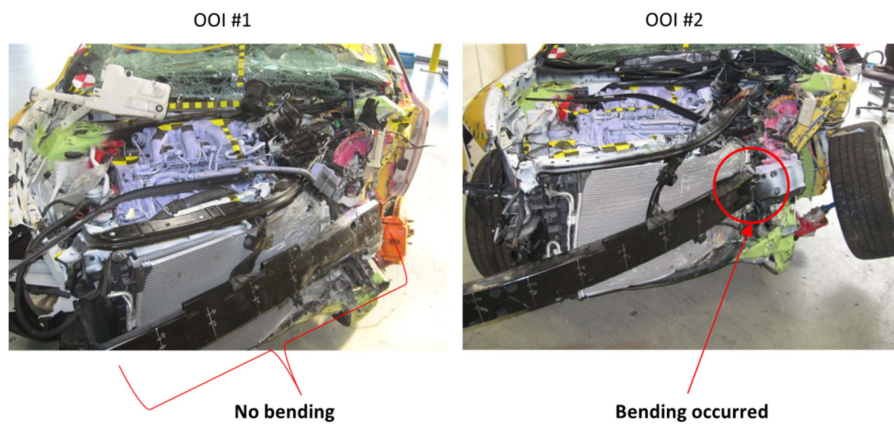


Figure 29. Photographs of bumper reinforcement beam deformation

The difference in floor deformation between OOI#1 and OOI#2 is presumed to be due to the following sequences. Initially, the deformation mode of the front longitudinal member differs, and larger rearward displacement occurs in OOI#2 than in OOI#1; then the dash lower cross member connected to the front longitudinal member undergoes large deformation toward the cabin side, this results in larger floor deformation in OOI#2 than in OOI#1. In a series of OOI research tests, NHTSA has conducted the repeatability evaluation using three same vehicles [4] (Figure 30). The variation of floor Row 1 deformation were at a similar level to the test results in this study as shown in Figure 24.

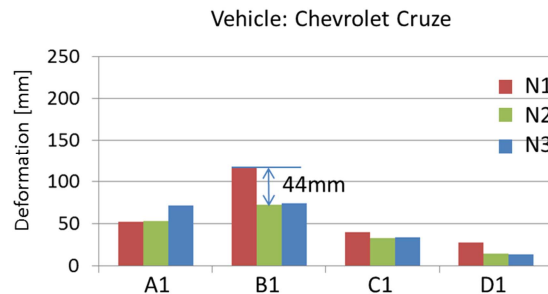


Figure 30. Result of floor deformation in NHTSA research test

Difference in vehicle G and velocity Figure 31 compares the vehicle deceleration (G) and Figure 32 compares the vehicle velocity. Deceleration was measured at the vehicle’s center of gravity, and velocity was calculated by

integrating G. It is seen that the peak G values differed by a factor of 7G between the longitudinal direction and by a factor of 12G between the lateral direction. However the overall wave shapes and timing of the peaks were similar in both the longitudinal and lateral directions between OOI#1 and OOI#2. Longitudinal velocity differed by 2km/h, but lateral velocity was almost the same.

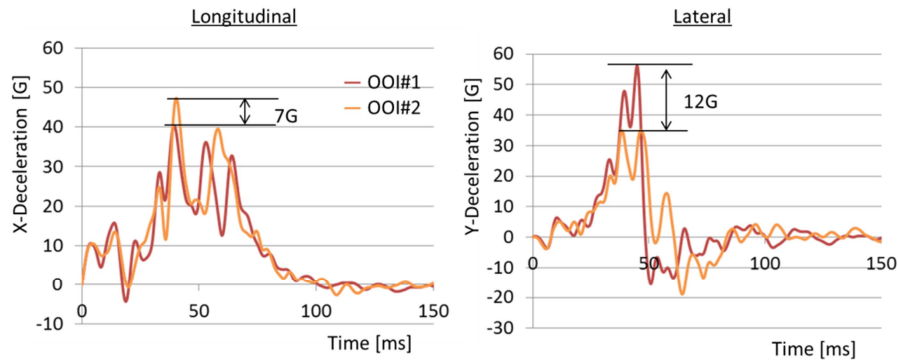


Figure 31. Comparison of vehicle deceleration

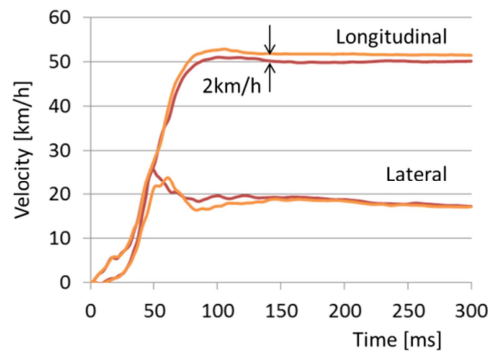


Figure 32. Comparison of vehicle velocity

DISCUSSION AND CONCLUSION

Real-world frontal impact accidents were classified into 9 crash configurations based on the method in the literature [7], [8]. The most frequent accident types are Full-engagement and Offset, followed by Small overlap accidents in that order. Small overlap and Offset accidents were then reclassified in terms of two directions: Offset-Oblique, Offset-Colinear and Small Overlap-Oblique, Small Overlap-Colinear and three collision partners: vehicle, pole, and other object. It was found that an Offset-Oblique-Vehicle accident similar to the offset oblique impact (OOI) test was the second most frequent crash configuration next to Full-engagement. However, this Offset-Oblique-Vehicle accident accounts for only approximately 10% of all frontal impact accidents. Regarding crash severity, in the AOOI, the resultant Delta-V of approximately 56 km/h covers a cumulative accident coverage of 90%. In the OOI tests, a strong correlation was seen between the resultant Delta-V and vehicle weight and the resultant Delta-V of lighter vehicles tended to be higher than 56 km/h. The lightest vehicle is higher than 64km/h in the offset deformable barrier (ODB) impact test. Therefore it is thought that additional vehicle structural countermeasure for lighter vehicles to address the current OOI test procedure may produce stiffer vehicles and shorter crash pulses and in consequence negatively affect the safety of vulnerable elderly drivers. As for the representativeness of the percentages of serious injuries, a large difference was seen between the accident data and the test results, especially for head injuries (BRIC). Differences between the accident data and the test results were also seen for lower extremity injuries, especially acetabulum and femur injuries.

Regarding repeatability of the OOI test, vehicle deformation, G values, and velocity were compared by conducting two tests using the same midsize sedan. The results showed that G values and velocity did not show any notable difference. However, floor deformation differed due to a difference in the deformation mode of the front

longitudinal member, which was caused by a difference in the bending location of the member and the bumper reinforcement beam. This difference in floor deformation was similar to the difference reported in a couple of OOI reserach tests previously carried out by NHTSA. The amount of this difference in floor deformation may affect the details and dimensions of countermeasures. These results suggest that further studies are required to validate the introduction of the OOI as a new crash test procedure in regulatory testing or NCAP.

REFERENCES

- [1] Rodney W. Rudd, Mark Scarboro, James Saunders, “Injury Analysis of Real-World Small Overlap and Oblique Frontal Crashes”, 2011 ESV, Paper Number 11-0384.
- [2] James Saunders, Matthew Craig and Daniel Parent, “Moving Deformable Barrier Test Procedure for Evaluating Small Overlap/Oblique Crashes”, 2012 SAE, No 2012-01-0577.
- [3] James Saunders and Dan Parent, “Assessment of an Oblique Moving Deformable Barrier Test Procedure”, 2013 ESV, Paper Number 13-0402.
- [4] James Saunders and Daniel Parent, “Repeatability of a Small Overlap and an Oblique Moving Deformable Barrier Test Procedure”, 2013 SAE, No 2013-01-0762.
- [5] James Saunders and Daniel Parent, “Repeatability of a Small Overlap and an Oblique Moving Deformable Barrier Test Procedure”, 2013 SAE, No 2013-01-0762.
- [6] Yasuhiro Dokko and Takahashi Hasegawa, “Evaluation of Thoracic Injury of the Occupants in Small Overlap/oblique Impact Using a Human FE Model”, 2013 JSAE, No152-20135332.
- [7] Erik G. Takhounts and Vikas Hasija, “An Operational Definition of Small Overlap Impact for Published NASS Data”, 2013 STAPP, No 243-266.
- [8] Kaye Sullivan, Scott Henry and Tony R. Laituri, “A Frontal Impact Taxonomy for USA Field Data”, 2008 SAE, No 2008-01-0526.
- [9] NHTSA, “NASS Analysis in Support of NHTSA’s Frontal Small Overlap Program”, 2011.

GLOSSARY

AOOI: Accident Oblique Offset Impact

OOI: Oblique Offset Impact

PDOF: Principal Direction of Force

IARV: Injury Assessment Reference Value

KTH: Knee Thigh Hip

BRIC: Brain Rotational Injury Criterion

A MODEL OF VEHICLE-FIXED BARRIER FRONTAL CRASH AND ITS APPLICATION IN THE ESTIMATION OF CRASH KINEMATICS

Zuolong, Wei
Hamid Reza, Krimi
Kjell Gunnar, Robbersmyr
University of Agder
Norway

Paper Number 15-0161

ABSTRACT

The study of vehicle crash process is of great importance in transportation safety. The crash pulses of vehicles during the fixed barrier impacts can reflect the crashworthiness of the vehicle structure. In this paper, a mathematical model of vehicle kinematics during the frontal crash is investigated. This work is based on the analysis of crash response signals and vehicle structure. The proposed model uses piecewise linear functions to describe the trend of crash impulse and ignores the residual oscillations. To study the model variance, the crashes in various speeds and a full car crash in complex condition are compared. At the end of paper, the crash performance of a vehicle crash is predicted according to the proposed model and therefore demonstrates its effectiveness and usability.

INTRODUCTION

Crashworthiness is one of the core topics in the passive safety of vehicles and plays an important role in the condition that the impact cannot be avoided. Generally, the analysis of crashworthiness is based on the related crash responses, i.e. the displacement, velocity and acceleration, of critical parts of a vehicle in full car crash tests. However, these tests are required appropriate facilities, one or more cars with measuring devices, experienced staff and a long time to prepare. It means they are complicated, expensive, long-lasting and therefore not easy to realize [1]. This is especially true in the early stage of vehicle design. Therefore, vehicle designers and researchers made a lot of effort to build numerical models to describe the crash processes. Up to now, various technologies are used to model the vehicle crash. Typical crash models may be classified into three broad categories [2]: 1) Detailed nonlinear finite element models. These models have excellent performance in the estimation of structural crashworthiness. However, before these crash models could be used, they usually require the details of the vehicle structure and materials. This limits the use of FE models in the design process. 2) Multibody models and multibody based lumped parameter models. As FE models, the multibody models also suffer the complexity. Consequently, the multibody based lumped parameter models make a compromise between the accuracy and complexity. Most of these models consist of energy absorbing (EA) elements with masses connected to both ends [3]. Reference [4 and 5] are typical studies on the lumped parameter models. 3) Functional approximation or response surface models. The functional approximation method is widely used in academia and industry. And reference [6] provides an overview of its use in the research of crashworthiness. To achieve better approximation, some advanced technologies are also introduced in this area, such as wavelet [7] and neural network [8]. Most of these models focus on the crash response signals themselves and can hardly be related to the vehicle structure. So the physical meaning of these modes is not clear.

In the proceeding of the study, a piecewise linear model is proposed to represent the vehicle-rigid wall frontal crash. Compared to existing models, this model is developed based on the analysis of crash responses and therefore can reflect the performance of vehicle structures in crashes.

The rest part of this paper is organized as follows: In the next section, the crashworthiness structure is introduced firstly. Afterwards, the proposed model is proposed. In this section, the modelling procedures will be presented in detail and the influences of crash condition are also discussed. After that, an estimation of vehicle kinematics is given as an application of the proposed model. The conclusion goes finally.

VEHICLE STRUCTURE

Most of modern commercial cars have unibody construction, i.e. a single entity forms a car's body and frame. The vehicle body is usually made of steel or aluminum that is stamped with the appropriate cross members and everything is mounted directly to it. In this paper, only the frontal crash of unibody construction is studied.

To improve the crashworthiness, the vehicles are meticulously designed. As an integration, the vehicle structure would transmit the impact load in a proper way, i.e. load-carrying path. In addition, there are some weak components arranged as crumple zone. During the crash, the crumple zone will deform and absorb energy and ensure the rest parts of the vehicle are safe. In the local design, the material and shape of beams, shells and connectors are also considered to achieve better energy-absorbing performance.

Load-carrying Path and Crash Process

Generally, vehicles have a high relative velocity in the crashes. For this reason, the frontal structures always have enough space for the crashworthiness design. In many vehicles, there are three paths to transmit the impact load:

- 1) Path1: Accessories - Front bumper and Crash box - Front longitudinal beam-Engine - Firewall
- 2) Path2: Upper wing beam - A pillar - Guard beams of door;
- 3) Path3: Sub-frame - Sill beam

For most cases, the first path affords more than half of the total energy in crashes. Accordingly, the ideal crash process contains several stages:

- 1) Accessory crush. This is designed to protect the pedestrian. This stage is very short and nearly has no influence on the energy and velocity of vehicles.
- 2) Bumper crash and Crash box. The bumper is helpful in the low-speed crashes. Its ability for the energy absorbing is limited.
- 3) Longitudinal beam collapse. This part is responsible for crash compatibility, i.e. to protect the opposing vehicle in some extent and make the total lost lower in crashes.
- 4) Engine compression. Engine should be seen as a mass with limited deformation in crashes. In some high speed crashes, it will crush into the firewall and be compressed a little.
- 5) Firewall deformation. Firewall is much stronger than other components to protect the passenger cabin.

Crashworthy Structures

In most vehicles, longitudinal beams are designed as the crashworthy structures and employed for the energy absorbing. Although, the longitudinal beams can be various in terms of the material, section shape and processing technology, they follow the same requirement in design to optimise its performance:

- 1) No deformation in low speed crashes; Collapse progressively and absorbing the energy effectively in high speed crashes.
- 2) Having repeatable and reliable failure mode to ensure its performance in different crashes.

For this reason, the crashworthy structures of vehicles always experience a stable process of collapse during different crashes. In this process, the deformation follows a linear trend and have a series of oscillations.

To sum up, the crash processes of vehicles yield to an internal pattern, which is controlled by the load-carrying path and beam collapse mode. For this reason, a functional model is proposed to present the vehicle crash process.

CRASH MODEL

During a crash, the response signals contain several parts, which are corresponding to the crash stages. A piecewise model can be therefore identified by the accelerations and external force.

Piecewise Linear Model

There are some mathematical models of crash response in the literature, such as sine, triangular, and haversine [9]. However, none of them consider the vehicle structure and consequently are neither precise enough nor adjustable for different crash scenarios. To illustrate the proposed modelling process, NHTSA Test 5677, in which Yaris is crashing to a rigid wall in 56km/h, is employed for example.

Model structure The response of vehicle crashes can be recorded by the acceleration signals (crash impulses). Figure 1 shows the acceleration signal of the left rear seat during the crash and the proposed model structure.

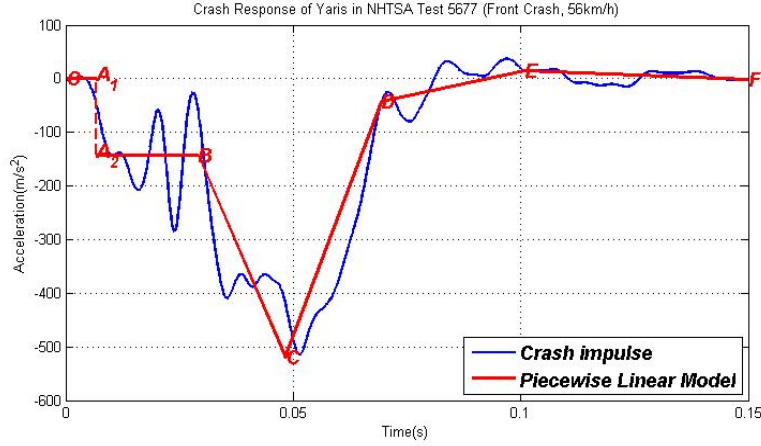


Figure1. Piecewise linear model structure for front crash of sedans.

Comparing with load-carrying path and crash stages presented above, the physical meaning of the model structure is as follows:

- 1) Original-A1 segment: The accessory are crushed and bumper deform. In this stage, there is no significant acceleration.
- 2) A2-B segment: The crash box and longitudinal beam are working. During this time, the acceleration is stable around a level.
- 3) B-C-D segment: The longitudinal beam keeps working and the engine is crashing to the firewall. The force worked on the firewall makes the sharp slowdown of the cabin.
- 4) D-E-End segment: Restitution process. The crumple area is fully compressed and most energy are absorbed. Some internal energy is released and leads the oscillation of velocity.

Although some local oscillations (the high frequency component of acceleration signals) are lost in this model structure, it reflects the trend (base mode) of acceleration in a full crash. Because the integration of the oscillations approaches zero [10], this model can keep a good performance in the estimation of velocity and displacement.

Time of model nodes In the presented model structure, the time and value of each node (i.e. A1, A2, and B~F) are to be decided. For O-A₁ stage, the acceleration is small and the variation of velocity is tiny. The end of this stage can be set as:

$$T_A = t_0, \text{ when } \Delta v(t_0) = \int_0^{t_0} a(t) dt = 1\% \times v_{init} \quad (1)$$

and

$$Acc_{A_1} = 0 \quad (2)$$

For node F, T_F is the end time of signals and the acceleration Acc_F is the value of end time. The times of other nodes are discussed in this part and the accelerations will be studied in the next part.

Comparing to A₂-B, the main feature of B-C-D process is that the engine is compressed by the firewall. The contact force slows down the cabin drastically. Correspondingly, the reacting force makes the deceleration of engine turn smaller (See Figure 2). So the time of B, T_B , is the time of minimum engine deceleration.

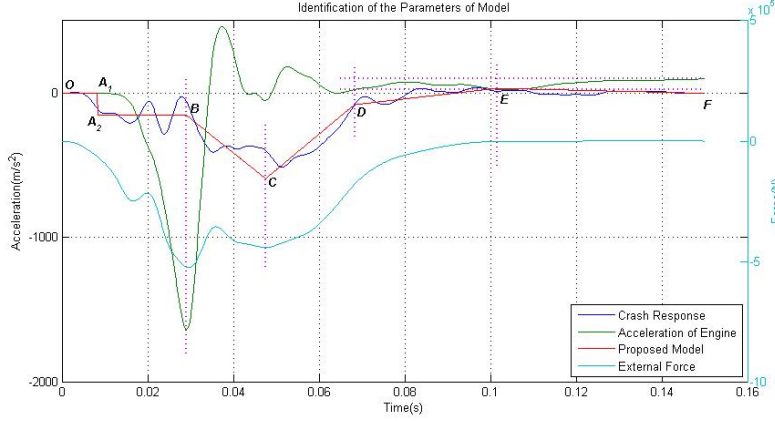


Figure2. Time Identification of Proposed Model Structure.

After T_B , the engine experiences a “step response” like process with the input of the reacting force from firewall and finally arrives the stable value when the time finished. So T_B can be set as the time when engine acceleration arrives the steady area. A recommended steady area can be seen from the maximum to the minimum value of engine acceleration after the T_E (will be given later).

Node C refers to the maximum deceleration in the crash process. Of course, it can be decided directly by the minimum point of crash response. However, in some cases, Acc_C is not significantly lower than the neighborhood and therefore T_C suffers a great uncertainty. This is because of the combined effect of the oscillations from engine and rest part of the vehicle. And neither of them plays a leading role. For these cases, an alternated method is given as below.

It should be noted that the crash response signal is measured from one point of the vehicle body. That means it cannot reflect the general response exactly perfect. To solve this problem, the external force, which works on the vehicle is to be studied (See Figure 2).

As shown, the first maximum force is corresponding to the node B and contributes to the maximum deceleration of the engine. The second maximum force is related to the Node C, as the engine acceleration is not significant at that period. So, T_C equals to the time of the second maximum force.

For the restitution stage, T_E is the time when external force falls to 1% of the maximum value.

Accelerations of model nodes The proposed model is hoped to make the error of acceleration and velocity small. For convenience in computation, the accelerations of B~E should ensure 1) $Acc_B \sim Acc_E$ locate near the real crash response; 2) the interaction of the proposed model, i.e. the velocity of model, is same with the real crash response at times T_B , T_D and T_F . So we can set $Acc_D = a(T_D)$ arbitrarily and decide the rest accelerations as follows:

1) To ensure

$$\int_0^{T_B} Acc(t) dt = Acc_B * (T_B - T_A) = \Delta v(T_B) \quad (3)$$

Acc_B is set as

$$Acc_B = \frac{\Delta v(T_B)}{T_B - T_A} \quad (4)$$

2) To ensure

$$\int_{T_B}^{T_D} Acc(t) dt = \frac{1}{2} Acc_B * (T_C - T_B) + Acc_C * (T_D - T_B) + \frac{1}{2} Acc_D * (T_D - T_C) = \Delta v(T_D - T_B) \quad (5)$$

$$\int_{T_D}^{T_F} Acc(t) dt = \frac{1}{2} Acc_D * (T_E - T_D) + Acc_E * (T_F - T_D) + \frac{1}{2} Acc_F * (T_F - T_E) = \Delta v(T_F - T_D) \quad (6)$$

Acc_C and Acc_E are set as

$$Acc_C = \frac{1}{T_D - T_B} \left[\Delta v(T_D - T_B) - \frac{1}{2} Acc_B * (T_C - T_B) - \frac{1}{2} Acc_D * (T_D - T_C) \right] \quad (7)$$

$$Acc_E = \frac{1}{T_F - T_D} \left[\Delta v(T_F - T_D) - \frac{1}{2} Acc_D * (T_E - T_D) - \frac{1}{2} Acc_F * (T_F - T_E) \right] \quad (8)$$

Models for Various Speed

To show the variance of the proposed model, a series of crashes are simulated by the FE method. In these crashes, the 2010 Toyota Yaris is crashing to a rigid wall at the speed of 20km/h, 25km/h, 32km/h, 40km/h,

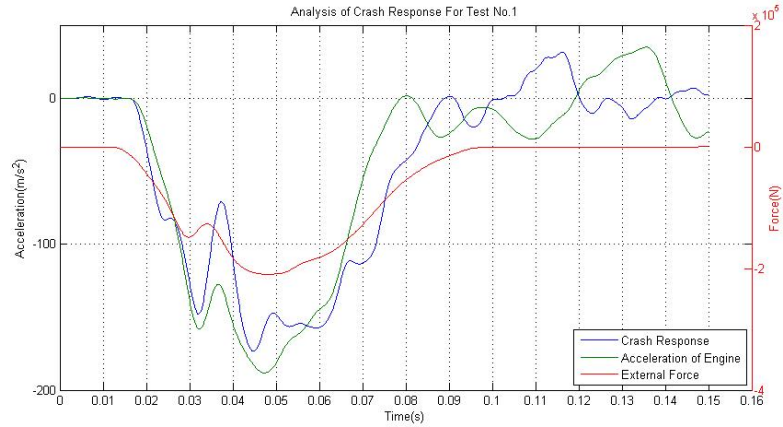
48km/h, 56km/h and 65km/h. The FE model of Yaris comes from the National Crash Analysis Center (NCAC) of George Washington University. The parameters of the modelling results are shown in the table (See Table 1).

Table1.
Parameters of modelling results for crash simulations in various initial velocities.

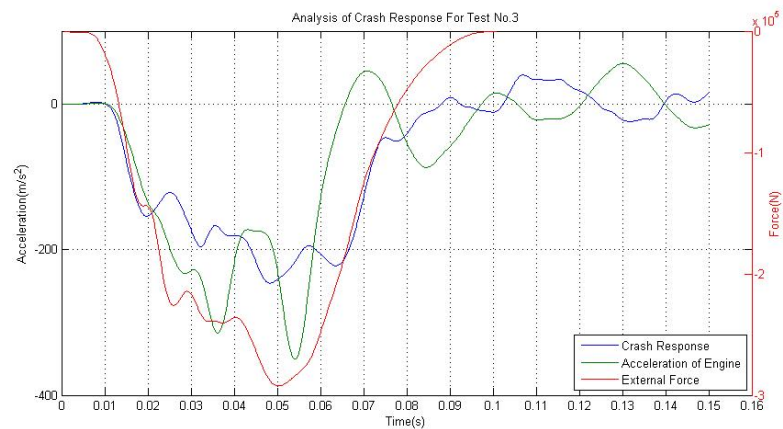
No.	Initial Velocity	At(s)/ A1(m/s ²)	Bt(s)/ B(m/s ²)	Ct(s)/ C(m/s ²)	Dt(s)/ D(m/s ²)	Et(s)/ E(m/s ²)	Ft(s)/ F(m/s ²)	Note
1	20km/h	0.0203 0	<i>0.0473</i> <i>-114.4992</i>	<i>0.1159</i> <i>-127.7229</i>	0.0736 -93.6547	0.1026 22.6533	0.1499 2.0482	Bad
2	25km/h	0.0172 0	0.0368 -125.1086	0.0569 -199.2543	0.0749 -87.6170	0.0985 20.3931	0.1499 -0.5908	Good
3	32km/h	0.0145 0	<i>0.0541</i> <i>-178.0036</i>	<i>0.1058</i> <i>35.2196</i>	0.0933 -3.2184	0.0989 -1.1863	0.1499 14.3759	Bad
4	40km/h	0.0125 0	0.0403 -187.4030	0.0516 -285.4251	0.0774 -84.9810	0.1030 37.3893	0.1499 -17.9486	Good
5	48km/h	0.0111 0	0.0337 -195.5635	0.0578 -379.2445	0.0745 -110.9681	0.0927 25.4419	0.1499 17.3587	Good
6	56km/h	0.0102 0	0.0330 -195.0890	0.0474 -484.4808	0.0873 40.1901	0.0963 40.0699	0.1499 -12.1832	Good
7	65km/h	0.0096 0	0.0278 -202.8010	0.0456 <i>-399.5320</i>	<i>0.1042</i> <i>44.3387</i>	0.1049 <i>21.1624</i>	0.1499 -22.8631	Bad
8	20km/h	0.0203 0	0.0323 -97.2563	0.0481 -172.514	0.0736 -93.6547	0.1026 22.6533	0.1499 2.0482	Good after adjustment
9	32km/h	0.0145 0	0.0362 -150.5192	0.0503 -229.4992	0.0933 -3.2184	0.0989 -1.1863	0.1499 14.3759	Good after adjustment
10	65km/h	0.0096 0	0.0278 -202.8010	0.0456 -500.0374	0.0905 38.564	0.1049 35.1197	0.1499 -22.8631	Good after adjustment

This table shows that:

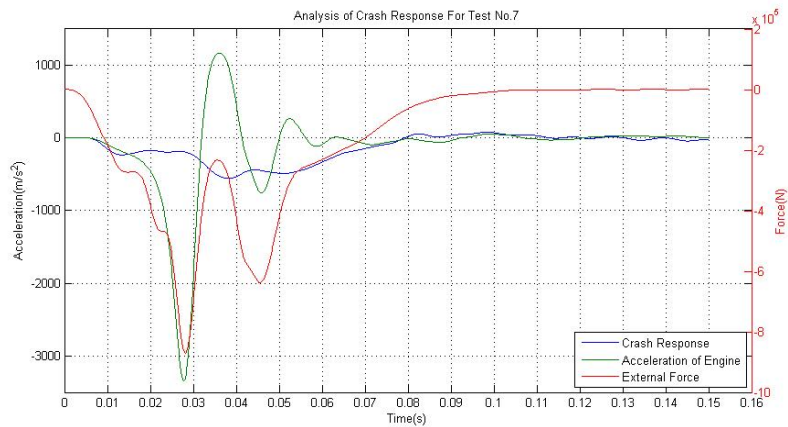
- 1) Generally speaking, the model has good applicability for the crashes with the initial velocity from 25~56km/h.
- 2) For the No. 3, the model has a wrong identification of T_B and T_C and therefore fails to fit the crash response. By studying the crash responses of 32km/h crash (See Figure 3b), it can be found that the engine acceleration at 0.0362s is the first local minimum value with the abrupt turn of trend. According to the physical meaning, this abrupt turn refers to the contact between the engine and firewall and T_B should be 0.0362s. Consequently, T_C is 0.0503s. After this adjustment (as No. 9), the model fits the crash response well. This is because of the less compression of the engine in the lower speed crashes. So for the crashes with initial speed lower than 32km/h, it is highly recommended to check the model again according to the physical meaning.
- 3) No. 1 suffers similar problems with Test 3 and can be adjusted (as No. 8) to achieve good performance. However, the minimum value is not much lower than other values in this crash response (See Figure 3a). Specifically, the process B~D (i.e. the engine influence) is not as significant as other crashes. This means the crash process, as well as model structure, is different from high speed crashes. For this reason, the proposed model may cannot represent the responses well for the crashes with initial velocity lower than 20km/h.
- 4) No. 7 is for the 65km/h crash and have a problem in the identification of T_D . In the crash responses (See Figure 3c), there are oscillations with big amplitude in the process D~E and lead the wrong identification. Obviously, in this crash, the vibration of the engine is much stronger than 56km/h crash. An adjustment can be made manually to improve the model (as No. 10). But it should be mentioned that for a higher speed crash, the model can hardly present the crash process very well.



a) Crash Responses and References of No.1 Simulation



b) Crash Responses and References of No.3 Simulation

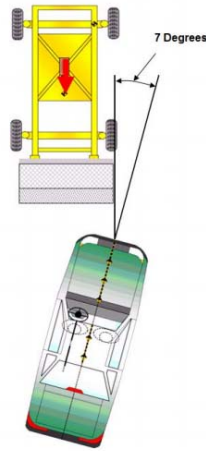


c) Crash Responses and References of No.7 Simulation

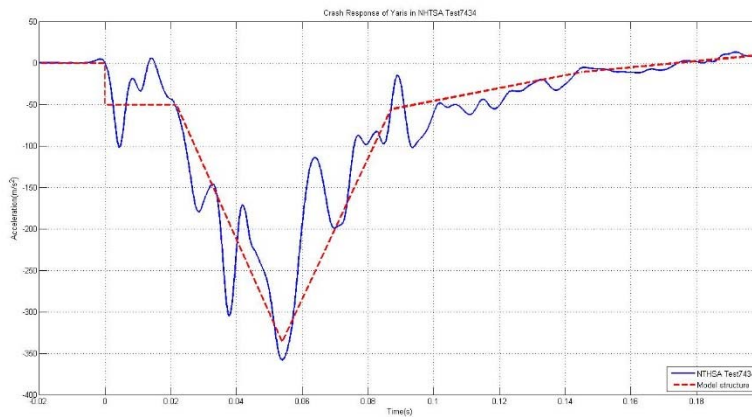
Figure3. Crash Responses and References (a. No.1; b. No.3; c. No.7).

Complex Condition

In this subsection, a full car crash test will be studied. In this crash, the Yaris is crashed by a moving deformable barrier (RMDB) with a target speed of 86.7 km/h. The crash mode is 7° angle and 20.6% offset (See Figure 4a). The test data come from NHTSA Test 7434.



a) Configuration of NHTSA Test 7434



b) Crash Responses and Modelling of NHTSA Test 7434

Figure4. NHTSA Crash Test 7434 (a. Crash Configuration; b. Crash Response)

From this response, we can find that:

- 1) Because of the deformable barrier, the maximum acceleration in this test is 358.3208m/s^2 in negative direction, which is near the value in 40km/h rigid wall crash. So it is possible to have an experience that the maximum acceleration of a deformable barrier crash can be estimated by the rigid wall crash with half speed. Of course, this is a rough estimation and the barrier should have similar mechanical characteristics as the vehicle body.
- 2) In $0\sim 0.02\text{s}$, the bumper, crash box and longitudinal beam are deforming. But due to the offset, only left half part of the crush zone is crushed and therefore this crash response during this time is different from 100% overlap crash. The most important difference is the average value in this period is about 50m/s^2 , which is about only 1/ the Acc_B in No. 4 of Table 1. In other words, the absorbed energy is much lower than the full overlap crash
- 3) There is also a process like B-D in the model, which indicates that the engine is also crushed into the firewall and compressed. This shows all the crashworthiness structures will work in the crashes with an offset.

In conclusion, this crash test can also be described roughly by the proposed model structure, shown as the red dash line in Figure 6b. However, some local performances are different, such as the mode of B-C stage. And consequently the related parameters should also be revalued.

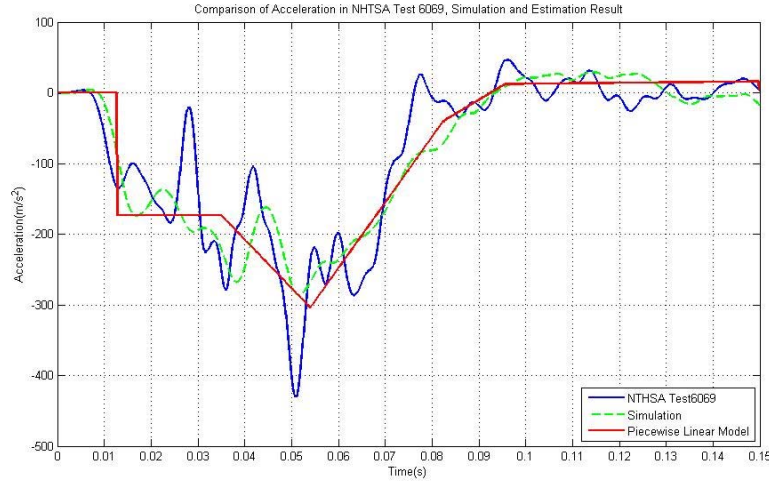
ESTIMATION OF VEHICLE KINEMATICS

The proposed model can be used for the estimation of vehicle kinematics. The NHTSA Test 6069 can be used as an example. The crash condition is: 39.6km/h full overlap crash to a rigid wall barrier. To make an

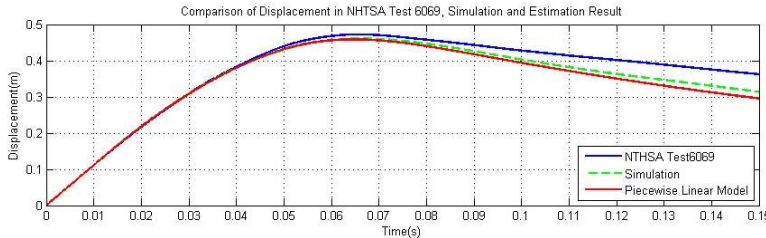
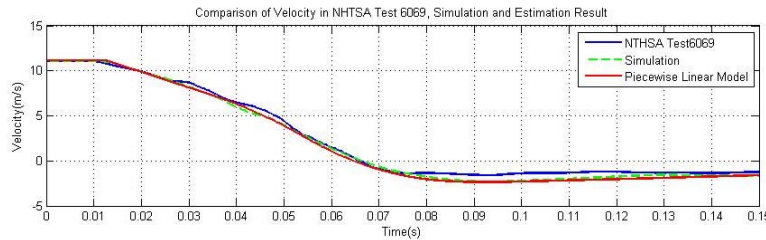
estimation, the parameters of the proposed model can be set as the average value of No. 5 and No. 9 in Table 1. That is $A_t = 0.0128$, $Acc_A = 0$, $B_t = 0.0350$, $Acc_B = -173.0414$, $C_t = 0.0541$, $Acc_C = -304.3719$, $D_t = 0.0825$, $Acc_D = -40.4034$, $E_t = 0.958$, $Acc_E = 12.3273$, $F_t = 0.1499$ and $Acc_F = 15.8673$.

Note: the T_D of No. 9 is obviously higher than other T_D . This may be because of the uncertainty of simulations. To get better estimation, the estimation of T_D and Acc_D should be adjusted as the average of No. 2-6, as the 39.6km/h is the average of the corresponding velocities.

The estimated model will be compared with the Test 6069 and simulation result (See Figure 5).



a) Acceleration Signals



b) Velocity and Displacement Signals

Figure5. Validation of the estimation (a. Acceleration; b. Velocity & Displacement)

As shown in Figure 5, the estimated results fit the test and simulation very well. The displacement error (about 0.0668m) at the end of time, which is similar with the simulation (about 0.0460m).

CONCLUSIONS

Comparing to finite element models and multibody modes, the mathematical models have advantages on conciseness and usability. For this reason, the mathematical models can be used in the early design of vehicles, as well as accident reconstruction. This paper presents a novel modelling scheme of crashes, which is based on the acceleration signals and vehicle structure. The proposed model can reflect the crash process clearly and therefore describe the crash response exactly. In addition, this model suits for the crash in various conditions

by adjusting the parameters. At the end of paper, an estimation of vehicle kinematics shows the good performance of the proposed model for a frontal crash at 40km/h.

REFERENCES

- [1] Pawlus, W., Robbersmyr, K. G. and Karimi, H. R. 2014. "Investigation of vehicle crash modeling techniques: theory and application." *International Journal of Advanced Manufacturing Technology*, 70(5-8), 965-993.
- [2] Hamza, K. T. 2008. "Design for vehicle structural crashworthiness via crash mode matching". ProQuest.
- [3] Huang, Matthew. 2010. "Vehicle crash mechanics". CRC press.
- [4] Kamal, M. M. 1970. "Analysis and simulation of vehicle to barrier impact." No. 700414, SAE Technical Paper.
- [5] Pawlus, W., Robbersmyr, K. G. and Karimi, H. R. 2011. "Mathematical modelling and parameters estimation of a car crash using data-based regressive model approach." *Applied Mathematical Modelling*, 35(10), 5091-5107.
- [6] Simpson, T. W., Booker, A. J., Ghosh, D., Giunta, A. A., Koch, P. N. and Yang, R. J. 2004. "Approximation methods in multidisciplinary analysis and optimization: a panel discussion." *Structural and multidisciplinary optimization*, 27(5), 302-313.
- [7] Karimi, H. R. and K.G. Robbersmyr. 2011. "Signal analysis and performance evaluation of a vehicle crash test with a fixed safety barrier based on Haar wavelets." *International Journal of Wavelets, Multiresolution and Image Processing*, 9(1), 131-149.
- [8] Zhao, L., Pawlus, W., Karimi, H. R. and Robbersmyr, K. G. 2014. "Data-based modeling of vehicle crash using adaptive neural-fuzzy inference system." *Mechatronics, IEEE/ASME Transactions on*, 19(2), 684-696.
- [9] Varat, M. S. and Husher, S. E. 2003. "Crash pulse modelling for vehicle safety research. In Proceedings of International Technical Conference on the Enhanced Safety of Vehicles. " National Highway Traffic Safety Administration.
- [10] Chou, C. C., Le, J., Chen, P. and Bauch, D. J. 2001. "Development of CAE simulated crash pulses for airbag sensor algorithm/calibration in frontal impacts." In 17th International Technical Conference on the Enhanced safety of Vehicles, Amsterdam.

EFFECT OF FMVSS 226 COMPLIANT CURTAIN AIRBAGS ON THE BRIC RESULT OF A HYBRID III 50TH% DUMMY DURING AN OBLIQUE IMPACT

John Cadwell

Eugene Lee

Aviral Shrivatri

Shiro Ohara

Toyota Gosei North America Corporation

United States of America

Hiroaki Yamada

Michihisa Asaoka

Toyota Gosei Co., Ltd.

Japan

Paper Number 15-0367

ABSTRACT

The proposed oblique impact test with a Research Moving Deformable Barrier (RMDB) by the National Highway Traffic Safety Administration (NHTSA) is designed to represent crashes involving partial longitudinal structural engagement between vehicles. The RMDB moves at a speed of 56mph (90kph), with a small overlap of 35% and an impact angle of 15°, into a stationary vehicle. In addition, the newly developed Test Device for Human Occupant Restraint (THOR) dummy and the Brain Injury Criterion (BrIC) are used to evaluate the injury risk. The implementation of these test modes and measurement techniques will raise the bar for performance of passive safety systems.

Meanwhile, the introduction of the Federal Motor Vehicle Safety Standard 226 (FMVSS 226) as a countermeasure for ejection mitigation during a rollover has increased the occupant protection area of side curtain airbags (SCAB). As a result, SCAB designs have incorporated increases in height, width, and depth, depending on the interaction of the airbag with the vehicle's interior. This dimensional change in FMVSS 226 compliant SCAB, while yielding positive results in side impact and rollover crashes, may also play a critical role in the prevention of injury for the NHTSA oblique test mode. This study examines the effect of the expanded occupant protection coverage of FMVSS 226 compliant SCAB on BrIC results during an oblique impact. This study used publicly available oblique pulse data (published by NHTSA) in a Finite Element (FE) model with a Hybrid III 50th% dummy to perform an oblique impact test. The interior environment of the FE model was obtained by digitizing a generic buck and morphing available FE models from the National Crash Analysis Center (NCAC) database. The FE model was validated with a belted 35mph frontal impact test (FMVSS 208) and then used for the oblique impact analysis. This study examines three oblique FE models, each consisting of a different configuration of restraint systems. The first configuration did not utilize a SCAB; the second configuration had a non-FMVSS 226 compliant SCAB; and the third configuration had a FMVSS 226 compliant SCAB. In order to assess the effect of SCAB design, only the upper body results of the dummy were compared and analyzed. Differences in injury response were observed between the three configurations when evaluating the head acceleration, head rotation, and chest deflection. A significant improvement was observed in the BrIC result for the FMVSS 226 compliant SCAB when compared with the other two restraint system configurations tested. Though this study is design-specific, appropriate explanations are provided to support the study.

INTRODUCTION

Despite continuous improvement to passive restraint systems, serious injuries and fatalities still occur during a crash event, even when all restraint systems operate as designed. Recently, oblique vehicle-to-vehicle impacts have been identified as a high risk scenario for occupants by the National Highway Traffic Safety Administration (NHTSA), and further supported by Rudd *et al.*, [2011]¹, wherein the vehicle's longitudinal structural members are only partially engaged. NHTSA has developed a test procedure to address this crash mode, refining the criteria for an oblique test method as a 35% overlap, at an angle of 15° (345 Degrees PDOF), impacting a stationary vehicle with a newly developed (Research Moving Deformable Barrier) RMDB that travels at 56mph (90kph)². This test mode has

introduced new challenges in occupant safety system design, as the resulting kinematics cause limited engagement of the frontal and side restraint systems by the occupant. This has led to an increased focus in the automotive industry on the protection of the occupant by the side and curtain airbags during these types of crash modes. Early research of the occupant kinematics and resulting injury modes in the oblique condition led to the creation of the Brain Injury Criterion (BrIC), presented in its most current form by Takhounts *et al.* [2013]³. The BrIC is measured using the X-, Y-, and Z-axis angular velocities of the head, and is intended to capture the risk of brain injuries as a supplement to the translational acceleration measurement used to calculate the Head Injury Criterion (HIC). Due to the occupant kinematics found in oblique crash conditions, a high level of head and torso rotation and excursion may result, making BrIC a critical measurement for establishing safety system performance. The FMVSS 226 test protocol was formally introduced in 2013 to prevent the ejection of occupants during a rollover crash, and has led to improved SCAB coverage in the X-, Y-, and Z-directions in-vehicle. This study will examine the effect of the utilization of an FMVSS 226 compliant side curtain airbag (SCAB) as it relates to occupant kinematics and BrIC results during an oblique test.

METHODS

Background

The newly developed NHTSA oblique test condition is specified as a Near-Side collision, wherein the RMDB impacts a stationary vehicle at 90kph, with a 35% overlap and an impact angle of 15° (Figure 1).

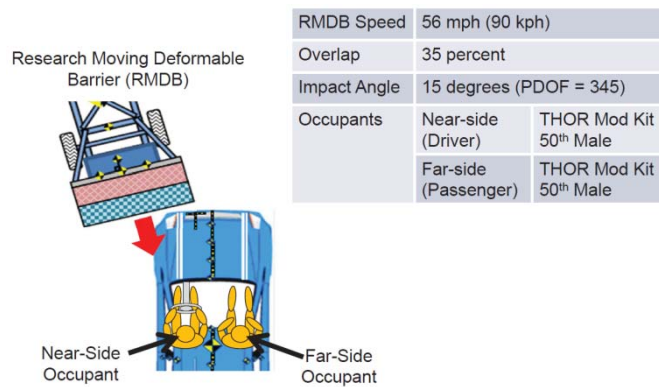


Figure 1. NHTSA Oblique RMDB Test Configuration.

Previous research has found that the new NHTSA oblique test mode introduces an increase in injury risk primarily to the Head, Chest, and Lower Legs, due to the angle of impact and intrusion levels observed in testing⁴. BrIC is a recently established head injury metric developed by Takhounts *et al.* [2013] which uses the maximum angular velocity (ω) measured about the X-, Y-, and Z-axes to determine the risk of injury to the brain due to rotational velocity of the head. For this study, BrIC was calculated using the equation in Figure 2.

Critical Angular Velocity	Rad/s
ω_{xC}	66.25
ω_{yC}	56.45
ω_{zC}	42.87

Where ω_x , ω_y , and ω_z are maximum angular velocities about X-, Y-, and Z-axes respectively, and ω_{xC} , ω_{yC} , and ω_{zC} are the critical angular velocities in their respective directions.

$$BrIC = \sqrt{\left(\frac{\omega_x}{\omega_{xC}}\right)^2 + \left(\frac{\omega_y}{\omega_{yC}}\right)^2 + \left(\frac{\omega_z}{\omega_{zC}}\right)^2}$$

Figure 2. BrIC Calculation based on Takhounts *et al.* [2013].

This study is concerned with the design and presence of installed SCABs, and their effect on both the BrIC value, and the overall reduction in head rotation.

Model Development and Validation

Before developing an oblique test method in computer-aided engineering (CAE), dummy kinematics and injury performance for an NCAP frontal crash were examined and validated using data from (3) developmental sled tests performed in-house. In order to correlate with the frontal NCAP sled testing, a Hybrid III dummy was used in the CAE environment.

For the frontal model validation, safety system components were chosen to match those used in the developmental sled program, and demonstrated good stability. The components used included a driver airbag (DAB), knee bolster airbag (KAB), and a 3-point seatbelt utilizing a pre-tensioner and load limiter. Simulations were then performed in CAE using the acceleration data used in the sled environment, and the results were analyzed. Upon reviewing the results, the CAE tests showed good correlation in Head, Chest, and Pelvis acceleration in both magnitude and phase, while Chest Deflection showed good correlation during loading, but exhibited a shorter duration than was observed on sled. Femur force was measured for both left and right femurs, and while the right femur showed good correlation to NCAP sled test data, the left femur exhibited higher magnitude and duration of loading than the physical tests (Figure 3). After evaluating the injury response by the upper body, it was decided to move forward with development of an oblique test setup in CAE, as the correlation to physical sled testing for occupant response in a frontal impact was good.

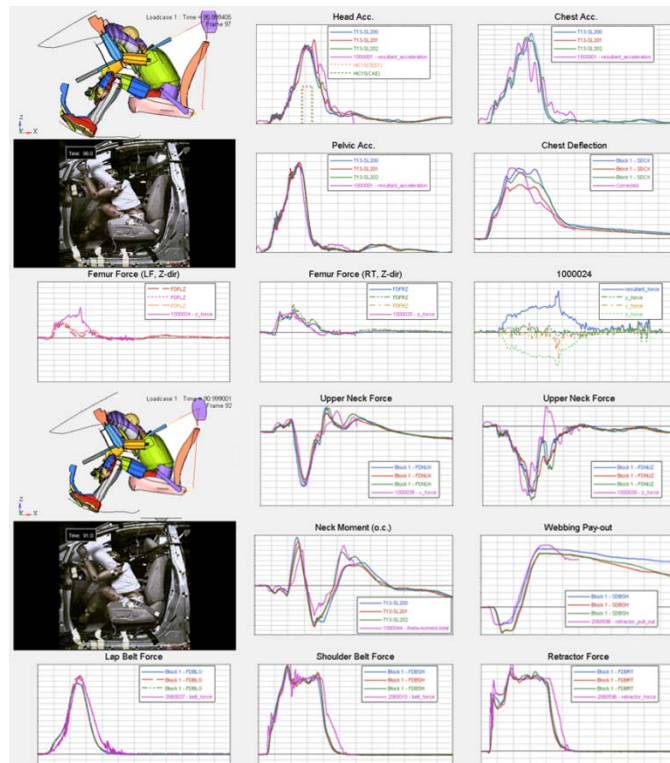


Figure 3. Frontal Impact Validation with Sled Series.

Three test conditions were chosen for examination of the SCAB effect on occupant kinematics in the oblique test condition. The first condition consisted of running the simulation with no SCAB present, utilizing only the DAB, KAB, and a pre-tensioning seatbelt with load limiter. In order to examine the benefit of an FMVSS 226 compliant SCAB, two SCAB models were used for the two subsequent tests. The first SCAB was a non-FMVSS 226 compliant, 2-row airbag, with a 50L capacity and an inflator whose output was 230kPa. Meanwhile, the FMVSS 226 compliant SCAB that was used in this experiment had a volume of 62L, and an inflator output of 350kPa. In the FMVSS 226 compliant SCAB, additional cells were added (Figure 4), and the airbag coverage was expanded in both the X- and Y-directions, relative to the vehicle coordinate system.

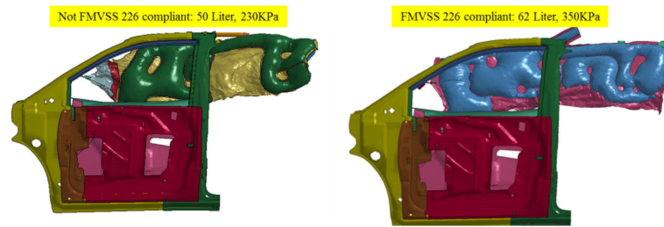


Figure 4. Comparison of Non-FMVSS 226 compliant, and FMVSS 226 compliant SCAB.

In order to establish an oblique acceleration to be used in the CAE model, a desktop review of NHTSA-published oblique pulse data was performed in order to find a pulse representing a stiff vehicle response. The acceleration data from the NHTSA database was selected⁵, and the X- and Y-direction accelerations were input into CAE, with an impact location at the front left corner of the vehicle. This allowed the model to experience the same vector of acceleration as the NHTSA test, without incorporating vehicle rotation into the study. A Hybrid III 50th male dummy was used for the CAE oblique testing. The Hybrid III exhibits a slightly different kinematic response and lower injury values than the THOR in physical testing when a significant vehicle Y-displacement is observed⁶. However, the Hybrid III model is very stable, and since the physical dummies are readily available, CAE oblique test results could be more easily confirmed at a later time through sled testing. The dummy was positioned using the setup numbers from the frontal sled tests, providing a uniform starting point for each simulation. SCAB modeling utilized a roll fold, and was then inflated at a time-to-fire (TTF) consistent with the published data, using the corpuscular particle method available in LS-DYNA to achieve full and representative deployment.

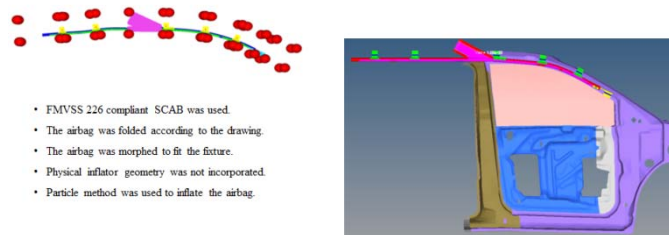


Figure 5. SCAB Morphing and Inflation.

Once the variables for the simulation were set, tests were performed for each of the three SCAB conditions, and results were compared.

RESULTS

The simulation results for the SCAB performance and occupant behavior are presented and discussed below. Each of the three conditions simulated created marked differences in occupant kinematics as well as occupant injury response. The BrIC value, which is the injury factor of interest in this study, is evaluated in relation to the presence and design of the SCAB for each simulation.

Occupant Kinematics

For all three CAE simulations, the occupant exhibited forward and outboard movement consistent with that found during NHTSA oblique testing. The overall occupant kinematics were very similar in each test, as the seatbelt response was consistent throughout the experiment. However, in the absence of the SCAB, the occupant's head showed the greatest lateral movement of any configuration, as the head was unrestrained in its movement in the Y-direction (Figure 6).

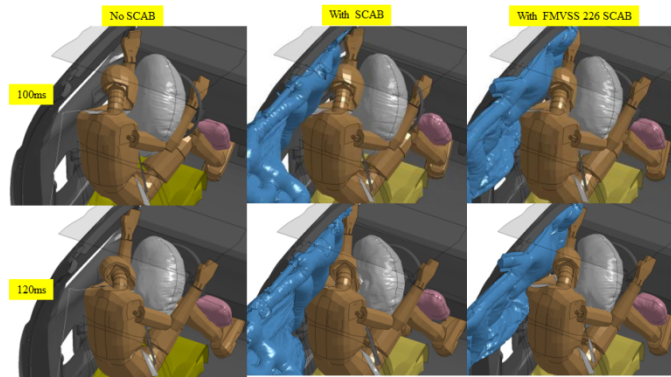


Figure 6. Simulation Results - Occupant Kinematics Comparison.

The head angular velocities for CAE were compared to the published data for the NHTSA oblique test⁵ (Figure 7). The magnitude of the velocity for each direction of rotation was exhibited slight differences, but the location and timing of each peak were consistent between CAE results and the published data. This comparison demonstrated that kinematically, the CAE model was representative of the motion seen by the occupants in the NHTSA oblique test method.

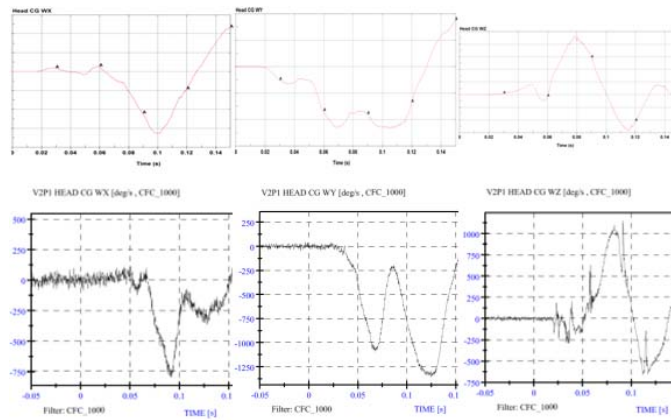


Figure 7. Head Angular Velocity - CAE vs NHTSA Results.

As seen in Figure 8, the increased chamber size in the Y-direction of the FMVSS 226 compliant SCAB creates contact with the occupant's head sooner in the crash event, limiting lateral movement and minimizing rotation. The early contact creates a counter-rotation effect that reduces the overall angular velocity for the event.

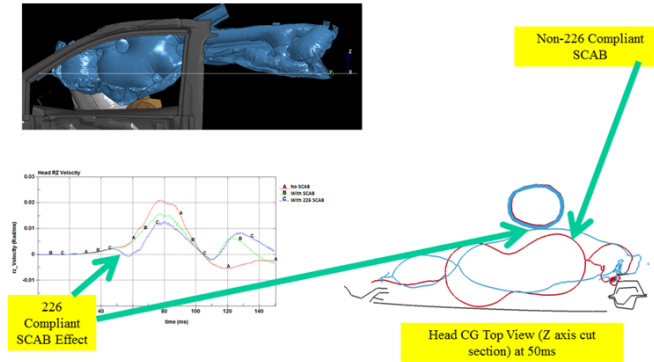


Figure 8. Head Rotation about Z-axis - 226 SCAB Reduction Effect.

BrIC Performance

In the baseline study, with no SCAB present in the simulation, the occupant exhibited forward and outboard movement. The DAB was contacted left-of-center, and the occupant’s head proceeded to move outboard toward the door trim; however, the occupant’s head made no contact with the door. The head experienced significant angular velocity about the X-axis (41.124 rad/s), as well as an elevated ω_z (21.163 rad/s), resulting in a BrIC score of 0.8725. Of the three CAE simulations, the baseline test resulted in the highest BrIC score. The second test incorporated a SCAB into the safety system design, yielding changes in the kinematics of the occupant. In this simulation, the occupant trajectory was similar to the baseline study; however the presence of the SCAB guided the head during forward movement, reducing the ω_z to 15.931 rad/s, while the ω_x result (41.552 rad/s) matched the baseline, and a reduction of 5.517 rad/s was seen in ω_y . The BrIC score for the second simulation was 0.8647.

In the final simulation, a change in occupant head kinematics was observed during interaction with the DAB and SCAB. The FMVSS 226 SCAB contacts the occupant’s head earlier in the crash event, inducing a counter-rotation that limits the magnitude of the peak angular velocity (Figure 8). As a result, ω_z was reduced to 12.772 rad/s, the lowest of all three of the simulations, while ω_x saw a reduction as well, showing a peak angular velocity of 25.519 rad/s. These reductions in angular velocity resulted in the lowest BrIC score for all three scenarios, at 0.655, representing a 24.2% reduction in BrIC when compared to the non-FMVSS 226 compliant SCAB. The BrIC values for each test are shown in Figure 9 and Table A1 in Appendix A.

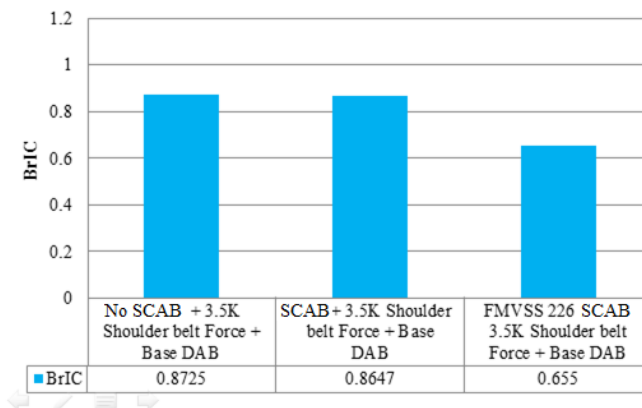


Figure 9. BrIC Review for SCAB Configurations.

Figure 10 shows the head angular velocity characteristics for each direction of rotation. Of note within this data is the reduction in magnitude of rotation about the X- and Z-axes for the FMVSS 226 compliant SCAB.

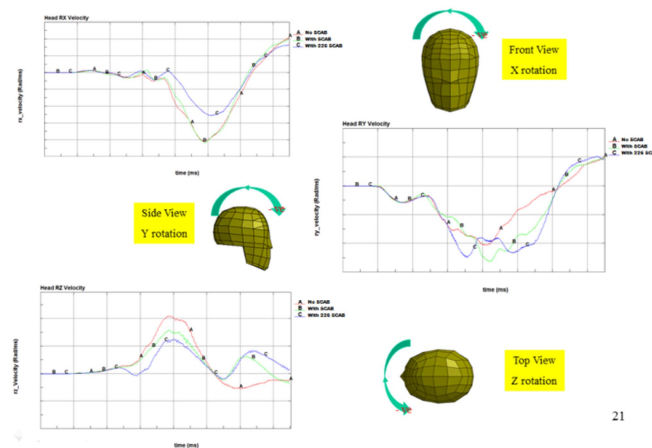


Figure 10. Head Angular Velocity Comparison.

CONCLUSIONS

This study has demonstrated that early engagement of a driver side occupant's head in an oblique impact using an FMVSS 226 compliant SCAB can reduce the rotation and angular velocity about the X- and Z-axes, thus reducing the overall BrIC score in a CAE test environment. This study acknowledges several limitations, including, but not limited to, the following:

- This study shows vehicle- and design-specific results using CAE. An analysis of a broad range of vehicle platforms and SCAB designs would be beneficial to reinforce the results reported herein.
- Using the Hybrid III CAE model may underrepresent injury risk in certain body regions. Additional CAE research using the THOR model may provide further insight into the effect of the FMVSS 226 compliant SCAB on BrIC.

Further CAE and sled testing is recommended to verify the performance of different FMVSS 226 compliant SCAB designs in different vehicle environments.

REFERENCES

- [1] Rudd, R., Scarboro, M., and Saunders, J., "Injury Analysis of Real-World Small Overlap And Oblique Frontal Crashes." 22nd International Technical Conference on the Enhanced Safety of Vehicles, Paper number 11-0384, (2011)
- [2] Saunders, J., Craig, M., and Parent, D., "Moving Deformable Barrier Test Procedure for Evaluating Small Overlap/Oblique Crashes." SAE Paper 2012-01-0577, (2012)
- [3] Takhounts, E., Craig, M., Moorhouse, K., McFadden, J., and Hasija, V., "Development of Brain Injury Criterion (BrIC)." Stapp Car Crash Journal, Vol. 57, (2013)
- [4] Saunders, J., and Parent, D., "Repeatability of a Small Overlap and an Oblique Moving Deformable Barrier Test Procedure" SAE Paper 2013-01-0762, (2013)
- [5] National Highway Traffic Safety Administration, Vehicle Crash Test Database, Test No. 8097 (<http://www-nrd.nhtsa.dot.gov/database/VSR/veh/VehicleInfo.aspx?LJC=8097>)
- [6] Guerrero, M., Butala, K., Tangirala, R., and Klinkenberger, A., "Comparison of the THOR and Hybrid III Responses in Oblique Impacts," SAE Technical Paper 2014-01-0559, (2014)

APPENDIX A

Angular Velocity (Rad/s)	No SCAB – CAE Result	With SCAB – CAE Result	With FMVSS 226 SCAB – CAE Result
ω_x	41.124	41.553	25.519
ω_y	20.539	26.253	24.784
ω_z	21.163	15.931	12.772
BrIC	0.8725	0.8647	0.655
HIC15	280.9	311.7	492.5

Table A1. BrIC & Angular Velocity Detailed Results.

STUDY ON THE SAFETY PERFORMANCE OF THE REAR SAFETY GUARD WITH AIR BAG FOR TRUCK

In-Song PARK,
Smart Air Chamber Co., Ltd.
Republic of Korea

Kyung-Won YUN, Kwang-Jong PARK, Hyo-Jun KIM
Smart Air Chamber Co., Ltd.
Republic of Korea

Paper Number 15-0033

ABSTRACT

Although the Korea government promotes the movement of safe traffic to reduce deaths in traffic accidents, the number increases every year.

Especially more and more accidents and casualties are reported from the cases of car collision to the back of the vehicles parked for managing car accident on road, cleaning of main roads, side roads and medial strip, and road repair.

Therefore, it has been along that the government should be responsible for taking a protective measure for road users.

71 cases have been reported to occur during highway repair and maintenance. As the result, 8 were dead and 76 were injured, showing the death rate of 11.3%, which is quite high.

So it seems urgent to take some action against it.

America and European countries legislate that vehicles of road repair and maintenance should be mandatorily equipped with shock absorber on car but our country lacks in a legislative measure, which is asked to be done.

Accordingly, this study compares the performance standards of shock absorber for road maintenance vehicle by applying country to establish the criteria.

In addition, it tries to interpret in theory the Rear Safety Guard using Air Bag and compare the safety performance test of a vehicle with the Rear Safety Guard manufactured in accordance with related laws and that using Air Bag.

Based on the result of the safety performance on the 60km/h Rear collision Test, this study proposes improvement in related regulations and laws in an attempt to reduce collision and death by proposing the Traffic Injury Prevention effect of the Rear Safety Guard using Air Bag.

INTRODUCTION

Deaths & casualties by vehicles are getting grow though government provide more developed safety standard in order to reduce them.

Especially, rear-end collisions to the working trucks on the road, which are on cleaning road, treating accident or road maintenance, cause fatal injuries.

That's why social responsibilities for them has been issued since long time ago.

For the last 10 years, 71 cases of rear-end collisions to the working trucks in the highway have incurred, of which 8 persons were dead, 76 persons were injured, which shows remarkable 11.3% of death rate. Accordingly, we need to take urgent measurement against them.

Especially, Under-ride accident, which means rear-end collision car burrow down beneath under working truck, cause fatal influence to the passenger life.

Nowadays, it is compulsory to install Rear Safety Guard in order to prevent such under-ride accident.

It is possible to prevent under-ride accident if Rear Safety Guard is installed as per current installation intensity standard. However, it regulates only shock absorption which may cause fatal shock to the passenger.

This Study issues necessity of regulation amendment to reduce passenger casualties and guides characteristics of shock absorption Rear Safety Guard. In order to provide comparison data, we make use of both Airbag Rear Safety Guard and the Conventional Rear Safety Guard in the performance test of rear collision with 60km/h velocity.

STRUCTURE OF REAR SAFETY GUARD AND THEORETICAL CONSIDERATION

Structure of Rear Safety Guard

Comparing structure of both Rear Safety Guards, the Conventional Rear Safety Guard has cross section of quadrangle beam and Airbag Rear Safety Guard is consist of Control Case and Borer fixed bracket. Control Case prevents rebound of rear-end collision vehicle with air occupied space using TPU (Thermoplastic Polyurethane).

Therefore, difference between the both Rear Safety Guards is, the Conventional Rear Safety Guard has only quadrangle beam to endure loading specified installation intensity by standard, however, Air bag Rear Safety Guard consist of rear Bracket enduring loading specified by standard, at the same time, air in the TPU absorbing 1st shock by TPU Elongation & Control case under low velocity and Borer absorbing 2nd shock by emitting air, simultaneously, minimizing rebound of rear-end collision vehicle.

Air bag Crush Movement Theory

The follows theoretical formula becomes as follows

A body, which has mass m with initial velocity v^0 , drops toward an elastic body.

Assume that the deformation of an elastic body is one-dimension and the material is compressible in order to make a formula for describing the moving of a colliding body.

σ is true stress and ε is true strain.

$$\sigma = f(\varepsilon), \varepsilon = \ln \frac{l}{l_0}$$

l_0 is the initial thickness of an elastic body, and l is the thickness after deformation.

$$F = \sigma A = f(\varepsilon) A$$

Volume changes after deformation because an elastic body is compressible

$$\alpha A_0 l_0 = A l$$

α is the rate of volume, A_0 is the initial area of deformation, and A is the area after deformation.

$$\text{If } l_0 - l = x, \text{ then } A = \alpha \frac{l_0}{l_0 - x} A_0$$

$$F = \alpha f(\varepsilon) \frac{l_0}{l_0 - x} A_0$$

Therefore, the momentum equation of the colliding body is

$$m \frac{d^2 x}{dt^2} = -\alpha f(\varepsilon) \frac{l_0}{l_0 - x} A_0$$

Considering the effect of gravity, the equation is as follows

$$m \frac{d^2 x}{dt^2} = -\alpha f(\varepsilon) \frac{l_0}{l_0 - x} A_0 + mg \text{ Formula of(1)}$$

Two initial conditions are necessary to solve the above equation. In case of small deformation, we can rewrite equation as

$$\frac{l_0}{l_0 - x} \cong 1$$

$$f(\varepsilon) = E\varepsilon = E \ln\left(\frac{l_0}{l_0 - x}\right) \cong E \frac{x}{l_0}$$

If we neglect the effect of gravity

$$m \frac{d^2x}{dt^2} = -\alpha E \frac{x}{l_0} A_0 \text{ Formula}$$

Formula of (2)

If we solve the equation (2) with two initial conditions, $x(0) = 0$ and $\frac{dx}{dt} = V_0$
The formula becomes as follows

$$x(t) = V_0 \sqrt{\frac{ml_0}{\alpha EA_0}} \sin \sqrt{\frac{\alpha EA_0}{ml_0}} t$$

And equation (1) becomes

$$F = m \frac{d^2x}{dt^2} = -V_0 \sqrt{\frac{\alpha EmA_0}{l_0}} \sin \sqrt{\frac{\alpha EA_0}{ml_0}} t$$

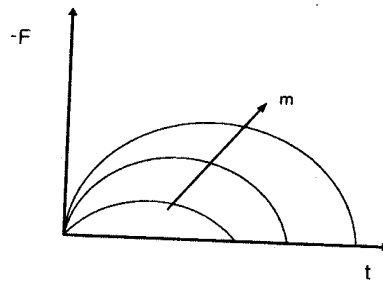
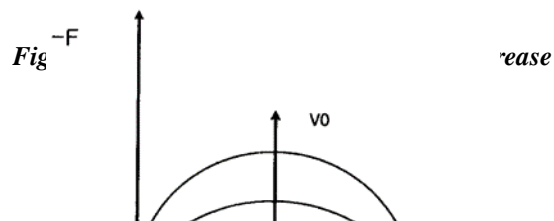
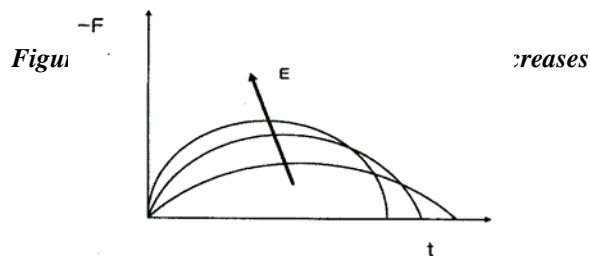


Figure 1. *F-t* curve in the mass of the colliding body increase



We can recognize that the relation between force and time is sine curve. Let us consider the effect of several variables.

The more the mass of the colliding body increases, the more the magnitude of the force and the period increase. When the elastic modulus increases, the force increases and the period become shorter. When the initial velocity increases, the force increases, but the period stays same.

A body, which has mass m with initial velocity V_0 , drops toward an elastic body. Assume that the deformation of an elastic body is one dimension and the material is compressible in order to make a formula for describing the moving of a colliding body. σ is true stress and ϵ is true strain drops toward an elastic body. Assume that the deformation of an elastic body is one-dimension and the material is compressible in order to make a formula for describing the moving.

The tensile strength of the thermoplastic polyurethane is 440 kgf/cm² and the tensile stress(at 300% elongation) is 260 kgf/cm².

TEST AND CONSIDERATION

Test Facility

Collision test facility strictly follows clause No. 102 evaluation on passenger protection at the time of collision of Vehicle safety standard.

Towing collision test facility was made to test 60km/h velocity of collision.

Figure1, Figure2 shows collision test facility and test method respectively.

Test standard is Head-on center impact of Figure.2 (a).



Figure 4-(a). Cable Draw Type collision Test Equipment

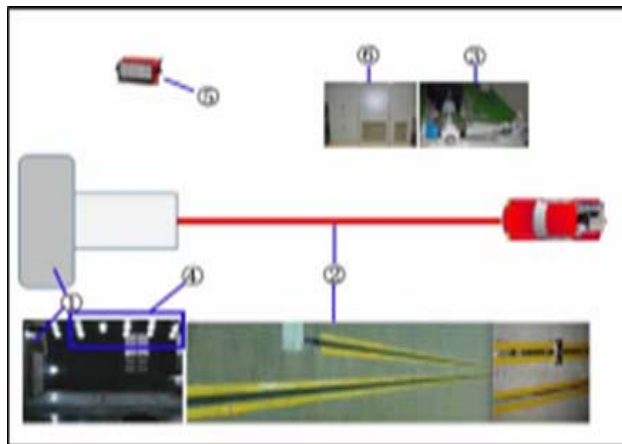


Figure4-(b).System diagram.

(Note)

- ① Collision test facility for this Study consists of fixed collision wall
- ② Driving road
- ③ Driving motor
- ④ Lighting facility
- ⑤ Data accumulator
- ⑥ Control unit

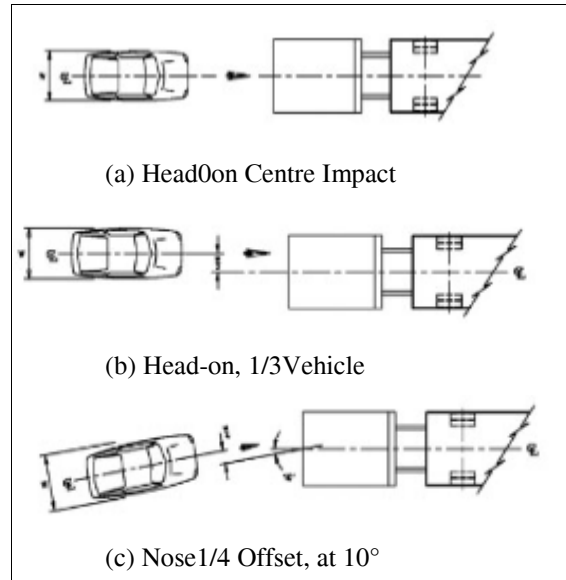


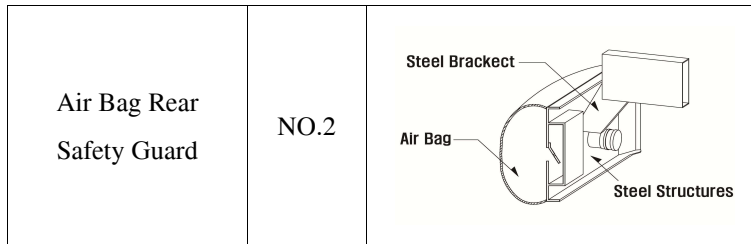
Figure 5. Test standard for crash absorption facilities

Testing

Collision testing This is to find shock absorption performance of the Conventional Rear Safety Guard and mobility of rear-end collision vehicle at right after collision. We designed both types of Rear Safety Guard to meet the conditions of rear-end collision vehicle. Table.1 shows types of test specimens for trial impact tests.

Table 1
A kind of test specimens for trial impact test

Specimens		Section(size)
Conventional Rear Safety Guard	NO.1	<p>Impact Steel Beam</p> <p>Steel Bracket</p>



(Note) NO.1 : Steel impact beam + steel structure bracket

NO.2 : Air Bag impact cushion + Steel impact structure + Steel structure bracket

The characteristics of respective tests are that fundamental structures of the both types of Rear Safety Guard are same.

However, Airbag Rear Safety Guard is assembled by air injected airbag. Those airbag's material, size, pressure, part price and weight are being studied through structure analysis and accurate testing.

Once it is accomplished, various types of products will be produced, which are able to meet each types of test.

Collision test Test performance of high speed rear-end collision tests follows American NCHRP Report 350 standard Shock Absorption Facility Test and U.K Design Manual for Roads and Bridges(TD49/07,Volume8 Section4, Part7), Requirements for Mounted collision Cushions standard. And 60km/h rear-end collision performance test was done in order to find collision performance of the both types of Rear Safety Guard.

Ten (10) tons of truck manufactured in 2003 for test installed both types of Rear Safety Guards with its total weight of 10,340kgs and midsize sedan of its weight of 10,340kgs was also used for rear-end collision vehicle.

The testing started that midsize sedan collided truck with Conventional Rear Safety Guard. After collision, its Conventional Rear Safety Guard was replaced with Airbag Rear Safety Guard for retesting. Same collision test method was applied to the Airbag Rear Safety Guard truck.

The test vehicle was installed with data accumulator inside test vehicle, acceleration meters at X,Y,Z axis and yaw sensor.

Tape switch for lighting was installed to sense impact at collision point.

500f/s high speed digital camera and video camera installed at left, right and upper right in order to record collision. Fig.3 shows collision test.

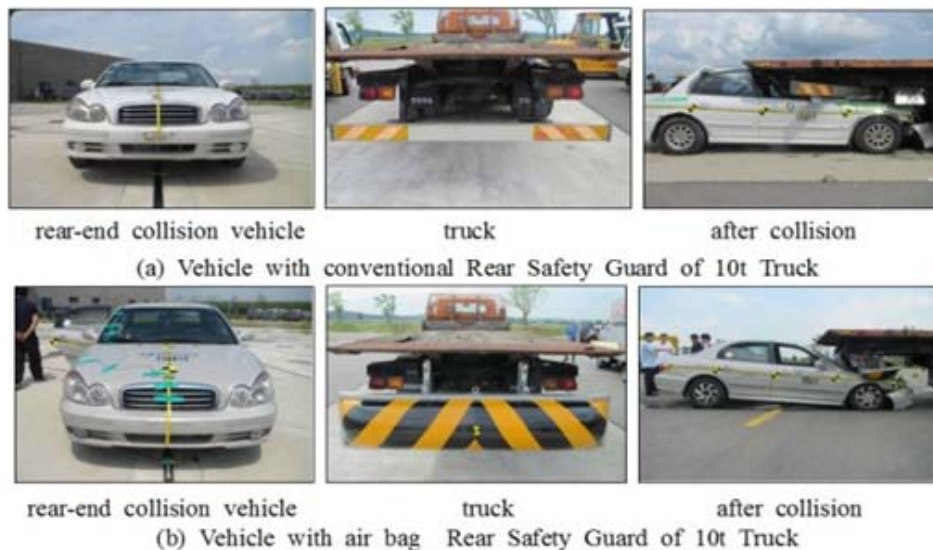


Figure6. The scene of the car collision test of Rear Safety Guard for 10ton Truck.

ANALYSIS AND CONSIDERATION

As follows Fig 7, Fig 8, Fig 9 Fig 10 showed that the 60km/h rear-end collision performance test results for both types of Conventional Rear Safety Guard and Air Bag Rear Safety Guard.

This study practical use evaluation standards is THIV 44km/h, PHD 20g, ASI 1.9G

The analysis for passenger protection performance index data by 60km/h collision performance test shows, at first, according to the test of Conventional Rear Safety Guard equipped truck, Yaw sensor detected data was maximum of $+112.5^\circ$ at 0.23 second and minimum of -51° at 0.24 second, and, acceleration index (ASI) was 50msec at composition of x,y,z axis direction, it was maximum 1.3(G'S) at 0.1890 ~ 0.239 second according to analysis result.

Theoretical Head Impact Velocity (THIV) shows 35.1km/h at 0.2149 second, which is synthesized value of x, y axis, and Post-Impact Head Deceleration (PHD) shows 17.1(G'S) at 0.2269~0.2369second, which is 10m second average synthesized value of x,y direction.

At second, in case Airbag Rear Safety Guard was installed, Yaw sensor detected data was maximum of -50° at 0.16 second and minimum of $+19^\circ$ at 0.45 second, and, Acceleration Severity Index (ASI) was 50msec at composition of x, y, z axis direction, it was maximum 0.9(G'S) at 0.0199~0.0609 second according to analysis result.

Theoretical Head Impact Velocity (THIV) shows 28.9km/h at 0.1269 second and Post-Impact Head Deceleration (PHD) shows 8.4(G'S) at 0.1269~0.1369second.

As follow in brief for above mentioned test data.

The results of data analysis, in case of Conventional Rear Safety Guard, shows Yaw effect based on z axis sharply rotate around $100\sim 150^\circ$ to the + direction at 0.15~ 0.25 second, however, in case of Airbag Rear Safety Guard, it shows $11\sim 50^\circ$ to the - direction at 0.15~ 0.25 second.

Especially, in case of Conventional Rear Safety Guard, it absorb collision force 0.10~ 0.20 second after collision, however, in case of Airbag Rear Safety Guard, it absorb whole collision force at the same time of collision.

From the under-ride's view, in case of Conventional Rear Safety Guard, passenger may have severe casualty because rear-end colliding car burrow down beneath under working truck, however, in case of Airbag Rear Safety Guard, passenger may have much less casualty because collision absorption occurs at the early time of collision.

The current regulation on Rear Safety Guard specifies to certify structure rigidity through only component test, which is revealed to be lack of prevention for the passenger casualties.

So, it is necessary to amend regulations on structure and test evaluation method of Rear Safety Guard because Rear Safety Guard bracket structure rigidity should be improved to prevent submarine effect by under-rider at collision.

Furthermore, there is no collision absorption performance standard.

So,we recognized that not only evaluation standards for injury THIV,PHD, ASI but also under ride situation level is should be provision of safety regulation.

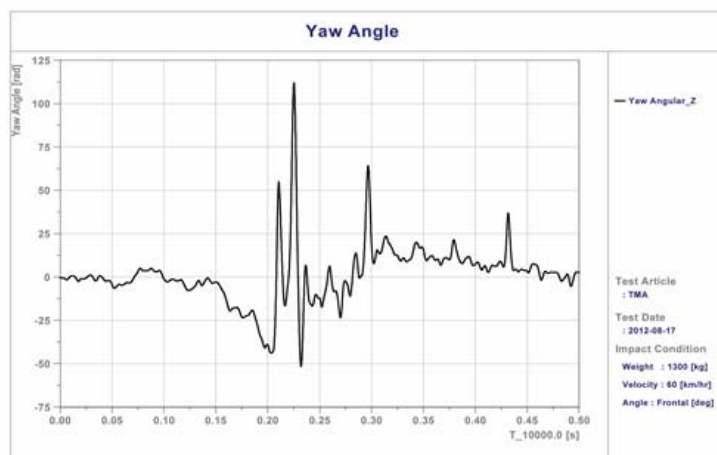


Figure7-(a). YAW data-Conventional type installed



Figure7-(b). YAW data-Air bag type installed

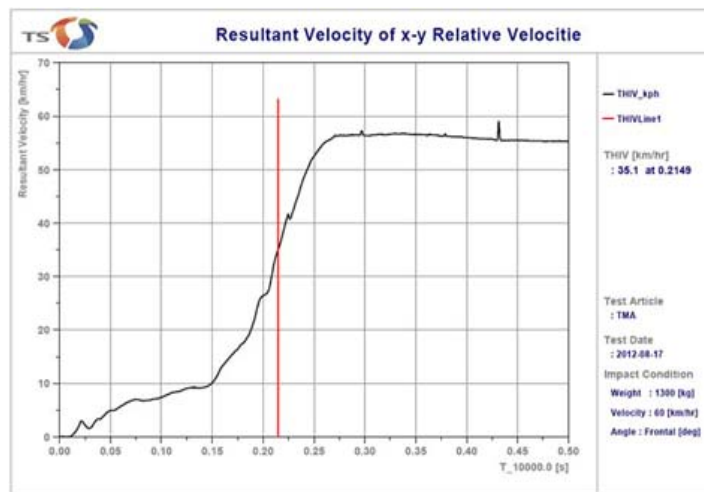


Figure8-(a). THIV data- Conventional type installed

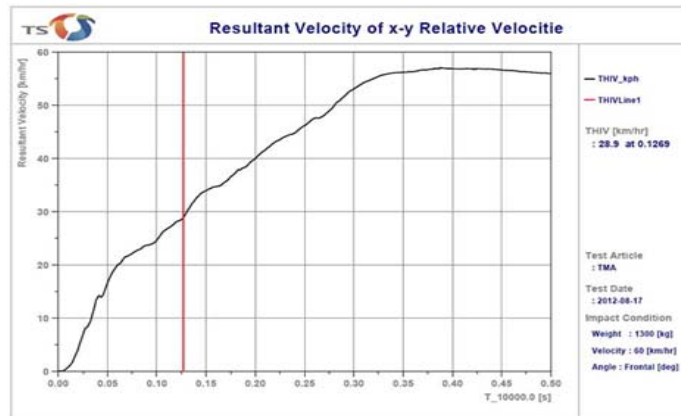


Figure8-(b). THIV data-Air bag type installed

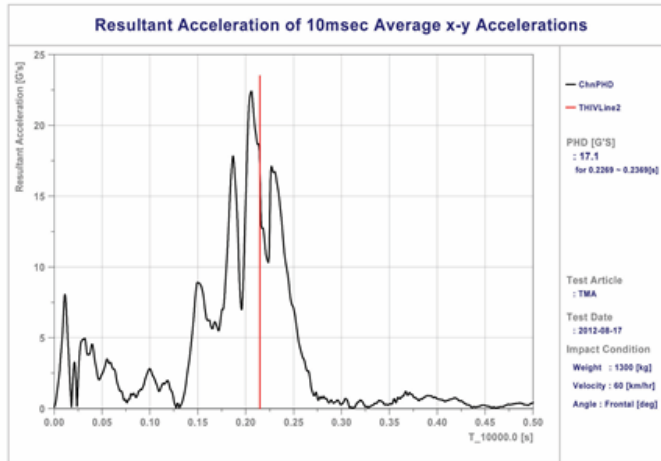


Figure9-(a). PHD data- Conventional type installed

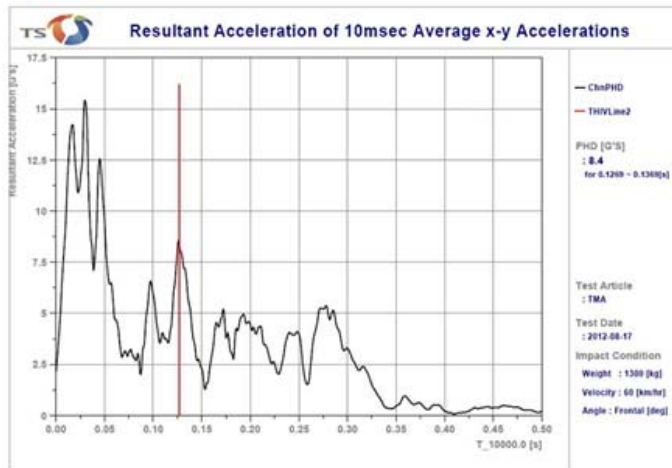


Figure9-(b). PHD data-Air bag type installed

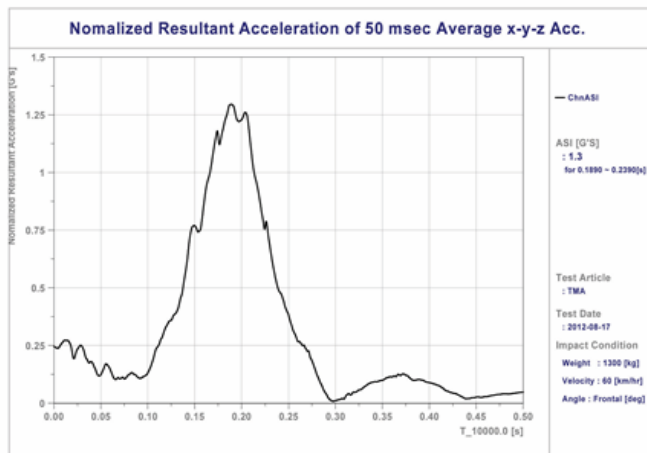


Figure10-(a). ASI data- Conventional type installed

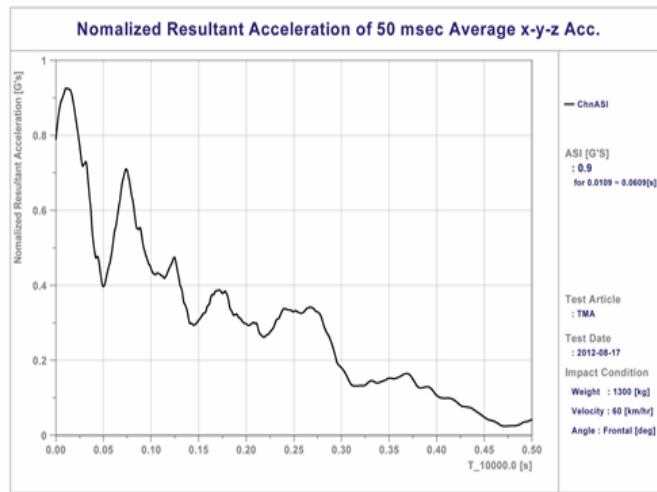


Figure10-(b). ASI data-Air bag type installed

CONCLUSIONS

We have considered the related regulation to improve Rear Safety Guard. And, the analysis results of 60km/h rear-end collision performance test by installing both types of Rear Safety Guard are as follows.

1) Rear-end collision performance test of both types of Rear Safety Guard shows that Airbag Rear Safety Guard inferior 12% of THIV, 49% of PHD and 69% of ASI to them of Conventional Rear Safety Guard.

2) Mobility of rear-end collision vehicle at collision shows that Airbag type of Rear Safety Guard equipped vehicle less burrowed down beneath truck due to less Under-ride effect. Accordingly, airbag Rear Safety Guard with polyurethane revealed to much reduce passenger casualty.

3) Rear-end collision vehicle equipped with Conventional Rear Safety Guard burrowed down beneath the truck up to front window of rear-end collision vehicle because Conventional Rear Safety Guard couldn't absorb collision force.

It means that it is difficult for Conventional Rear Safety Guard to prevent passenger casualty. Therefore, structure rigidity and evaluation method for passenger casualty such as THIV, PHD and ASI should be improved by adopting Truck Mounted Attenuator (TMA) evaluation method.

4) Need to provision that the under ride situation levels on Rear-end collision vehicle because of cause to reduce deaths in traffic accidents,

5) We can recognize that Air Bag Truck Mounted Attenuator (TMA) is superiority absorbing performance on collision base on the showed similar trend for the Air Bag Theoretical Formula and 60km/h rear-end collision test result of complete vehicle attached Air Bag Truck Mounted Attenuator (TMA).

Hence, it is possible that reduce deaths traffic accidents on rear and the other dictions collision, in case of the much more study to commercialize and improvement of quality for Air Bag Truck Mounted Attenuator (TMA).

REFERENCE

- [1] Ahn, K. H., "A study on the collision motion of polyurethane TPU airbag", Seoul univ. Textilepolymer depart, pp. 20~32, 1992.
- [2] Park, I. S., "A study on the vehicle safety at a high speed collision and the vehicle damageability and repairability at a low speed collision", Kook min univ, pp. 40~60, 2000.
- [3] Lee, H. B., Han, M. S., "Automobile design engineering", Wonchang publish co., pp. 195~207, 1998.
- [4] S. P Timoshenko. J. N Goodier, "Theory of Elasticity", McGRAW-HILL, pp. 485~504, 1970.
- [5] S. H. Crandall. et. al., "Introduction to the mechanics of Solid". McGraw-HILL, pp.323~325, 1978.

- [6] E.Kreyzig, "Advanced engineering mathematics", JOHN WILEY & SONS, pp. 73~75,1993.
- [7] Ministry of Land, Transport and Maritime Affairs of Korea "Guidelines for installation and maintenance of road safety facilities." 2012
- [8] Ministry of Land, Transport and Maritime Affairs of Korea "Handbook for genuine vehicle collision test for protecting vehicle facilities" 2012
- [9] Gyeong Woo, Kim "Study for mobility of passenger car collision and design of collision absorption facilities"
- [10] DaeHyung, Jang "Study for collision mobility of collision absorption considering passenger safety" Korean Society of Civil Engineers. 2006
- [11] R.H. Macmillan, Dynamics of Vehicle Collision," Proceeding of the International Association for Vehicle Design, Special Publication SP5 Channel Islands, UK, 1983
- [12] H. E. Ross, Jr., D. L. Sicking, and R. A. Zimmer, Recommended Procedures for the Safety Performance Evaluation of Highway Features," NCHRP Report 350, Transportation Research Board, Washington, D.C., 1993
- [13] CEN, "Road restraint systems Part 1: terminology and general criteria for test methods, EN 1317-1, European Committee for Standardization 2010.
- [14] Tae-Ho Yoon, Young-Me Cha, Jong-Il Yook, Jong-Gyu Baek, Hee-Jae Kim "Study on Composite material's bullet-proof effect improvement by adding urethane resin." The Korean Society for Composite Materials 2011.

DefinitionS/AbbreviationS

- ATMA** Air Bag Truck Mounted Attenuator
- THIV** Theoretical Head Impact Velocity
- PHD** Post-Impact Head Deceleration
- ASI** Acceleration Severity Index

MPDB-Mobile offset progressive deformable barrier

A new approach to cover compatibility and offset testing

Volker, Sandner
Andreas, Ratzek
ADAC e.V
Germany

Paper Number 15-0389

ABSTRACT

For more than 25 years the German Automobile Club ADAC is conducting tests to show the consumers and Industry the compatibility of passenger cars. With the upcoming off road vehicles in the 90's, the structural and mass difference between the compact and the small executive cars according the Off roaders was huge. The geometries in the vehicle front structures were totally different and did not align in case of a frontal impact. In combination with less performing structures for offset crashes the outcome in a car to car offset frontal impact tests was dramatically worse. Not only the smaller and lighter car showed poor performance also the crash structure of the large off roader failed. A decade later the passenger cars have become much safer due to consumer test programs and regulatory demands. But still these cars are showing a different behaviour in a car to car impact than in a car to barrier impact.

The different results of ODB tests, car to car impacts and the accident analyse showed that there is a need to find a test solution which will show this performance in a full size crash and allow analysing and rating the result.

Several tests with vehicles, barriers and different test conditions have been carried out to find a solution to reproduce real life behaviour and a possibility to rate the vehicle according its aggressiveness and compatibility, which lead to a mobile barrier solution with a progressive deformable element.

INTRODUCTION

Passenger cars have become much safer over the last years, not least thanks to comprehensive consumer testing programmes. The vehicles comply with most of the requirements of the Euro NCAP standard crash configurations.

The Euro NCAP frontal impact assesses the vehicle's self protection potential under the precondition that the car's supporting structure is ideally hit in the crash. Since single-vehicle accidents account for over 50% [1] of road deaths and over 40% of severely injured occupants, self protection is a decisive aspect of passive safety. ADAC accident research data shows, however, that severe injuries may be due to the fact that the supporting vehicle structures fail to meet. To ensure optimal accident protection, it is essential that the supporting vehicle structure is hit and that the crumple zone absorbs energy while the cabin remains stable. However, ADAC accident research data shows that this is not always the case. In many collisions, e.g. the longitudinal member is not hit (*Figure 1*) or the cross member detaches from the frame. In such case, the crumple zone cannot be fully utilised and the cabin deforms. This reduces survival space which means that the restraint systems fail to prevent the occupants from hitting the steering wheel or dashboard and sustaining severe injuries.



Figure 1: *If the supporting vehicle structure is not hit in a crash, the impact energy causes cabin deformation*

In 2010, ADAC introduced a new test set-up to assess the compatibility of vehicles. The test procedure should address the majority of the collisions not covered by the standard. In the test, the test vehicle impacts a special, honeycomb-shaped element, leaving a characteristic indentation whose surface is scanned for evaluation after the test. The indentation scan allows an assessment of a vehicle's sensitivity to nonstandard crash constellations. Moreover, the test assesses the partner protection of the vehicle's crumple zone and the load the vehicle causes to smaller vehicles in a collision. This vehicle to mobile barrier test with a progressive deformable Element was named ADAC compatibility test or MPDB test.

To achieve additional reductions in the injury risk of car occupants, extended research into passive safety will be required. Assessing a vehicle's self protection potential under ideal load conditions will no longer be sufficient. The effective interaction of different vehicles ("compatibility") and a large front-end shield are becoming increasingly important.

ACCIDENT STATISTICS

In 2009, 183,785 car occupants [1] were in a road accident involving a maximum of two parties: approx. 64% of them were in a car-to-car accident, 23% in single-vehicle accidents, 9% in accidents involving HGV and buses and approx. 4% in accidents involving other road users.

Considering exclusively accidents causing severe or fatal injuries, the percentage of single-vehicle accidents increases considerably (see Table 1 and Figure 2).

Table 1:
Car occupants involved in accidents in Germany by crash opponent and injury severity

Crash opponent	Car occupants (single-vehicle and two-vehicle accidents)			
	No. of occupants involved in accidents	of which		
		killed	severely injured	slightly injured
Single-vehicle	42,773	932	10,962	30,879
Passenger car	118,173	516	11,630	106,027
HGV, bus	16,425	307	2,435	13,683
Other	6,414	51	757	5,606

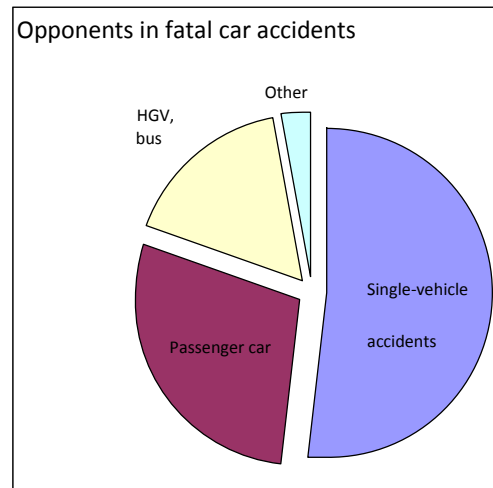
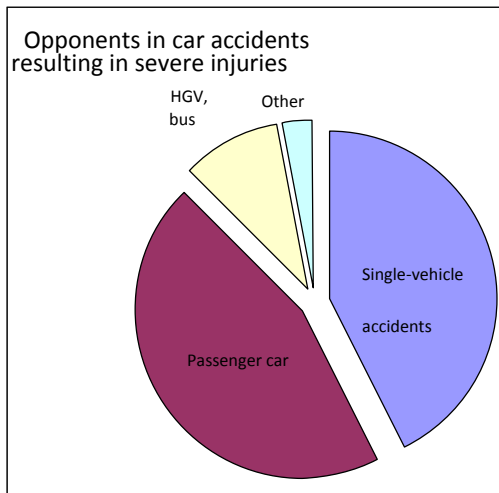
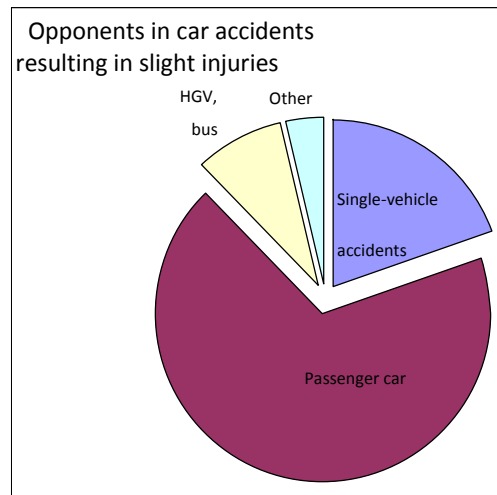
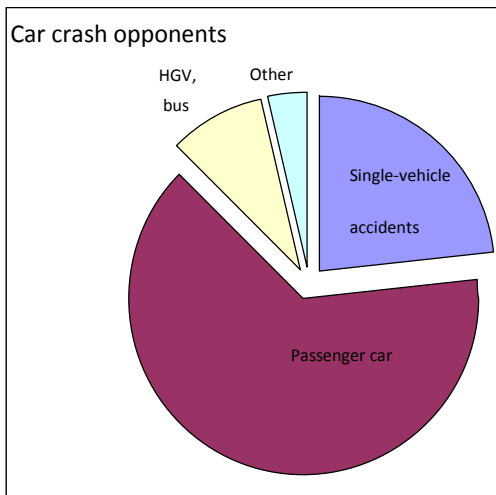


Figure 2: Car crash opponents (top left) and crash opponents by injury severity of car occupants

According to ADAC accident research data, the vehicle class only has a minor influence on the severity of the injuries car occupants sustain (Table 2). There are two reasons:

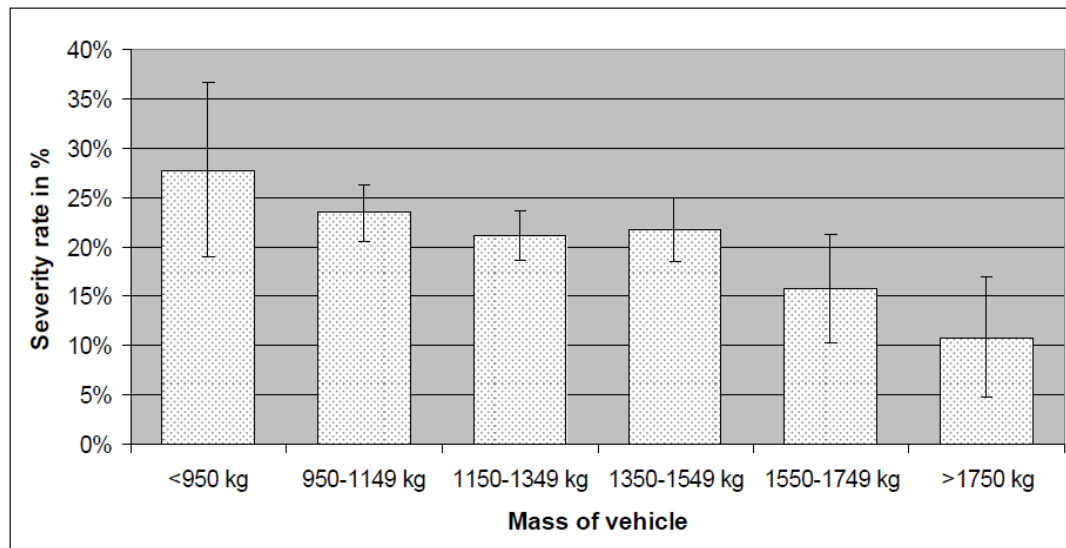
- ADAC accident research concentrates on severe accidents; approx. 39% of them are single-vehicle collisions and 14% involve utility vehicles. In these two types of accidents, the vehicle's self protection potential is essential while the high vehicle weight and a more rigid front end have little advantage. The only asset is the larger crumple zone of large cars.
- The analysis considers all types of collisions. Large vehicles have the greatest advantage in front-end collisions.

Table 2:

Percentage of slightly, severely and fatally injured car occupants (ADAC accident research; vehicles built in 2000 or later)

	Supermini	Family	Luxury
Slightly injured	37%	38%	45%
Severely injured	60%	60%	53%
Fatally injured	3%	2%	2%

Considering exclusively two-car front-end collisions, it becomes obvious that injury severity is relatively strongly affected by vehicle mass. Figure 3 shows that the risk of getting seriously or fatally injured in a crash is approximately twice as high in very light vehicles (<950kg) (over 27%) as in very heavy vehicles (>1750kg).



: severity rate in frontal impact according to the mass of the vehicle.
 Vehicle designed since 2000 or registered since 2004.

Figure 3: Percentage of severely and fatally injured in car-to-car front-end collisions by vehicle mass[2]

WHAT DOES COMPATIBILITY INCLUDE

Compatibility refers to the interaction of colliding vehicles. The following issues are especially important:

- **Weight difference:**

When two vehicles of different weight crash into each other at identical speed, both vehicles will move in the heavier car's direction of travel. While the impact causes the lighter car to brake to a standstill and then accelerate rearward, the heavier car is braked from its speed of travel to a residual speed.

Vehicle deceleration depends on the change in speed during the crash ($\Delta v = \text{pre-crash speed of travel} - \text{post-crash residual speed}$) and is a decisive factor for determining accident severity and the occupants' injury risk. Since speed change is smaller in the heavier passenger car, loads on the occupants are lower in the heavier than in the lighter vehicle.



Figure 4: Upon impact, the heavy SUV causes the light supermini to skid rearward

- **Different front-end rigidity:**

The test set-up used for vehicle approval based on ECE R94 and the Euro NCAP frontal impact includes an offset collision between two cars of identical weight which travel at the same speed. For this test, it is essential that impact energy is absorbed by the crumple zone before the cabin starts to deform. To ensure that the vehicle's own "pushing" mass causes only the crumple zone to deform, heavy vehicles have higher front-end stability than light vehicles. Although heavy vehicles usually have a longer deformation distance, the structural force required to cause front-end deformation is significantly higher in heavy vehicles than in light vehicles.

If two different vehicles crash into each other, the crumple zone of the lighter car will be the first to deform because of the vehicles' different rigidities. As a result, the load on the small vehicle may become too high relatively quickly while the crumple zone of the larger vehicle remains mostly intact.



Figure 5: Post-crash deformation is considerably stronger in the small vehicle (left) than in the more rigid large vehicle (right)

- **Different front-end geometries:**

The deformable element used in the Euro NCAP frontal impact and the ECE R94 vehicle approval is comparatively soft and absorbs only little energy while maximum load is exerted. Modern vehicles penetrate the element (blue in Figure 6), and the longitudinal member transfers the impact energy directly to the metal plate behind.



Figure 6: Since the current front-end element absorbs only little impact energy, energy is transferred to the large and stable metal plate behind the element

Longitudinal member position and dimensions as well as transverse member stability (cross members connecting the left and right longitudinal members; red in Figure7) are of minor significance. In this standard crash, even a single longitudinal member jutting out of the vehicle like a spear can transfer the impact energy to the large metal plate behind the deformable element.



Figure 7: *The dimensions and position of supporting structures in modern cars vary considerably*

More often than not, cars colliding head-on cannot support each other because their supporting structures do not meet, causing the crumple zone to remain mostly intact while the cabin deforms. In most cases, this results in very severe injuries to the occupants (Figure 8). The smaller the front-end overlap and the higher the collision speeds, the more serious are the consequences of geometric discrepancies. An approach by IIHS is covering exactly this kind of small overlap situation, by using just 25% of the vehicle width.



Figure 8: *If the supporting vehicle structure is not hit in a crash, the impact energy causes cabin deformation*

DEVELOPMENT OF CAR TO MOBILE DEFORMABLE BARRIER TEST

As the car to car impact was the starting point the initial setup of the car to barrier test should be close as possible. The impact speed of 56kph and the overlap of 50% of the small car were taken over. In several European projects, such as APROSYS, the actual average mass of passenger cars in Europe were discussed for the side impact barrier. While taken into account the number and type of cars actual on the market as well as actual selling numbers, the compact car class, shows the highest number actual on European roads. In driving condition these class will be approximately 1400kg heavy. The mass of the mobile barrier was set to this weight, which is already covered by the FMVSS 208 side impact barrier, which is the base for the impacting trolley.

First impact tests

The initial starting point for the test specification was the car to car impact test between two cars of the same mass range and size. This test was carried out according the actual car to car impact specifications with 50% overlap of the small car and 56kph impact speed. In this test, also the vehicles were out of the same vehicle class, both longitudinal did not match (see Figure 9)



Figure 9: car to car impact at 56kph

In a second test the yellow car was replaced by the mobile barrier equipped with the PDB Element. All other parameters were not changed (see Figure10)



Figure 10: car to mobile barrier impact at 56kph

Comparison of deformations:

A direct comparison between the vehicle pulses, the vehicle deformations and the 3D measurement showed that the MPDB test loaded the tested vehicle in a different way than in the car to car impact.



Figure 11 : car to car test (left picture), car to MPDB test (right picture):

Differences detected after the impacts were are more or less undeformed footwell area, the trans fascia beam and A-pillar section showed rupture, the instrument panel intruded the passenger compartment. Compared to cases of the ADAC accident research and also compared to the car to car test those deformations are quite uncommon and lead to the decision to implement changes in the test setup and improve the performance of the test results.

The top of the PDB element is compareably high (appr. 900 mm) and in the upper part more or less undeformed. So it is quite likely that the upper part of the PDB is stiffer than an average car. During the test, the PDB put a lot of energy into the car, especially in the area of the waist line. Following changes were applied to the barrier due to that fact.

- 1. reduce the ground clearance of the PDB by 75 mm**
- 2. reduce the overall height of the PDB by 135 mm**

3. reduce the test speed to 50 kph

A second impact test with the changes mentioned was performed and the vehicle pulse as well as the 3D measurement and the deformation of the car were quite close and comparable see deformation pictures in Figure 12.



Figure 12: Comparison of deformations car to car test (left picture), new car to MPDB test (right picture):

The overall result of the new test setup could be recognized after the detailed analyses of the vehicle tested according to the new boundaries. Not only the overall picture shows a comparable deformation, also the detailed view below the dashboard, the deformation of the A-pillar and the intact trans fascia beam offer no big differences between the 2 tests. But there are still less deformations in the footwell area of the MPDB tested car. The conclusion is, that deformations of the PDB are more homogeneous – the upper part is also loading the tested vehicle.

Test setup car to MPDB

The new test setup of compatibility crash test simulates a head-on collision with a 50% overlap between the vehicle to be assessed and an approx. 1400kg moving trolley with a PDB, made of alloy, representing a typical, widely used small family car (see Figure 13). The vehicle and the trolley are travelling at identical speed.

The ground clearance of the PDB barrier is 150mm while the height of the barrier is 750mm above the ground and one alloy box with a stiffness of 0,34MPa and a second block with progressive stiffness, both covered with an alloy sheet.

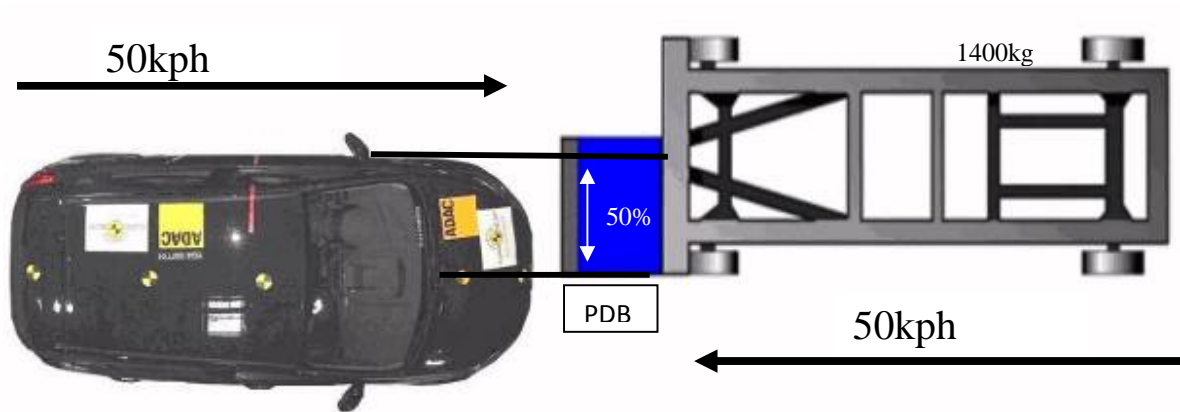


Figure 13: Test set-up of the compatibility crash test

To assess the occupants' injury risk, two 50% H3 dummy on each of the two front seats and restrained a Q6 child dummy in an appropriate CRS on the right rear seat were installed. Dummy installation and instrumentation as well as vehicle load and measurement were in compliance with the Euro NCAP test protocol. Also the Dummy assessment was carried out according Euro NCAP assessment protocols.

METHODE OF THE COMPATIBILITY ASSESSMENT

The compatibility assessment includes the analysis of the indentation the colliding vehicle leaves on the deformation element upon the impact as well as the change in trolley speed. The assessment comprises the steps below:

1. Determining the assessment area:

The first step includes determining the area of the PDB that is relevant for assessment in dependence of the vehicle dimensions and other framework conditions:

Width Ideally, the front-end shield spans the entire width of the passenger car to be able to absorb impact energy in the crumple zone also in accidents where overlap is minor. To take this into account, the assessment area represents 45% of the vehicle width.

Because of the crash kinematics (rotation of the vehicle and trolley), force is exerted on the side edges of the deformation element which, as transverse load, causes unrealistic deformation to the honeycomb structure. As a result, the edges cannot be assessed and the assessment area ends 200mm from the PDB's side edges.

Height To ensure that the structures of the colliding vehicles meet upon the impact and to lower the risk of overriding or underriding the barrier, the supporting structure must be mounted between 250 and 650mm above the ground. This takes the different vehicle classes into account and complies with additional requirements (e.g. RCAR bumper test, HGV underrun protection).

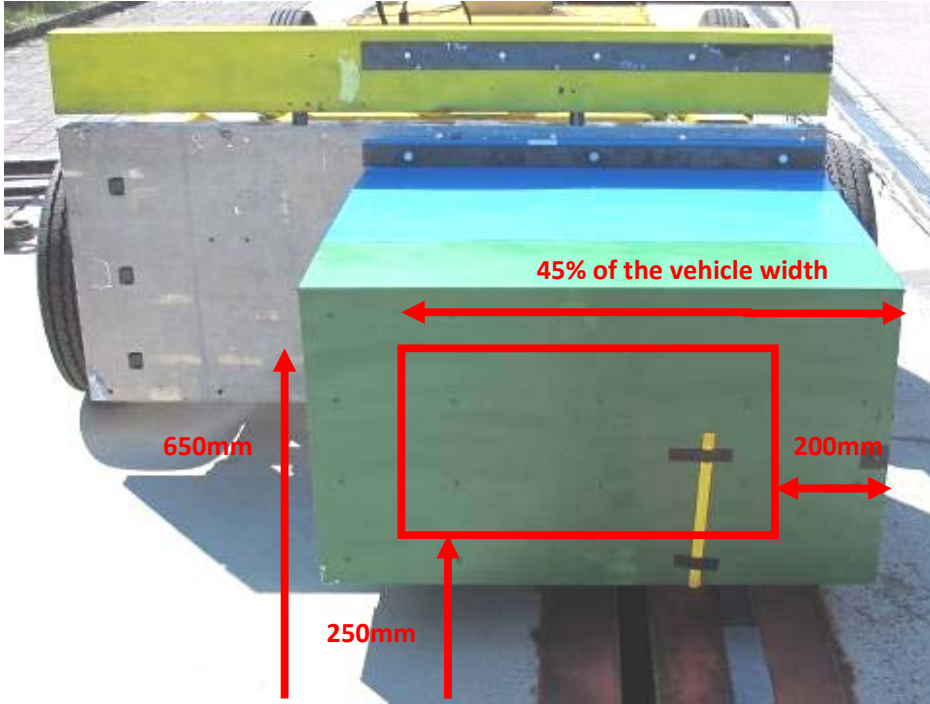


Figure 14: Determining the assessment area

2. Assessing indentation homogeneity/geometry:

Ideally, the vehicle front end should have homogeneous rigidity in the entire assessment area (see Figure 14). Both very rigid longitudinal members that penetrate the colliding vehicle like a spear and very soft areas that do not provide support for the colliding vehicle and barely dissipate or absorb energy are a disadvantage. A vehicle meets the above criteria if it leaves a homogeneous and large indentation in the PDB.

The homogeneity assessment comprises a statistical evaluation of the intrusion depth in the area under assessment. For this purpose, the average intrusion depth and the standard deviation (a measure for the mean variation of the measured values around the average) are determined. A greater standard deviation means a more inhomogeneous deformation of the barrier and results in a poorer homogeneity rating.

3. Assessment of the energy impacting on the colliding vehicle:

Two criteria are used to assess front-end rigidity and the energy impacting on the colliding vehicle:

- **Energy impacting in the PDB assessment area:** Great differences in the rigidity of colliding vehicles may cause impact energy to be absorbed only by the less rigid vehicle while the crumple zone of the more stable vehicle remains intact. Very high front-end rigidity therefore has a detrimental effect on partner protection. PDB deformation depth enables the assessment of front-end rigidity and impact energy. To lower the risk of excessive loads on the colliding vehicle, it is essential that the vehicle tested absorbs kinematic energy in its own crumple zone.
- **Change in trolley speed:** Since for technical reasons impact energy assessment focuses only on the assessment area as defined above, we do not consider the entire amount of energy impacting on the colliding vehicle in our test. Therefore, we also assess the change in trolley speed. While a change by less than 50kph is a plus, a change by more than 50kph is a drawback.

Examples of different front structures

The following tables will show the results of 3 family cars tested in the last test series and according the latest version of the assessment. All cars have been tested also by IIHS according the small overlap test. The results in the compatibility test are showing very different behaviour of front structures. In the 1st example the vehicle shows a single load path of extreme stiffness and a very weak cross member. While example 2 has several load paths in height and is also covering the outside areas of the longitudinal. This vehicle scores well in the small overlap and the compatibility test. The 3rd vehicle shows also 2 load pathes in the front, but also a weak cross member. The longitudinal is too stiff, but less aggressive than in example 1. The 3rd car has a good rating in small overlap tests too.

Table 3:

Example 1 family car

Post-crash vehicle	The vehicle is a family car with a very inhomogeneous crumple zone consisting of two longitudinal members which are interconnected by an unstable aluminium cross member. The cross member spans the width of the longitudinal members, leaving the area in front of the front wheels unprotected. In front of the suspension strut domes, the vehicle has two short, but rather flat, longitudinal members (shotguns). However, they are placed too far to the rear and top to absorb deformation energy in the test. Maximum deceleration of the vehicle upon the impact was 38g. The change in speed was
--------------------	--

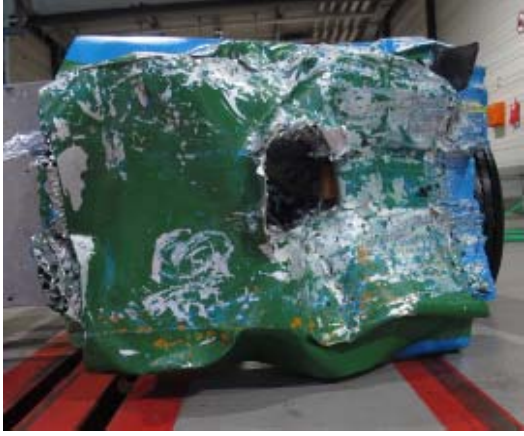
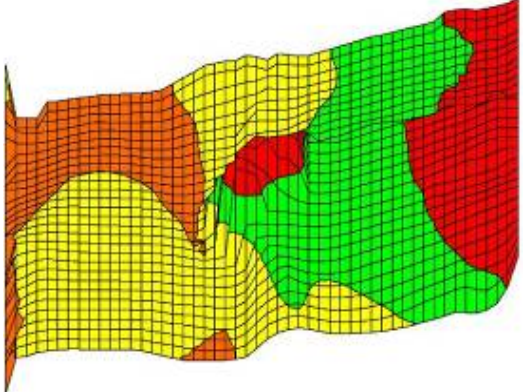
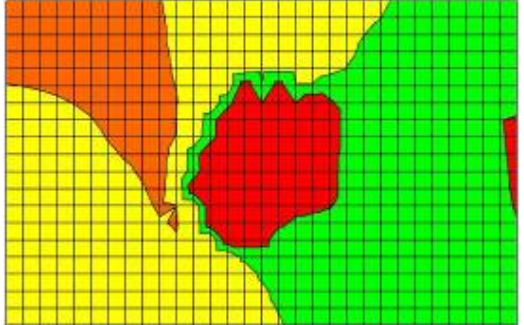
	57kph.	
Post-crash PDB	<p>PDB deformation upon the impact is extremely inhomogeneous with the longitudinal member punching a deep hole into the barrier and the engine block causing strong deformation to the PDB edges (on the right in the photo). Where the vehicles front wheel impacts the PDB, intrusion of the PDB which absorbs approx. 93kJ is, however, minimal. The PDB trolley's maximum deceleration upon impact was 35g. The change in speed was 63kph.</p>	
Digitised post-crash PDB front	<p>This illustration shows the entire front of the PDB and the different intrusion depths. Intrusion depth colour scheme:</p> <p>Orange 0 to 160mm Yellow 160 to 320mm Green 320 to 480mm Red >480mm</p>	
Post-crash PDB assessment area	<p>This illustration shows the PDB area that is relevant for compatibility assessment.</p> <p>The green area of the indentation left by the Audi's front end is well-suited to absorb energy in a crash, while the red area is much too rigid. On the other hand, the yellow and orange areas are too soft.</p>	

Table 4:
Example 2 family car

<p>Post-crash vehicle</p>	<p>The vehicle is a family car with a relatively homogeneous crumple zone. It consists of three horizontal planes connected on the right and left with vertical profiles:</p> <ul style="list-style-type: none"> • The main load path consists of two longitudinal members interconnected by a steel cross member. There is an additional connection from the longitudinal members to the suspension strut domes in front of the wheels. • A steel lock support of somewhat weaker dimensions is located above the main load path and is connected to the suspension strut domes on either side. • Below the main load path is another steel cross member which spans the width of the longitudinal members. <p>What makes the vehicle design unique are its structures located outside the longitudinal members and in front of the front wheels. These structures are intended to dissipate the impact energy over a large area and absorb energy in crashes with little overlap.</p> <p>Maximum deceleration of the vehicle upon the impact was 71g. The change in speed was 58kph.</p> 
<p>Post-crash PDB</p>	<p>Rather large areas of the element are deformed by the impact. There are no major holes in the surface, but the individual members on the vehicle front have left visible indentations. The PDB trolley's maximum deceleration upon impact was 29g. The change in speed was 58kph. The barrier absorbs 76kJ of energy in the crash test.</p> 

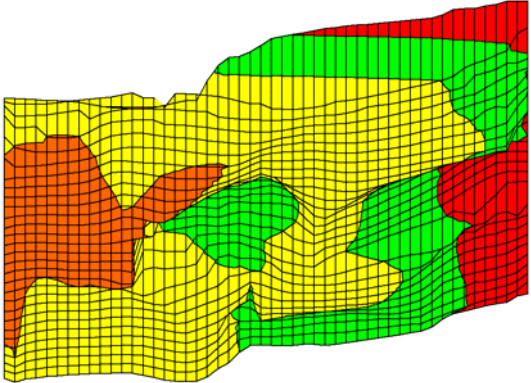
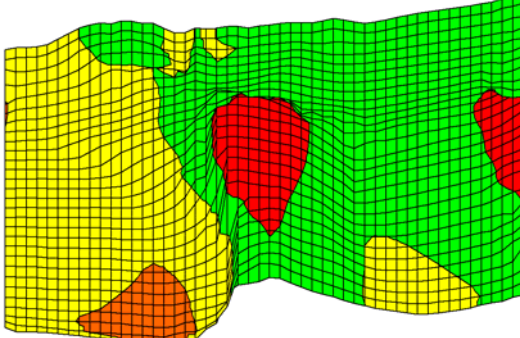
Digitised post-crash PDB front	<p>This illustration shows the entire front of the PDB and the different intrusion depths. Intrusion depth colour scheme:</p> <p>Orange 0 to 160mm Yellow 160 to 320mm Green 320 to 480mm Red >480mm</p>	
--------------------------------	--	--

Table 5:
Example 3 family car

Post-crash vehicle	<p>The front end of the vehicle comprises several load paths:</p> <ul style="list-style-type: none"> • The main load path consists of two longitudinal members connected by a steel cross member. • Underneath the longitudinal members, there is an additional steel cross member whose outer edges rest on the chassis sub-frame. • In front of the suspension strut domes, the vehicle has two additional short, longitudinal members (shotguns) stably connected to the main load path. These members are intended to protect the cabin in crashes with little overlap. <p>Maximum deceleration of the Vehicle upon the impact was 33g. The change in speed was 51kph.</p>	
Post-crash PDB	<p>The main load path of the vehicle leaves a vertical bend and a much deeper indentation than the other supporting structures. In this test, the PDB element absorbed 92kJ of energy. The PDB trolley's maximum deceleration upon impact was 38g. The change in speed was 58kph.</p>	

Digitised post-crash PDB front	<p>This illustration shows the entire front of the PDB and the different intrusion depths. Intrusion depth colour scheme:</p> <p>Orange 0 to 160mm Yellow 160 to 320mm Green 320 to 480mm Red >480mm</p>	
--------------------------------	--	--

CONCLUSIONS

Compliance with Euro NCAP frontal impact requirements is essential for good occupant protection. However, even vehicles with a very inhomogeneous front-end design may pass this test. In the event of a two-vehicle accident (or single-vehicle accident such as vehicle-tree collision), poor front end structural design may result in excessive local loads on the vehicle or its opponent and serious injuries for the occupants. Vehicle designers must therefore take additional requirements into account:

- **Adapted front-end geometries**

In today's vehicles, there is no standard for the mounting height of front-end supporting structures, i.e. mounting height may vary greatly from manufacturer to manufacturer and from car model to car model. Cross members are usually very flat and do not span the entire width of the vehicle. In addition, they are unstable, failing to dissipate the impact energy. As a result, there is poor energy absorption potential for the colliding vehicles.

Equipping a vehicle with a front shield consisting of wide multiple cross members (see Figure 15) may dramatically improve partner protection and self protection (e.g. when crashing into a tree). It helps dissipate the impact energy throughout a large area so that most of it is absorbed in the crumple zone. The shield should protect the area between 250mm and 650mm above the ground and ideally span the entire width of the vehicle. This construction will not only help for partner protection, also small overlap scenarios will be addressed with this construction.



Figure 15: *Frontal impact protection: disadvantageous (left) vs. advantageous (right) front-end construction*

- **Adapted front-end stability**

Vehicle mass has no influence on the deformation distance required to keep vehicle deceleration at an acceptable level. The long nose of a large and heavy vehicle can therefore be divided into a soft partner protection area and a rigid self protection area. This ensures that in a head-on collision with a light vehicle, the crumple zone of the large vehicle is able to absorb most of the energy rather than the small vehicle.

If the vehicle designers bear the above issues in mind, they will contribute to considerably lowering the injury risk in single-vehicle and car-to-car accidents. The risk of getting seriously or fatally injured is likely to decrease by approx. 7% [1] This would prevent over 150 road deaths and some 2100 serious injuries to car occupants on German roads each year.

The Euro NCAP roadmap for 2017-ff will also include an updated frontal impact scenario and will have to deal with the question self and partner protection. Possible frontal scenarios were examined in the last 5 years which will be taken into account for a new consumer frontal impact test scenario in 2020.

REFERENCES

[1] Federal Statistical Office Germany; road accidents 2012

[2] IRCOBI Conference 2010; C. Chauvel, S. Cuny, G. Favergon, N. Bertholon, P. Delannoy: Self-Protection and Partner-Protection for new vehicles

CRITICAL REVIEW OF THE CURRENT ASSESSMENT APPROACHES FOR FRONTAL CRASH COMPATIBILITY REGARDING THE EVALUATION OF STRUCTURAL INTERACTION

Emad Sadeghipour

Morris Fischer

Fabian Duddeck

Markus Lienkamp

Technische Universität München

Germany

Raffaele Ciardiello

Politecnico di Torino

Italy

Paper Number 15-0096

ABSTRACT

The assessment of structural interaction has been identified as the main challenge of the unresolved problem of frontal crash compatibility. With this background, two questions are raised: Does a better structural interaction correspond with higher safety and crash compatibility? Are current test approaches able to evaluate structural properties?

Considering the structural mechanics of collisions, it is hypothesized that a poor structural interaction does not necessarily result in lower safety and should be considered together with compartment strength and restraint systems. This hypothesis is confirmed by reviewing some crash results from other studies. A spring-mass vehicle model is also used to verify the hypothesis. Finally, a comprehensive simulation study is conducted to find the answers to the two questions. For this study three different variations of a vehicle model are created, which represent different structural properties of the passenger car fleet. The crash performance of these models is analyzed in different car-to-car and car-to-barrier tests.

Results of the car-to-car tests show that better structural interaction often makes the vehicle more aggressive. Generally, better structural interaction increases crash pulse and reduces intrusions. Depending on vehicle design and crash configuration, the intrusions or the crash pulse become more important as to why good or poor structural interaction cannot be overall related to more crash compatibility or occupant safety.

Our criticism of the current assessment approaches for frontal crash compatibility is the establishment of a direct link between good structural interaction and higher safety. These approaches do not consider the effect of higher crash pulses due to the better structural interaction. Our recommendation is to assess the partner protection through metrics about intrusions and crash pulse of the partner, without direct assessment of the structural interaction. Instead, the test configuration should be able to reflect structural properties in intrusions or crash pulse.

Results of the car-to-barrier tests show that the Progressive Deformable Barrier can reflect structural issues correctly. However, the developed metrics for this barrier result in incomprehensive interpretations. Results of the tests with other barriers are inconsistent with the structural properties of the vehicles.

Finally, an exemplary test concept with the Advanced European Mobile Deformable Barrier is presented as an alternative assessment approach. Simulation results of the proposed assessment approach show good consistency with the crash performance of the vehicles in the car-to-car tests. Combination of this test concept with the Full-Width Rigid Barrier test can be used to assess the safety and crash compatibility of passenger cars.

1. INTRODUCTION

Crash compatibility is known as a key component in improving vehicle safety and will become even more important in Europe's future road safety. This is due to the increasing market share of mini cars and sport utility vehicles in relation to other car segments [19], which increases the potential of incompatible collisions.

Although many studies [4, 15, 16] have been conducted in Europe to develop a proper assessment approach for crash compatibility, no assessment approach has been implemented yet. Important issues involving frontal crash compatibility for normal passenger cars have been identified as compartment strength, restraint systems, force levels and structural interaction (SI). Whereas restraint systems and compartment strength can be evaluated from dummy measurements and intrusion values, the assessment of SI is still an unresolved problem.

The issue of force levels consist of deformation forces of frontal structures and energy absorption management [4]. According to the matched pair analysis from the FIMCAR project, the deformation forces does not have a high

priority. Since the energy absorption management will also be considered in the assessment of SI, the focus of this study is on the issue of structural interaction.

Recently, two assessment approaches have been proposed from the FIMCAR project [1, 4]. The first approach is a combination of an offset test with the Offset Deformable Barrier (ODB) at 56 km/h and a full-width test with a Deformable Barrier and a load-cell wall (FWDB) at 50 km/h. A metric was developed in the FIMCAR project to establish a common interaction zone for the vertical SI; however, FIMCAR has not succeeded in developing a metric for horizontal SI in this approach.

The second approach is a test with a Progressive Deformable Barrier (PDB) or its mobile version. The developers see this barrier as the only configuration that can potentially assess horizontal load spreading. However, PDB still has validation and repeatability issues that must be resolved before its implementation. Furthermore, the association of the automotive industry worries about the misuse potentials of this barrier [17].

2. HYPOTHESIS: IMPACT OF STRUCTURAL INTERACTION ON OCCUPANT SAFETY

SI describes how the structures of a vehicle deform at the local level when interacting with a collision partner [14]. This definition includes two issues. First, with a poor load spreading, the energy absorption of the frontal structures is lower than its designed goal. The second issue is the structural stability, which prefers a homogeneous and robust reaction of the vehicle structures over different loading conditions. Neither of these aspects have a direct impact on occupants' injuries. The indirect impact has a dual meaning. On the one hand, poor SI can lead to intrusions by which occupants are exposed to contact injuries. On the other hand, poor SI can result in a higher deformation stroke that reduces the crash pulse in favor of restraint loadings on the occupants. Thus, poor SI does not necessarily correlate with lower safety and should be considered together with compartment strength and restraint systems.

Current assessment approaches define some requirements for good SI. In these approaches, the evaluation of separate metrics for SI, intrusions and dummy measurements determines the compatibility of the vehicle. This does not consider the influence of structural properties on crash pulse and intrusions.

Review of Some Crash Test Results

It has been observed in some real crash tests from different studies that poor SI could result in better occupant safety. In the test series 1b from the FIMCAR project [11], some supermini cars were tested in aligned and misaligned configurations. It is obtained that if the vehicle has a strong passenger compartment and front-end design, then the misalignment does not necessarily result in higher intrusions. In this case, the misaligned configuration results in less intrusion for the firewall. Most dummy criteria were also better by the test series 1b with misalignment. Similar results have been observed in the test series 2 (small family car vs. sport utility vehicle) of the FIMCAR project and the test series 3 (supermini car vs. small family car) of the VC-COMPAT project [2]. This confirms that poor SI does not necessarily result in lower safety. The impact of SI on occupant safety depends on the compartment strength and restraint systems of the vehicle and also the crash configuration.

Spring-Mass Vehicle Model

A spring-mass vehicle model from [7] has been further developed for this study. The model consists of two nonlinear springs as the main load paths and an elastic beam element as the bumper of the vehicle. The bumper represents load spreading on front structures; i.e. higher stiffness for the bumper corresponds with better SI for the vehicle. This model is calibrated to represent the Finite-Element-Model of the Toyota Yaris from [6]. The consistency between the kinematic of the spring-mass model and the Finite-Element-Model is verified in two tests against a rigid wall at 56 km/h with 50% overlap and full-width. The metrics of the Roadside Safety Verification and Validation Program from [8] are used for this verification.

Six variations of the spring model with different bumper stiffnesses are tested against a rigid wall at different speeds and with different overlap values. Figure 1 illustrates the results. The z-axis shows the maximum crash pulse in g. Colors indicate the value of the crash pulse, by which dashed red stands for high. The stiffness increases by a factor of two from SI-1 to SI-6. SI-2 represents the original Finite-Element-Model.

The results show that lower SI reduces the crash pulse by high overlaps. It is due to the extended deformation stroke. Higher SI is more desirable for low overlaps since the whole kinetic energy will be absorbed in crash structures, which prevents an impact of stiff compartment on the rigid wall. Hence, the ideal SI is a design parameter, which does not have an overall best case.

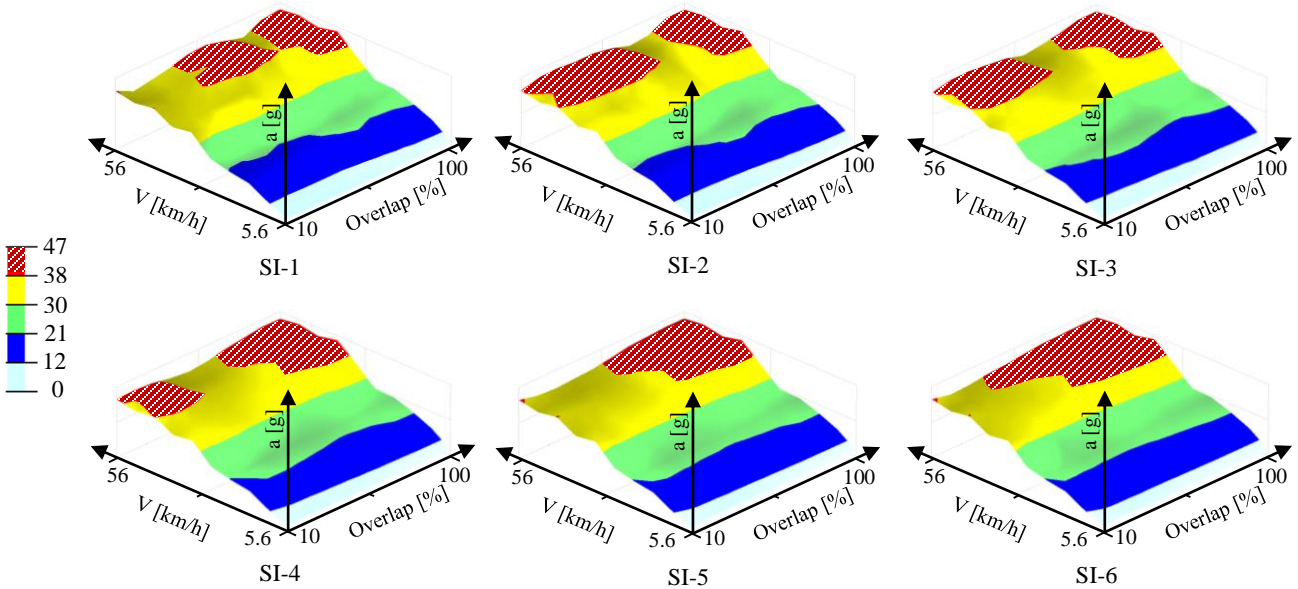


Figure 1. Crash pulses for different structural interactions (prioritized from poor to good SI).

3. SIMULATION STUDY

The previous section explained a hypothesis about the impact of SI on occupant safety. In this section, we are looking for answers to the following two questions:

1. Does a better SI correspond with higher safety and crash compatibility?
2. Are current test approaches able to evaluate structural properties?

To find the answers, a simulation study is conducted.

Reliability of the Simulation Study

In this part, the question of reliability of the simulation results is addressed. The different aspects are categorized into simulation models, evaluation criteria and the test catalog.

Simulation Models The Toyota Yaris Finite-Element-Model from [6] is used as the basic simulation model¹. This model is validated with crash tests against a Full-Width Rigid Barrier (FWRB) at 56 km/h and at 40 km/h and also against an ODB at 64 km/h with 40% overlap. The overall vehicle deformation and pulse were similar between tests and simulations [6]. This simulation model has also passed some additional tests with higher crash severity that confirmed the model robustness. Thus, this simulation model is considered a proper input for our qualitative simulation study.

The basic simulation model is changed to represent different structural properties of vehicles. Three variations are created from the basic model with considering the variations' feasibility. Each model represents a real car category with well-known SI characteristics. The models are ordered by their structural properties in Table 1.

To confirm the SI characteristics of the vehicle models, two simulation studies are conducted:

- The vehicles strike against the RCAR bumper from [18] at 56 km/h. This barrier can be used to evaluate the vertical homogeneity [9]. It is expected that vehicles with better structural properties have more homogeneity in the vertical deformations.
- The vehicles collide against the original Yaris model at 50 km/h with 50% overlap. This is the car-to-car baseline situation for the test ECE-R94, which is for the approval of vehicles in Europe with regard to the protection of the occupants in the event of a frontal collision. It is expected that vehicles with better structural properties have more homogeneity in the horizontal deformations.

¹ This model has been developed by The National Crash Analysis Center (NCAC) of The George Washington University under a contract with the FHWA and NHTSA of the US DOT.

Table 1.
Simulation models and their variations, ordered by SI characteristics.

#	Model Name	SI characteristics	Changes of the model in relation to the original Yaris model
1	Mini Electric Car (Mini E-Car)	poor horizontal SI poor vertical SI	1- Represents an electric mini car without motor block and radiator, which eliminates a load path in the middle of the vehicle. This reduces the horizontal load spreading. 2- The height of the vehicle is reduced by 50 mm due to the configuration of the suspension systems. This increases the occurrence possibility of vertical SI problems (e.g. over-/underride). 3- A battery pack is added to the luggage compartment to balance the mass of this variation with the basic model.
2	Electric car (E-Car)	poor horizontal SI	1- The same as No. 1 for the Mini E-Car 2- The height of the vehicle is the same as for the basic model 3- The same as No. 3 for the Mini E-Car
3	Basic-Model	Normal	Original Toyota Yaris model without any changes.
4	Strong-Car	good horizontal SI good vertical SI	1- The material of the front structure components (e.g. radiator frame) is changed to the highest-grade steel. 2- The thickness of the front structure components (e.g. radiator frame) is increased up to 100% (depending on the component). 3- The density of the changed components is scaled to maintain the same mass as the basic model.

Figure 2 illustrates the results of these simulation studies. The results are comprehensive and confirm the ordering of the structural properties. For better visibility, the plastic bumper and the hood are hidden. The main load path and the front structure are colored in red and the wheels are colored in black. To highlight the structures' performance, a triangle is created for each vehicle that exhibits the homogeneity of the deformations. A triangle with a greater base shows more inhomogeneity.

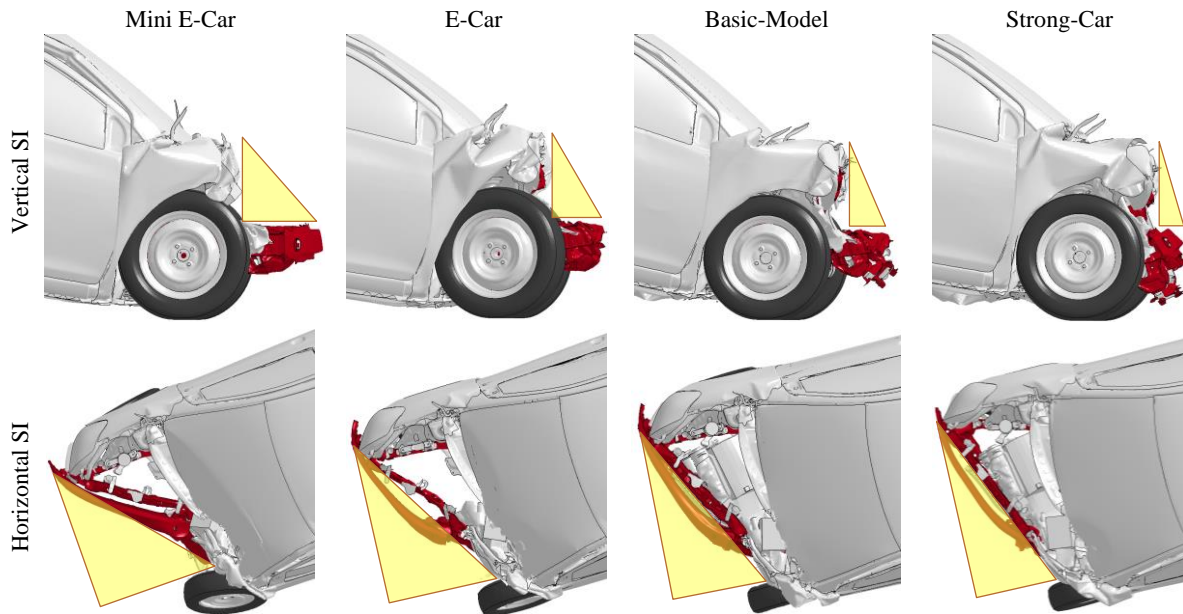


Figure 2. Validation of SI characteristics for the vehicle models.

Evaluation Criteria In this study, occupant safety is evaluated by intrusions and restraint loads. Points of vehicle crash metrics from [12] are used to measure the intrusions. This includes average intrusions in the toe-pan, maximum intrusion in the left and right knee-bolster for the driver, maximum displacement of the steering wheel and maximum displacement of the A-pillars. The Occupant Load Criterion (OLC) is used to evaluate the restraint loads on the driver. OLC considers the principle physical behavior of restraint forces applied to the occupant's chest. At the beginning, the occupant has a free flight

phase of about 65 mm and then it will be ideally restrained with a constant deceleration over 235 mm. This constant deceleration defined the OLC value, which corresponds with head and chest injury criteria [5]. Use of intrusion values and OLC, instead of the implementation of a dummy in the vehicle model, removes the dependency of results on the specific configuration of the restraint systems of the test vehicle.

Test Catalog To answer the questions from the beginning of this section, two series of car-to-car and car-to-barrier tests are analyzed.

The most important types of frontal collisions are considered in the car-to-car test series, with the original Yaris model as the bullet vehicle. These configurations are:

- Baseline test of ECE-R94 with 50% overlap and 100 km/h collision speed (50 km/h for each vehicle). This test represents a collision with a high risk of intrusions in the passenger compartment.
- Car-to-car collision with 75% overlap and 100 km/h collision speed (50 km/h for each vehicle). This test represents a collision with a high crash pulse for the restraint systems. It been observed in [13] that there is a high proportion of fatal and severe injuries in accidents with high overlap.
- Baseline test of small overlap and oblique test from [12] with 15° and 17% overlap and 112 km/h for the bullet vehicle. This test represents a collision with highly misaligned loads and high crash severity.

The most important test configurations for safety and crash compatibility are included in the car-to-barrier test series. Aside from ODB (from Euro-NCAP) and FWRB (from US-NCAP), the studied cases are PDB and FWDB from the FIMCAR project [1, 4].

4. RESULTS

Car-to-Car Tests

Simulation results are presented in Table 2. This section answers the first question: Does a better SI correspond with higher safety and crash compatibility?

Self-Protection Whereas vehicles with better structural properties have lower intrusions, better SI cause generally higher crash pulses and OLC values. Thus, there is no ideal structural property for all crash configurations.

There are two exceptions in the test results. By the high overlap test, the Mini E-Car with poor vertical SI has a higher OLC than the E-Car. This is due to a better coupling of wheels with the main load path because of the lower height of the vehicle, which causes a stiffer deformation zone. The other exception is that the Strong-Car with good SI has lower OLC values than the Basic-Model by the small overlap and oblique test. This is due to an impact on the stiff passenger compartment in the Basic-Model test, while the higher stiffness of the deformation zone by the Strong-Car avoids such an impact that reduces the crash pulse and the OLC value.

Partner-Protection Generally, the bullet vehicles have more intrusions and OLC values as they collide with vehicles with better structural properties. Hence, better SI makes the vehicles more aggressive.

There are two exceptions, by which the intrusion values of the bullet vehicle is less against the Strong-Car with good SI comparing to the test with the Basic-Model. By the small overlap and oblique test, better structural properties of the Strong-Car made it friendlier for the bullet vehicle regarding the intrusion values. The other exception is by the high overlap test, in which better structural properties resulted in less intrusion in the toe-pan and knee-bolster for the Strong-Car compared to the Basic-Model.

The results confirm the hypothesis that good or poor SI does not influence occupant safety directly. Structural issues, such as over-/underride, affect intrusion values and crash pulses. Depending on vehicle design and crash configuration, intrusion values or the crash pulse become more important as to why good or poor SI cannot be overall correlated to more or less occupant safety. It is also a design decision, if the passenger compartment should be stronger or the restraint systems should save occupants better. E.g., a supermini car could have a very short and stiff deformation zone, but a high-strength passenger compartment and good restraint systems. Therefore, an assessment of SI through some specific metrics that are independent from crash pulse and intrusions restricts the design's freedom.

Table 2.
Results of the car-to-car test series.

Crash configuration	Car	OLC [g]	Intrusion / Displacement [mm]			
			Toe-pan	Knee-bolster	Steering wheel	A-Pillar
Baseline test of ECE-R94 vs. Yaris (bullet vehicle) 50% offset 50 km/h for each	Mini E-Car	24.8	162	105	137	40
	<i>Bullet</i>	20.3	61	17	27	19
	E-Car	26.4	122	69	64	15
	<i>Bullet</i>	21.9	91	29	42	24
	Basic-Model	25.3	99	32	26	18
	<i>Bullet</i>	25.5	99	34	42	24
High Overlap test vs. Yaris (bullet vehicle) 75% offset 50 km/h for each	Mini E-Car	28.0	213	101	136	31
	<i>Bullet</i>	27.0	42	14	0	10
	E-Car	26.8	182	86	114	23
	<i>Bullet</i>	26.8	63	40	2	26
	Basic-Model	28.4	141	77	95	23
	<i>Bullet</i>	28.6	128	58	77	23
Small overlap and oblique test vs. Yaris (bullet vehicle) 15°, 17% offset 112 km/h for the bullet vehicle	Mini E-Car	22.6	317	267	420	287
	<i>Bullet</i>	27.5	76	7	11	17
	E-Car	27.5	251	207	251	75
	<i>Bullet</i>	28.0	132	26	38	24
	Basic-Model	30.2	174	92	111	54
	<i>Bullet</i>	34.5	171	73	84	31
Strong-Car	Strong-Car	29.2	158	82	128	46
	<i>Bullet</i>	37.4	159	54	57	67

Car-to-Barrier Tests

It is obtained in previous parts that good or poor SI cannot be overall correlated to more or less occupant safety. To consider the structural properties in the assessment of crash compatibility, either some metrics should predict the structural performance in real collisions, or the test configuration should reflect the structural issues in crash pulse and intrusions. This has been analyzed in this section for different barriers to answer the second question: Are current test approaches able to evaluate structural properties? Simulation results are presented in Table 3.

Full-Width Rigid Barrier Vehicles with better SI had higher crash pulses and, consequently, higher OLC values. However, in this test configuration, better SI is penalized with more intrusions. It is due to the nature of the rigid wall that exerts forces to components, which are not designed as load paths. Displacement on these components results in intrusions in the compartment. Thus, this test configuration does not reflect structural properties correctly. There is also no metric for this barrier to predict the structural performance in real collisions.

Offset Deformable Barrier Generally, vehicles with lower SI had lower OLC values. However, the intrusions do not correspond with structural properties. The Strong-Car with good SI has more intrusions in the toe-pan and less in other zones. Intrusions of the Mini E-car with poor vertical SI do not reflect any over-/underride problem. On the contrary, the intrusion values in its toe-pan are higher than in other vehicle models. Although the E-Car has a poor horizontal SI, its intrusion values are slightly less than for the Basic-Model. There is also no metric for this barrier to predict the structural performance in real collisions.

Full-Width Deformable Barrier A metric has been developed in the FIMCAR project for the FWDB to assess the vertical structural alignment. The loads are measured in eight rows on a load cell wall behind the deformable block. The vehicle must achieve minimum load requirements in rows 3 and 4 and can use loads in row 2 to help fulfilling this requirement under certain conditions. The minimum load requirement promotes structural alignment and the credit of loads from row 2 encourages vertical load spreading [4]. FIMCAR did not succeed in developing a metric for horizontal SI, whereas the E-Car with poor horizontal SI has passed this test; it got even better results than the Basic-Model for both OLC and intrusions. The developed metric rejected the Mini E-Car due to its poor vertical SI. However, the Strong-Car with good SI is also failed. The most controversial part of these results is that the Mini E-Car failed due to only 6.4% lower loads than the limit of the metric, whereas the Strong-Car with good SI failed due to 28.1% lower loads. Therefore, it is doubtful that the developed metric could predict the structural performance in real collisions.

It is obtained that vehicles with better SI had higher OLC values. As it is mentioned in [10], the intrusion values in this test configuration are generally low and similar for different SI characteristics. A clear trend for different structural properties does not exist and this barrier cannot reflect structural properties correctly.

Progressive Deformable Barrier Deformations on the barrier can be used to evaluate SI of the vehicle. There is also a concept for a Fail/Pass metric, which is based on the measurements of the loads in different heights. The criterion 99%ile of Digital Derivative in Y (DDY) in common interaction zone from [1] has been estimated for each vehicle. Lower values correspond to more homogenous vehicle deformation, which is in contrast with the structural priorities of the vehicles. Criterion (d) is another developed metric from [1], which might detect the load path of the vehicles. This metric could generally detect SI problems. However, the (d) scores are similar and since limits are not yet adjusted, the evaluation of the simulation results with Fail/Pass is not possible.

Generally, vehicles with lower SI had lower OLC values and higher intrusions. The over-/underride issue is also observed in the results of the Mini E-Car with poor vertical SI relative to the E-Car. Hereby, the steering wheel's displacement is higher, while other intrusion values for the toe-pan and knee-bolster are lower.

This barrier can reflect structural properties in intrusions and crash pulse of the test vehicle. However, the metrics for the partner-protection are ineffective.

Table 3.
Results of the car-to-barrier test series.

Crash configuration	Car	OLC [g]	Intrusion / Displacement [mm]				Metrics for SI (if any)
			Toe-pan	Knee-bolster	Steering wheel	A-Pillar	
US-NCAP vs. FWRB 100% overlap 35 mph	Mini E-Car	28.7	110	42	67	33	-
	E-Car	27.7	93	36	38	31	-
	Basic-Model	37.2	179	65	98	68	-
	Strong-Car	37	180	78	114	80	-
EU-NCAP vs. ODB 40% overlap 64 km/h	Mini E-Car	21	176	115	97	22	-
	E-Car	21.9	123	75	87	15	-
	Basic-Model	27.2	125	73	95	33	-
	Strong-Car	27.4	132	42	71	28	-
vs. FWDB 100% overlap 50 km/h	Mini E-Car	24.1	90	26	36	19	Failed
	E-Car	23.8	87	23	40	18	Passed
	Basic-Model	30.2	88	39	12	26	Passed
	Strong-Car	28.8	78	27	5	22	Failed
vs. PDB 50% overlap 60 km/h	Mini E-Car	23.0	168	83	120	23	99%ile DDY=1.4 (d) score = 3.4
	E-Car	21.8	193	86	80	24	99%ile DDY=1.7 (d) score = 3.2
	Basic-Model	28.0	106	37	38	25	99%ile DDY=2.8 (d) score = 3.6
	Strong-Car	27.4	89	27	23	22	99%ile DDY=2.8 (d) score = 3.5

5. ALTERNATIVE ASSESSMENT APPROACH

Our recommendation is to assess the partner protection through metrics about intrusions and crash pulse of the partner, without direct assessment of the structural interaction. Instead, the test configuration should be able to reflect structural properties in intrusions or crash pulse. An exemplary concept of such a test approach is presented in [10]. The vehicle strikes against the Advanced European Mobile Deformable Barrier (AE-MDB), the geometry and stiffness of which may represent the front-end of today's passenger car fleet [3]. Since the objective is the proof of this concept, the test configuration is not finalized in this study. The test vehicle collides at 50 km/h with 50% offset against the AE-MDB at 35 km/h. This results in an energy equivalent speed of about 56 km/h for both sides.

Besides the criteria for the crash pulse and intrusions of the test vehicle, acceleration pulse and forces behind the deformable blocks will be measured on the mobile barrier. Acceleration pulses will be converted to OLC and forces on the AE-MDB represent the risk of intrusions for the partner. Simulation results of the car-to-AE-MDB tests are presented in Table 4.

Table 4.
Results of the test vs. AE-MDB.

Crash configuration	Car	OLC [g]	Intrusion / Displacement [mm]				Other Criteria
			Toe-pan	Knee-bolster	Steering wheel	A-Pillar	
vs. AE-MDB 50% overlap AE-MDB 35 km/h Car 50 km/h	Mini E-Car	19.3	139	80	68	21	OLC _{AE-MDB} =16g max. F=73.2kN
	E-Car	19.2	142	85	79	17	OLC _{AE-MDB} =16.7g max. F=97.2kN
	Basic-Model	26.5	91	38	31	22	OLC _{AE-MDB} =25.1g max. F=222.8kN
	Strong-Car	25.5	71	33	22	19	OLC _{AE-MDB} =25.1g max. F=354.2kN

The simulation results are consistent with the results of the car-to-car tests; i.e. vehicles with better SI result in higher crash pulses for both sides, while intrusions of the vehicles with better SI are smaller. Better SI makes the vehicle more aggressive and causes higher OLC values and forces on the barrier, which is in agreement with the car-to-car tests results.

The override issue is also reflected in the Mini E-Car case where the intrusion values in the toe-pan and knee-bolster are less comparing to those of the E-Car. It is noteworthy that the test severity is too low for the displacement of the A-pillar and all values are quite similar.

6. CONCLUSIONS AND RECOMMENDATIONS

Better SI increases crash pulse and reduces intrusions. Depending on the vehicle design and crash configuration, intrusion values or the crash pulse become more important as to why good SI cannot be overall related to more crash compatibility. It is obtained that better SI makes the vehicle more aggressive. Current assessment approaches for the frontal crash compatibility establish a direct link between good SI and higher safety. These approaches do not consider the effect of higher crash pulses due to better SI and limit the design's freedom.

Among the current assessment approaches, the PDB is found as the only barrier that can reflect SI issues correctly. However, the developed metrics for this barrier resulted in incomprehensive interpretations.

Our recommendation is to assess the partner protection through metrics involving intrusion and the crash pulse of the partner without direct assessment of the structural interaction. Instead, the test configuration should reflect the structural properties in intrusions or crash pulse values. An exemplary test concept is presented and proved by simulations. The combination of this test concept with FWRB test can assess the safety and crash compatibility of the vehicles.

ACKNOWLEDGMENT

The project was independently funded by the Institute of Automotive Technology at the Technische Universität München.

REFERENCES

- [1] Del Pozo de Dios, E., Lázaro, I., Delannoy, P., Thomson, R., Versmissen, T. & van Nunen, E. (2013). *Development of a Structural Interaction Assessment Criterion Using Progressive Deformable Barrier Data*. 23rd ESV Conference Proceedings, Seoul
- [2] Edwards, M.J., de Coo, P., van der Zweep, C., Thomson, R., Damm, R., Martin, T., Delannoy, P., Davies, H., Wrigge, A., Malczyk, A., Jongerius, C., Stubenböck, H., Knight, I., Sjöberg, M., Ait-Salem Duque, O. & Hashemi, R. (2007). *Improvement of Vehicle Crash Compatibility through the Development of Crash Test Procedures*. Final Technical Report of VC-COMPAT
- [3] Ellway, J.D., van Ratingen, M., Versmissen, T., van Montfort, S., Langner, T., Dobberstein, J., Goutas, P., Gay, P., Malak, A., Denker, C., Hallack, J., Odanaka, K. & Ogihara, T. (2013). *The Advanced European Mobile Deformable Barrier Specification for Use in Euro NCAP Side Impact Testing*. 23rd ESV Conference Proceedings, Seoul
- [4] Johannsen, H., Adolph, T., Edwards, M., Lazaro, I., Versmissen, T., & Thomson, R. (2013). *Proposal for a Frontal Impact and Compatibility Assessment Approach Based on the European FIMCAR Project*. Traffic Injury Prevention, S105-S115, DOI: 10.1080/15389588.2013.790538.
- [5] Kübler, L., Gargallo, S. & Elsäßer, K. (2009). *Frontal crash pulse assessment with application to occupant safety*. ATZ worldwide, Volume 111, Issue 6, pp 12-17.
- [6] Marzoughi, D., Samaha, R.R., Cui, C. & Kan, C. (2012). *Extended Validation of the Finite Element Model for the 2010 Toyota Yaris Passenger Sedan*. Working paper of NCAC, 2012-W-005
- [7] Huang, M. (2002). *Vehicle crash mechanics*. Boca Raton, Fla.: CRC Press.
- [8] Mongiardini, M. & Ray, M.H. (2009). *Roadside Safety Verification and Validation Program (RSVVP)*. User's Manual of RVSSP 1.7
- [9] O'Brien, S. (2011). *Priorities for the Assessment of Frontal Impact Compatibility*. 22nd ESV Conference Proceedings, Washington, D.C.
- [10] Sadeghipour, E., Duddeck, F. & Lienkamp, M. (2014). *Crash Compatibility of Microcars: A Study on Current Test Approaches*. Crash.tech 2014, Munich (also published in Researchgate)
- [11] Sandqvist, P., Thomson, R., Kling, A., Wågström, L., Delannoy, P., Vie, N., Lázaro, I., Candellero, S., Nicaise, J.L. & Duboc, F. (2012). *Report on Car-to-Car Test Results*. Deliverable 6.1 from FIMCAR project (FP7)
- [12] Saunders, J., Craig, M.J. & Suway, J. (2011). *NHTSA's Test Procedure Evaluations for Small Overlap/Oblique Crashes*. 22nd ESV Conference Proceedings, Washington, D.C.
- [13] Thompson, A., Edwards, M., Wisch, M., Adolph, T., Krusper, A. & Thomson, R. (2011). *Report detailing the analysis of national accident databases*. Deliverable 1.1 from FIMCAR project (FP7)
- [14] Thomson, R., Johannsen, H., Edwards, M., Adolph, T., Lázaro, I. & Versmissen, T. (2012). *Documentation for a frontal impact and compatibility assessment approach: Part I*. Deliverable 6.3 from FIMCAR project (FP7)
- [15] N.N. (2006). *Improvement of vehicle crash compatibility through the development of crash test procedures*. Final technical report of project VC-COMPAT
- [16] N.N. (2007). *Car crash compatibility and frontal impact*. Final report of EEVC-WG 15 to steering committee
- [17] N.N. (2008). *Detailed discussion of the VDA position on the proposal for draft amendments to UN-ECE R94*. Retrieved February 21, 2015, from <http://www.unece.org/fileadmin/DAM/trans/doc/2008/wp29grsp/FI-03-09e.pdf>
- [18] N.N. (2010). *RCAR Bumper Test*. Issue 2.0 from Research Council for Automobile Repairs (RCAR)
- [19] N.N. (2013). *European Vehicle Market Statistics*. Pocketbook 2013, the International Council on Clean Transportation (ICCT)

The trolley test way of IIHS small overlap and side test - with minimized structure usage -

Park Un-chin

Song Ha-jong*

Kim Hyun-chul*

Florian Ganz**

Sudar Sankar**

Mario Wohlfahrt**

ABSTRACT

To develop a vehicle in low cost and early well-customized performance trolley test can be used efficiently. In this research, we will introduce how to make the trolley for the IIHS small overlap and side crash with substituting parts by CAE validation and show the good validation with real vehicle crash after the test

Key Word : Trolley, Buck, BIW, Vehicle Crash, Component Test, CAE, IIHS Small overlap, IIHS Side

1. Introduction

We use sled test often to tune the restraint system in the vehicle because of its repeatability and low cost. If we have something similar to this in structure performance test, it would be very useful to reduce the vehicle developing cost.

If we use the whole BIW that is useful way because we usually produce not the parts of front buck or side structure but the total of BIW to develop many kinds of performances and reduce the cost. But for the repeatability too many parts are used. For example at the IIHS small overlap test rear half part of the car can not be needed necessarily and at the IIHS side test right half and floor part not be needed so much. To see a certain point for some issues like lower arm dislocation, B-pillar breakage or door trim sharp edge, we should repeat the test several times.

If we use half structure it will be more useful to repeat and concentrate on that point. Also this way is more useful than one part component test like lower arm breakage test, B-pillar tensile test or door trim sharp edge test in the viewpoint of total structural test.¹⁾⁻⁴⁾

So, in this research we will introduce how to make the front buck trolley for IIHS small overlap structure test and side structure trolley with CAE validation. We tried to minimize the cost of manufacturing by making the substitutes for many parts like the engine, cowl cross bar at the IIHS small overlap trolley test and using only the side structure and doors at the IIHS side trolley test. We will judge the validation of this trolley test by comparing the results with full car crash.

2. Main Subject

2.1 IIHS small overlap trolley test

2.1.1 The concept of frontal small overlap trolley

To make the small overlap trolley we used ACTS Mobile barrier. The mobile modular crash device consists of four basic elements that can be combined in different configurations. This enables the fixing of bigger parts and has clear benefits regarding the matching of sizes, of CG positions and of weight of the tested vehicles. Also, different wheel and roller systems, as well as bushings can be adaptive. We use only rear half for the Forte IIHS small overlap test.



Fig.1 Configuration modular mobile crash cart

Table 1. The Spec of ACTS frontal mobile barrier

Detail	Adjustability	Unit	Length			
			2.600	3.200	3.800	
Width	50 mm steps	mm	from	900	900	900
			to	1.300	1.300	1.300
Mass	depending on width	kg	from	708	875	939
			to	828	1.046	1.110
Wheelbase	50 mm steps	mm	from	1.560	2.120	2.720
			to	2.160	2.720	3.320
Width	50 mm steps	mm	from	1.295	1.295	1.295
			to	1.695	1.695	1.695
Height	fix	mm	400	400	400	
Ground clearance	stepless	mm	from	100	100	100
			to	300	300	300

* Safety Performance Team 1 : Author or Co-Author

** Crash Simulation Team : Co-Author

*** ACTS (Advanced Car Technology System) : Co-Author

Its frame mass can be adjusted from 700kg to 2,800kg and additional mass can be adaptive and adjusted. Statistic simulation can be done for a longitudinal beam with 600kN force and a cross beam with 400kN. Also crash panel and basic frame can be adjusted with step less.

With this barrier, we decided to use the front Forte BIW from the forward to right in front of b-pillar. If we use the door and B-pillar the validation would be better but for the future use to minimize the part we did it. The cut area will be Also, we decided to remove all the trim an chassis parts except the parts related to the moving and the connection of engine to reduce the cost and improve the repeatability. Those parts are front wheels, lower arms, suspensions, a roll rod, an engine mounting, a transmission mounting, etc. The engine, front doors, cowl cross beam, delta glass and the first roof cross beam will be substituted by appropriate designed material by CAE. In case of wind glass and front seat they are removed. We couldn't install the front seat because rear seat mounting is removed.

We selected the Forte vehicle is the US model of 1.8 Nu engine auto transmission. This vehicle's intrusion is poor grade which has some deformation on the roofrail of B-pillar and the worst case of the deformation among the Hyundai-Kia vehicles, we believe if we are successful for the validation that can be available for the most of vehicles.

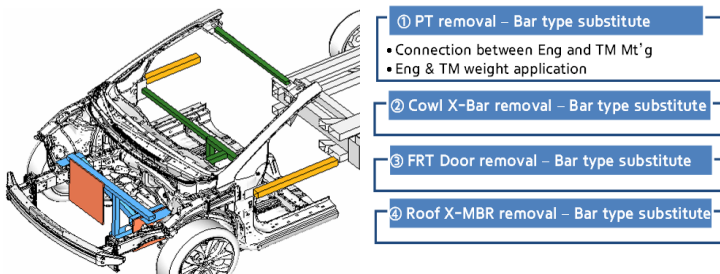


Fig.2 The concept of small overlap trolley

2.1.2 Substituting parts

In the IIHS small overlap test engine compartment doesn't influence so much as in frontal US NCAP test but during the crash the left hand front side member becomes to contact the transmission because it is bent by crash energy. So we designed substitution of transmission part side with the wall to block front side member bending at the same distance as real transmission.

Also the engine room weight distribution is important to fit the total vehicle weight distribution and determine the movement of powertrain. So we pick out the CG coordinates for engine and transmission each. And we added several 10 to 25kg weights to left and right positions of the upper beam to fit the CG. The Forte engine weight is 114kg and transmission 80kg. The

powertrain coordinates is (x:236 y:22.8 z:212) and the coordinate measured from (x:236 y:17.9 z:211). So they are so close.

The links to the vehicles are designed same as a vehicle. Bolting is done at the left transmission mount, the engine mount and roll rod with same direction with the vehicle assembly.

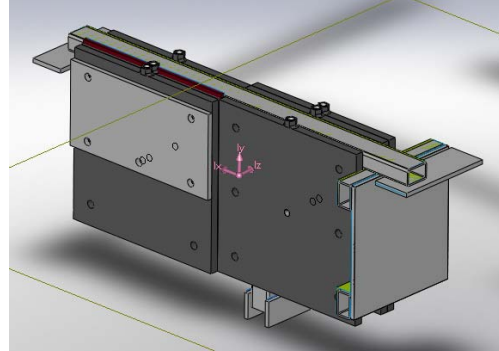


Fig.3 Powetrain substitute model



Fig.4 Powetrain mounting points

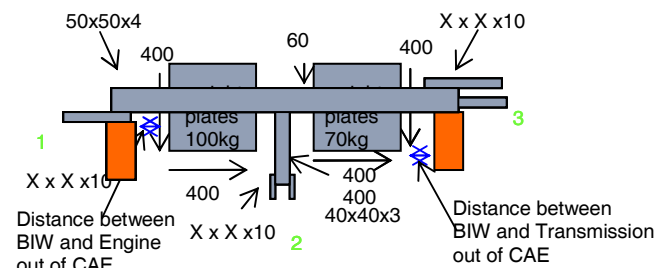


Fig.5 The concept of powertrain substitute

The links to the vehicles are designed same as a vehicle. Bolting is done at the left transmission mount, the engine mount and roll rod with same direction with the vehicle assembly.

For the front door we set the 2 bars instead of door assembly initially. But lower beam is removed at 2nd CAE validation. The links to the vehicles are designed same as a vehicle. Bolting is done at the 2 door hinge mountings.

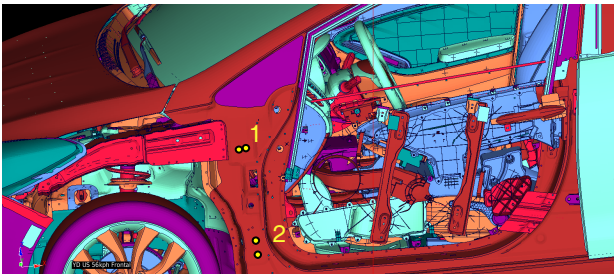


Fig.6 Front door mounting points

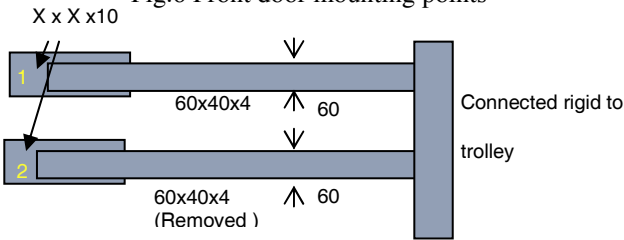


Fig.7 The concept of powertrain substitute

Also we designed the cowl crossbar substitute and 1st roof cross member to minimize the parts. When we get the structure assembly the cowl cross bar is not contained and the roof cross member is not the part of side structure like A-pillar and side sill.

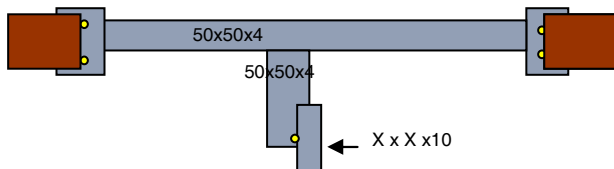
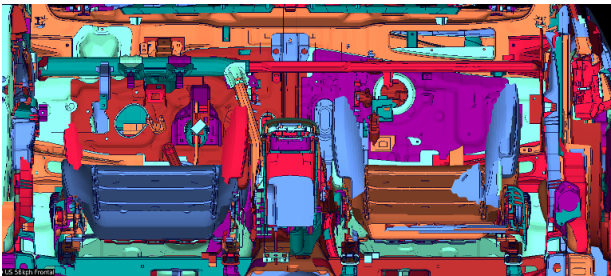


Fig.8 The concept of cowl crossbar substitute

All beams' material were S235 of plastic stress 235Mpa. And the surface area parts were welded to the trolley bracket

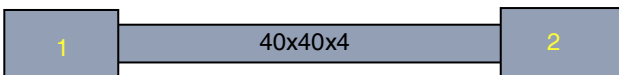
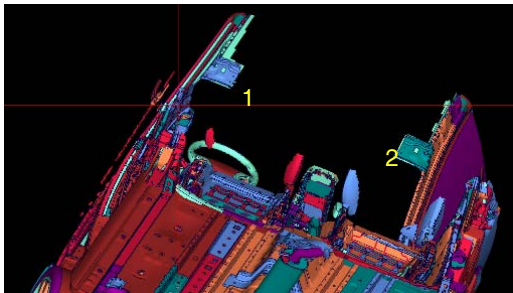


Fig.9 The concept of roof cross member substitute

2.1.3 CAE validation

From the 1st to 7th CAE validation we set the wheel rims rigidity, door substitute lower beam removal and most of the section size with thickness. But there was front side member upper moving. But when we did apply very weak connecting condition to the most of welding points as a trial at 5th CAE, there was no front side member upper moving. We can also assume this in the comparison of vehicle CAE and vehicle crash because we know most small overlap welding points are failure in Forte correlation experience.

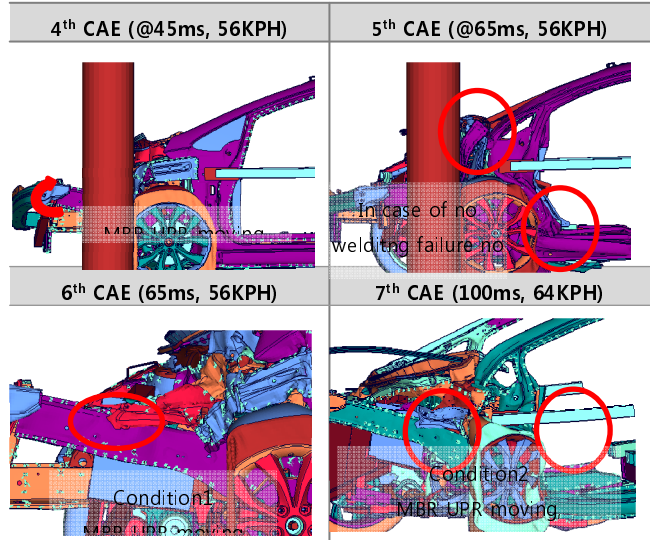


Fig.10 CAE validations from 4th to 7th

So we applied 3 times of welding condition adjustment. from 6th to 8th. Finally we weakened 27 welding points by engineering judgment the member upper going reduced enough. Also we set the final trolley test speed as not 64kph but 56kph, because in case of 64kph there was too much rotation of the vehicle. We also already knew the fact 56kph is better than 64kph in DM small overlap trolley tests research as an experience because there are many missing points like hood, chassis and trims.

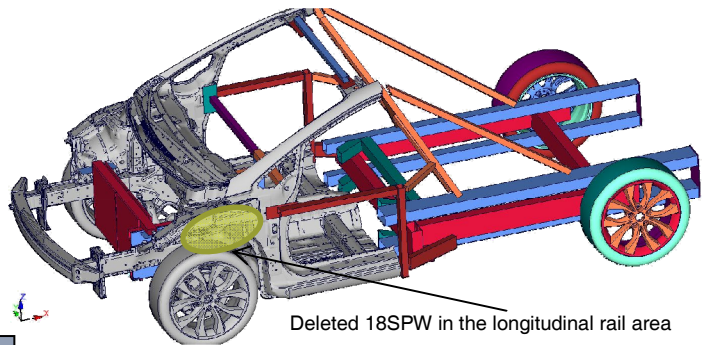


Fig.11 Final CAE validation model

2.1.4 Results of small overlap trolley test

We focused the validation on the contacting time of wheels, the dislocation time of lower arm A-point, the

rotation angle of vehicle and the structural deformation. As you see from table2 and fig11, the criteria matches very well. In case of structural deformation the result was closer to the full car than car CAE.

Table 2. Results summary of small overlap trolley

Item	Full car	Trolley
Tire contact	39ms	39ms
A pt. dislocation	42ms	42ms
Car rotation@200ms	19deg	20deg

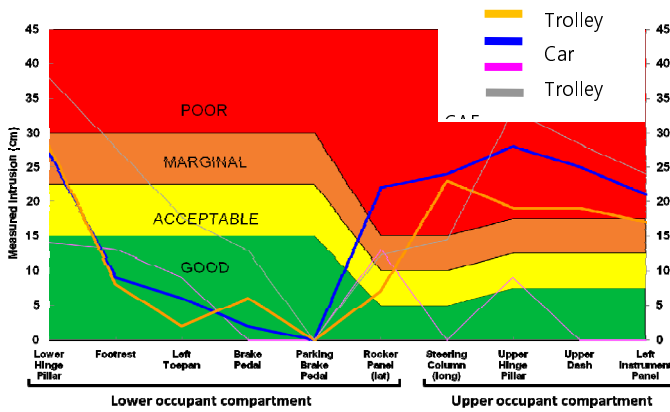


Fig.11 Structural deformation comparison



Fig.12 Video comparison with full car crash @ 200ms

As a result, this method for small overlap trolley test is valid. We can use this method for better crash performance developing with reduced developing cost. There were some points to be improved next time. Firstly, the wheel rotation for x-axis was different because we run the test without drive shaft. Secondly, the door substituting beam hinge mounting was broken and rear part was bended even it was indispensable. Next time we must invent better substituting system.

2.2 IIHS side trolley test

2.2.1 The concept of side trolley

To make the IIHS side trolley we used ACTS side

trolley. The trolley device consists of many beams and 13 inch wheels to be adjusted wheel base and wheel tread distance but there is the limit for the wheel base adjustment of the minimum value 1630, because the left wheels are inside comparing with rear car this is needed to be supported in case of 1570 wheelbase length car Forte. So CG positions and weight distribution can be easily adjusted. This trolley usually



Fig.13 Configuration of ACTS side trolley

Table 3. Characteristics of ACTS side trolley

- Different adaptation (B-pillar, hinges, doors, trims)
- Speed max = 65 km/h
- Angle max = $\pm 45^\circ$
- Weight max = 2500kg
- Different configurations (Buck vs. pole or barrier)

In this research our purpose is the total test of side structure. So we decide to attach the whole side structure with doors of none glass and whole inner parts. Because there was severe deformation at the roof rail and side sill area in the 1st CAE with just rigid connection between side structure and trolley we decide to attach bending bar with some distance for roof rail and "V" shape struts with several rectangular brackets. Also almost-none deformable area like A-pillar and C-Pillar we will make 3 rigid bars connection for each. All the supporting bars are changed for the size and shape through 8 CAE validations. Crash speed 50kph is same as vehicle's.

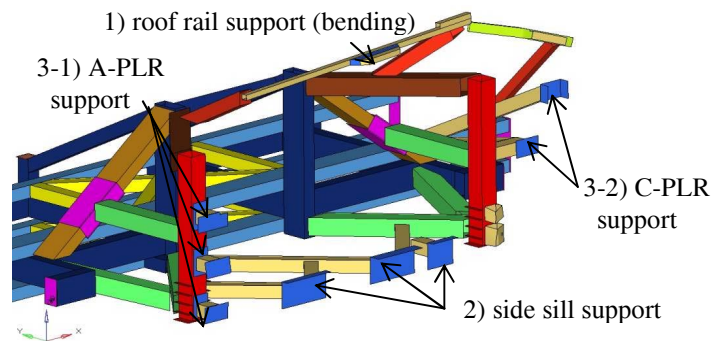


Fig.14 The connecting parts concept

2.2.2 CAE validation

At the first CAE validation, Vehicle side structure including roof and roof cross members are connected to trolley by rigid elements at A and C pillar and roof. As a result there was severe deformation at the roof rail and

side sill area because there was no support for them.

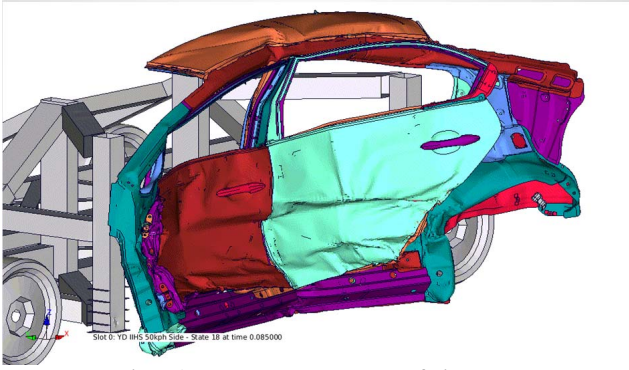


Fig.15 The 1st CAE result of side trolley

So we deleted roof and roof-beams at 2nd CAE, added trolley beams on the upper and lower area. Spec are like Fig.16. But as a result the roof rail have passed away over the trolley supporting beams and side sill rotation was too much.

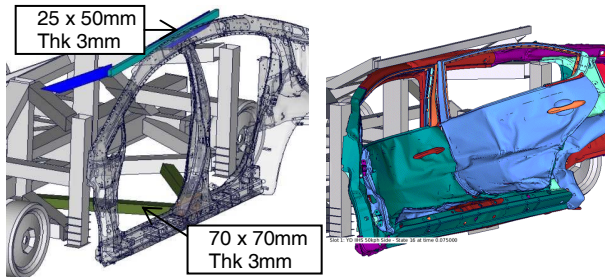


Fig.16 The 2nd CAE model and result

At the 3rd CAE, lower B-pillar support defined roof support with deformable profile between A and C pillar. Even there was still big rotation on the side sill and drop down of roof rail, the B-pillar profile became much closer to full car CAE.

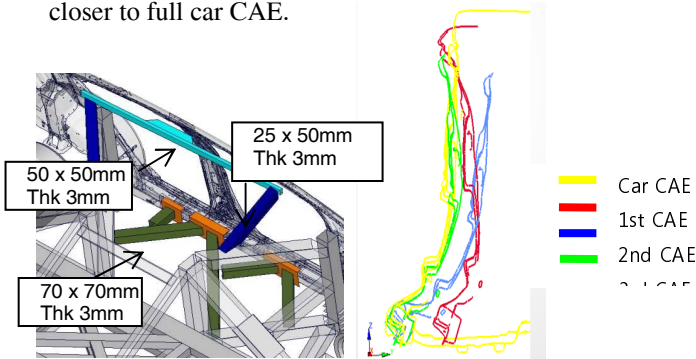


Fig.17 The 3rd CAE model and B-PLR profile (1,2,3rd)

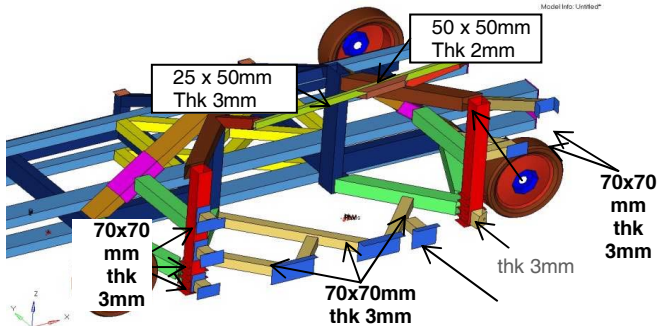


Fig.18 The 4th CAE model

At the 4th CAE, we added connections between trolley and vehicle at A & C-pillar to resist too much Z-axis rotation of them. As a result it is improved. Also we changed roof support beam thickness from 3 to 2mm to make more intrusion like full car CAE.

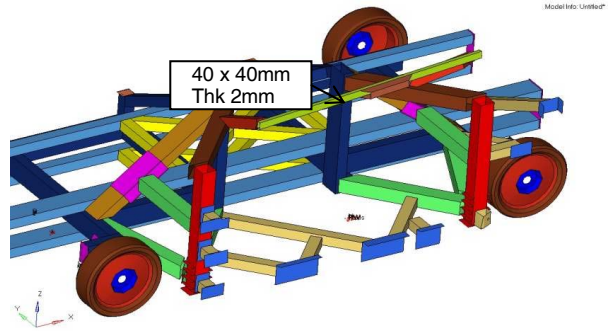


Fig.19 The 5th CAE model

At the 5th CAE, we weakened roof beam to prevent too fast spring back. as a result spring back was improved but the initial intrusion was too high.

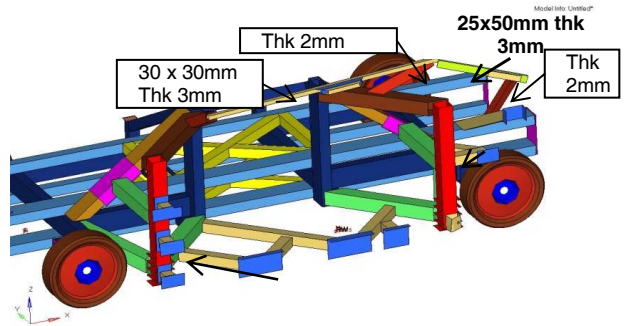


Fig.20 The 6th CAE model

So at the 6th CAE, we modified C-pillar support because we thought the rear part deformation of roof rail support makes too fast initial intrusion. Then we weakened roof beam more to prevent too fast spring back. As a result upper b-pillar intrusion became closer than 5th CAE.

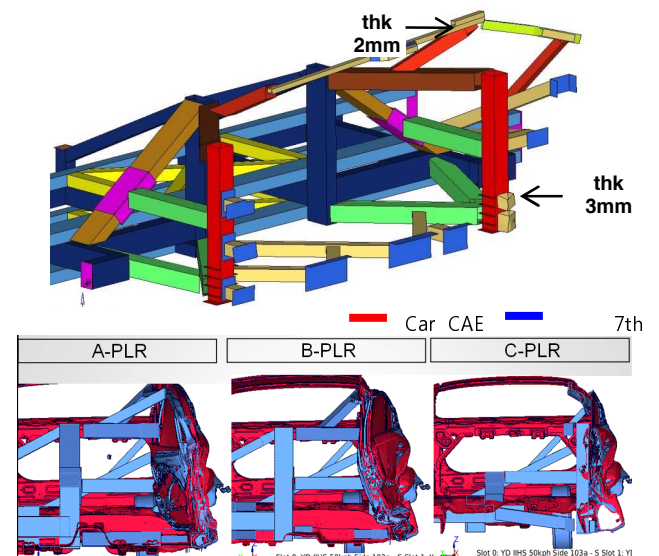


Fig.21 The 7th CAE model & A,B,C-PLR comparison

At the 7th CAE, we strengthen the rear of roof beam by adding one box and also added new box between trolley and sill at C-pillar to prevent C-pillar partial intrusion. As a result we got the successful validation to make the trolley. There were still some points not validated partially like front & rear door beltline bending point and B-pillar upper & lower rotation but even the full CAE is not

At the 8th CAE, we changed all the beams material from S355 to S235 because we cannot get the S355 soon. Also we changed some rigid parts to real modeling. As a result the intruding speed and permanent deformation was closer to the full car CAE than 7th CAE. 5)-6)

2.2.3 Results of IIHS side trolley test

Through the comparison of intruding speed, we've come to know this trolley has really close structural performance. In case of upper and lower part the intruding speed correlation was not so good as beltline height but the modes are clearly same.

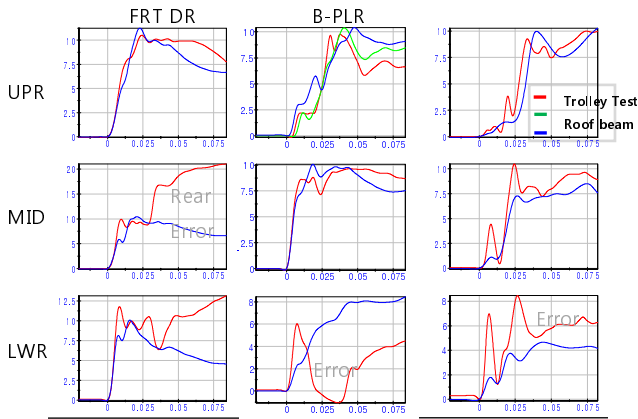


Fig.22 Comparison of UPR/MID/LWR intruding speed

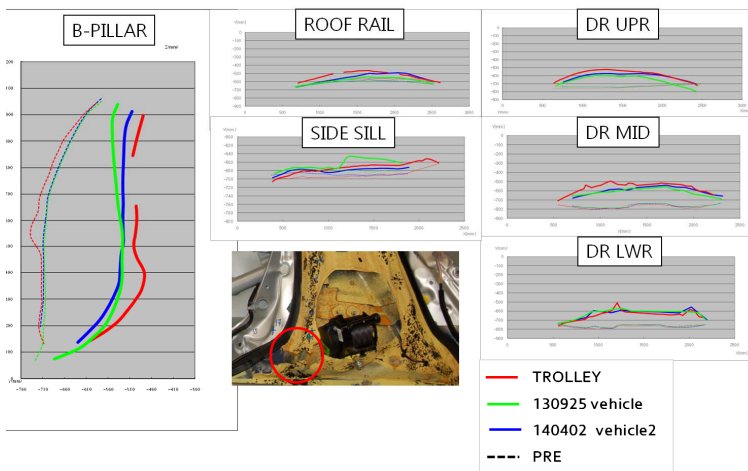


Fig.23 Comparison of static deformation

For the static deformation comparison, there were 50mm difference on the B-pillar lower, roof rail front and door upper/middle front. When we inspect the trolley, there was crack on the B-pillar lower inner panel. The reason was thought there was no front seat support in this

trolley. So we added seat support substitute (inner 10t thickness, outer 5t thickness) and run the CAE again. As a result B-pillar and front door deformation was much closer to the real vehicle and the high strain area of B-pillar disconnected place was reduced. This means the probability of B-pillar disconnection became lowered.

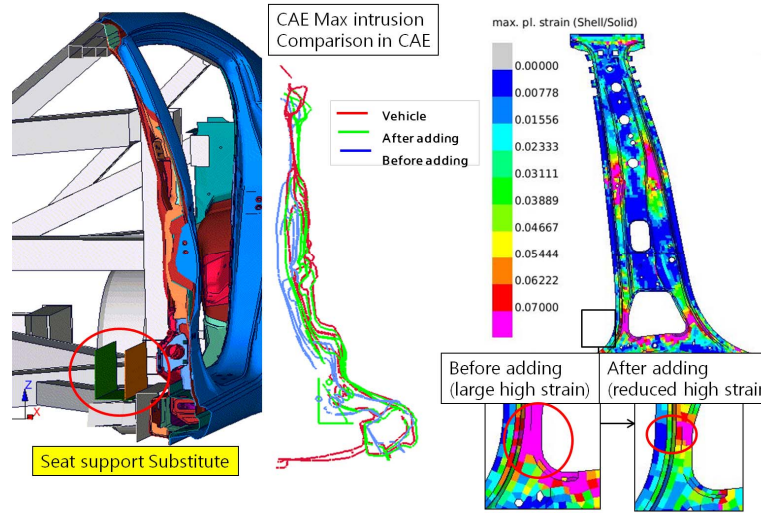


Fig.24 Seat support substitute CAE result

3. Conclusion

We made 2 kinds of trolley- IIHS small overlap and IIHS side, by using CAE validation for the Kia Forte vehicle. The correlation was very good even it's just made once and minimized parts because we concentrated on the important parts.

In case of small overlap trolley, we deleted many parts but we substitute powertrain, door, cowl cross bar and roof rail cross beam by creative ideas. All the strengths are tuned by CAE and CG points of powertrain and vehicle was set very accurately. As a result the trolley test many event time and structural values are really close to the vehicle test.

In case of side trolley, we designed many supporting beams and tuned them by CAE. Even if side structure deformation is complicated, there was not a big deformation in the roots like A/C pillar we install the beam by welding. Only the roof rail and side sill we applied very smart idea-making space and supporting by bending beams or rectangular brackets to realize the deformation better. As a result the trolley test many event time and structural values are really close to the vehicle test.

Now if we use these skills to develop a vehicle structure we can solve the main issue faster and with low cost because we can repeat the tests more easily. We expect test numbers side and smalloverlap could be reduced half. For one vehicle development the developing cost saving would be over \$210,000. We are planning this methodology adaptation from PD project.

■ **Patent:** Be submitted "Efficient IIHS smalloverlap structure trolley", "Efficient IIHS side structure trolley"

References

1. Jason R. Kerrigan "Design of a Dynamic Rollover Test System" UVA Center for Applied Biomechanics, 2011
2. Jeff R. Crandall, "Reproducing the Structural Intrusion of Frontal Offset Crashes in the Laboratory Sled Test Environment" University of Virginia, 2014
3. P. Michael Miller II, "A Compact Sled System for Linear Impact, Pole Impact, and Side Impact Testing" MGA Research Corp., 2002
4. Patrick M. Miller, "Evaluation Methodologies for Automobile Side Impact Development" MGA Research Corp. ", 1993
5. Karl Hoffmann, "Eine Einführung in die Technik des Messens mit Dehnungsmessstreifen", Herausgeber: Hottinger Baldwin Messtechnik GmbH, Sarmstadt
6. Herausgegeben von W. Beitz und K.-H., "DUBBEL TASCHENBUCH FÜR DEN MASCHINENBAU" 20. AUFLAGE

■ Author ■



Park Un-chin



Song Ha-jong



Kim Hyun-chul



Florian Ganz



Sudar Sankar



Mario Wohlfahrt